High Temperature Superconducting Microwave Devices

by

K.S. Kale

St. John's College

A thesis submitted in partial fulfilment of the requirements
for the degree of Doctor of Philosophy,
University of Oxford,
Trinity Term, 1996

Department of Engineering Science,
Parks Road,
Oxford
OX1 3PJ

High Temperature Superconducting Microwave Devices

K.S. Kale
St. John's College

A thesis submitted in partial fulfilment of the requirements
for the degree of Doctor of Philosophy,
University of Oxford,
Trinity Term, 1996

Abstract. This thesis describes investigations into the application of high temperature superconductors (HTS) for microwave devices. The ultimate aim of this research was to produce HTS components that would demonstrate the commercial potential of their use in spacecraft such as satellites or in base stations for terrestrial cellular communication systems. During the course of this research the surface resistance (R_s) of HTS thick and thin films deposited onto different substrates has been measured by a variety of techniques. These have been compared and contrasted with each other. There has been a particular emphasis upon the use of dielectric resonators as characterization tools and this thesis describes their use to measure the R_s of films and the loss tangents of the materials used in them. Consideration has been given to losses in the walls of the enclosures that surround dielectric resonators which is an area that has been neglected in previous work. Many of the films characterized had R_s values lower than normal conductors at the same temperature and frequency including a thick film which had an R_s of $2.7m\Omega \pm 8.0\%$ at 77K and scaled to 10 GHz which represents the second lowest result achieved in a thick film to date. Using such high quality films a number of devices have been made including microstrip resonators operating at 1.7-8.4 GHz, 5.58 GHz, 23 GHz and 24.75 GHz dielectric resonators and filters with centre frequencies from 5.58-13 GHz. Such devices have shown performance enhancements of up to 700% over their normal conductor equivalents. Benefits have been delivered in light, low volume packages which is of particular advantage to the satellite communications industry. Finally, there has been a demonstration, for the first time, of a tunable HTS thin film filter.

For my gurus.

Acknowledgements

Accomplishing a body of engineering research lasting three years single-handed is impossible and requires the help, assistance, encouragement and support of a number of individuals and institutions. This part of my thesis although small in size is the largest in content. The content consisting entirely of thanks.

The EPSRC, Department of Engineering Science and St. John's College, Oxford have provided valuable financial and domestic support throughout my course and your contribution is much appreciated. I would like to thank my supervisors Prof. Dew-Hughes and Dr. Edwards for their valuable comments and advice especially when it came to writing up. I am especially grateful to Dr. Edwards for his final piece of constructive criticism without which I would not have produced the world's first tunable HTS thin film filter. The HTS films, without which a single device could not have been made, were provided by the Materials Department, Oxford University. They also helped fill the large gaps in my HTS knowledge. So, thank you to Annette Bramley, Steve Morley (now at Nottingham University), John O'Connor, Mark Su, Bridget Glassey and Dr. Chris Grovenor.

I would like to thank Kalok Jim, Andy Street and Bori Minakovic for not only helping out with the engineering involved in this research, but for making working in the Department great fun. Thanks also to the guys down in the workshops and stores who provided mechanical construction advice and made the boxes for my devices.

Alan Jenkins has been a constant presence during this research; a teacher, a guide, a mentor, a supervisor, a wall to bounce my ideas off, an encourager, an endless source of microwave knowledge, a listener and a teacher of infinite patience. I have learned much more than just engineering from you. Thanks for being a true guru.

My greatest thanks go, as always, to my Mum and Dad.

Contents

Chapter 1

Introduction

Possible uses of high temperature superconductors (HTS) include very fast computers, high speed trains, energy storage, high field magnets, non-invasive medical diagnosis and communications [1.1-1.3]. To date the use of HTS in the latter has been widespread [1.4-1.6] and commercial with companies such as Conductus and Du Pont already manufacturing and selling HTS microwave devices. The reduced cooling costs of HTS compared to low temperature superconductors (LTS), which operate at around 4 K, has made such devices viable [1.7].

There are a number of properties of HTS that make them particularly adapted to microwave circuits.

1. **Very low rf losses**

   The rf losses of HTS have been shown to be around an order of magnitude lower than those for conventional conductors (see chapter 3). This has benefits for microwave devices such as filters, oscillators and resonators where low insertion losses and high quality factors are needed.

2. **Wide signal bandwidth**

   The non-dispersive property of HTS means that they can theoretically be used over an infinite bandwidth. Rf components such as mixers can be used to

process signals as high as THz [1.8]. In such application areas HTS can sometimes be the only way to implement the required function.

3. **Low power consumption**

With the high bandwidths that can be utilized with HTS a possible application might be high speed digital circuits [1.9]. Normal conductors generate high amounts of heat which presents a problem when trying to reduce the size of circuits. With superconductors there is an opportunity to make use of very small, high density digital structures and use them for high speed interconnects.

For the microwave communications field, HTS thin film technology developments have been critical [1.10]. They have made possible the design and fabrication of stripline family devices where HTS films are deposited onto low loss substrates [1.4]. Devices made in this way, such as filters and resonators, have demonstrated advantages in terms of lower noise, surface resistance, power losses, dispersion, weight and space requirements [1.8, 1.11]. Such advantages are particularly relevant to devices used in satellites where very small signals may be received and the cost of launching can be $20,000 per kilogram [1.12].

This thesis contains details of investigations into high temperature superconducting microwave devices and the characterization of the HTS films from which they are made.

The remaining part of this chapter begins with a glossary of superconductivity terms. This is followed by a discussion of the microwave theory of normal and superconductors. The chapter goes on to list the main types of HTS compounds that have been discovered and how they are synthesized and deposited onto substrates. It ends with a review of the low power applications of HTS.

Chapter 2 is a critical review of the different methods available to measure the surface resistance of HTS films. Descriptions of the various methods have been given and their various advantages and disadvantages.

Chapter 3 gives the results of surface resistance measurements made by the parallel plate resonator, end wall replacement, microstrip resonator, partial end wall replacement and dielectric resonator techniques. The results are compared and contrasted against each other and other films made in the world.

Chapter 4 focuses upon HTS microwave applications describing the different devices that have been fabricated. Detail is given as to their performance and how this improves upon conventional normal conductor technology.

Chapter 5 describes the different devices that have been made in Oxford. The performance of these devices show that by using HTS there are considerable advantages to be gained especially in terms of high performance in a small package.

Chapter 6 concludes this thesis with a review of the research demonstrating the value of HTS devices to satellite and mobile communications.

1.1 Superconductor Basics

This section will review some superconductor terminology as well as reviewing the particular characteristics that define a superconductor and its behaviour. This will form a basis of understanding for the following chapters.

1.1.1 The Superconducting Transition Temperature

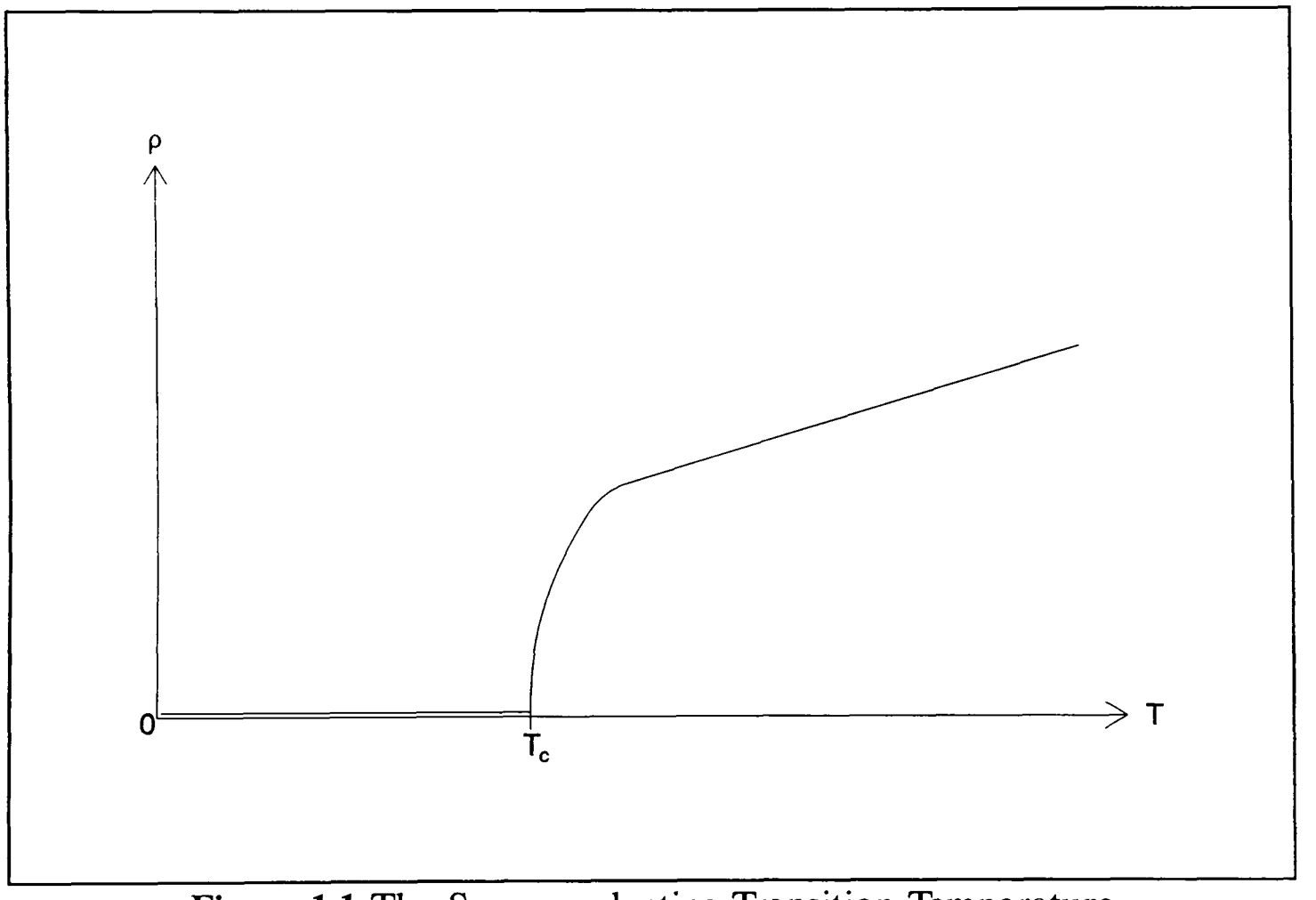

Figure 1.1 The Superconducting Transition Temperature

In 1911, Heike Kamerlingh Onnes discovered that when mercury was cooled its dc resistivity dropped sharply at about 4 K and when cooled further it exhibited no resistivity at all [1.13]. This new state was called the "superconducting state". Later,

other metals and alloys were also found to exhibit similar behaviour and the temperature at which the material lost all resistance was called the superconducting transition temperature or critical temperature (T_c). Fig. 1.1 illustrates the behaviour. The transition to the superconducting state is found to be sharp when the material is pure. For instance, a good gallium specimen may have a transition range of as small as 10^{-5} K, but as impurities are introduced the transition is broadened due to the disturbance in the crystal structure [1.14].

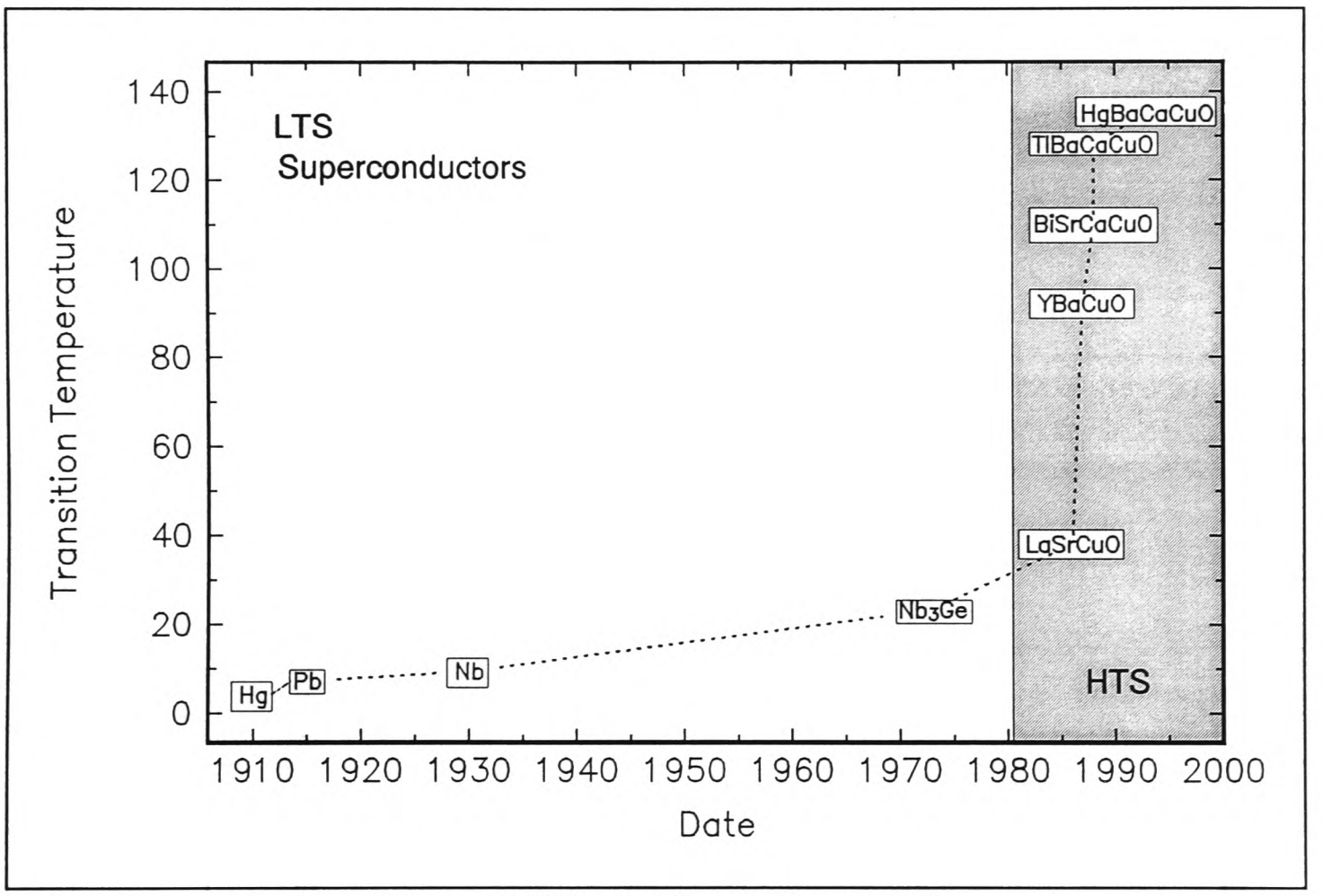

Figure 1.2 T_c vs Time [after 1.15]

For 75 years after Onnes' discovery the highest T_c recorded was still only 23.3 K for Nb_3Ge [1.16]. In 1986 though, two IBM researchers, Bednorz and Müller, discovered superconductivity as high as 30 K in the Ba-La-Cu-O system [1.17]. From this point onwards superconductors were classified into two types: low temperature

superconductors (LTS) and the new high temperature superconductors (HTS) that had cuprate structures. Fig 1.2 shows the progress to date in increasing the T_c for HTS.

1.1.2 The Meissner Effect

In 1933, Meissner and Ochsenfeld discovered that a metal in the superconducting state expels a magnetic flux from its interior [1.18]. This property has important thermodynamic implications. Consider a superconductor that is cooled in zero magnetic field (Fig. 1.3). Not surprisingly, the flux density in the material remains at

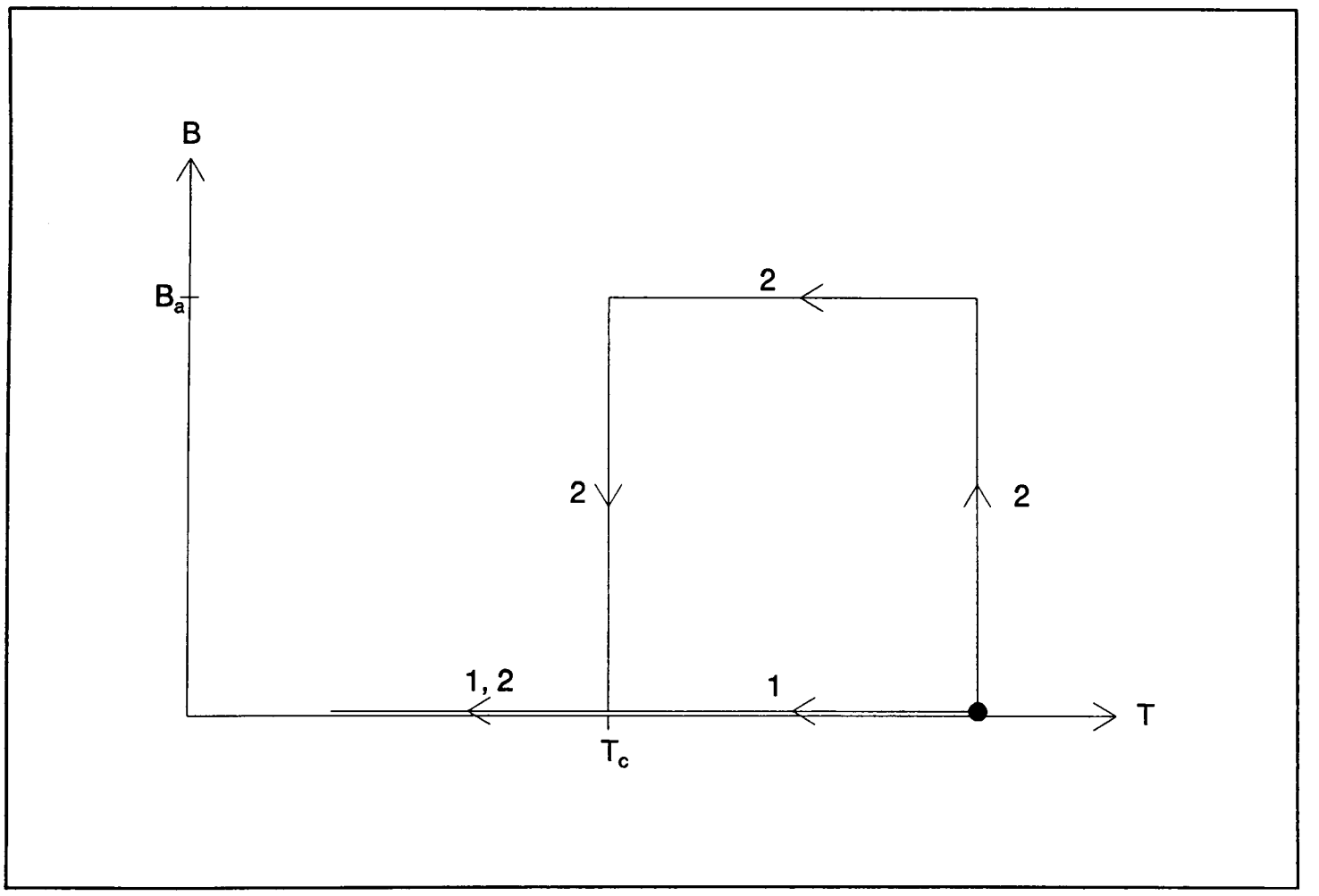

Figure 1.3 Superconductor Interior Flux Density vs Temperature

zero (line 1). However, if a field, B_a, is applied at $T > T_c$ the flux density in the material also takes this value. When the superconductor is cooled, at T_c the flux is expelled and the flux density drops abruptly to zero (curve 2). This is called (with injustice to Ochsenfeld) the Meissner effect.

This behaviour can be contrasted with that for a perfect conductor (Fig. 1.4). Once again when cooled in zero field the flux density in the material remains at zero. If B_a is applied and then the material is cooled the behaviour is different. The flux

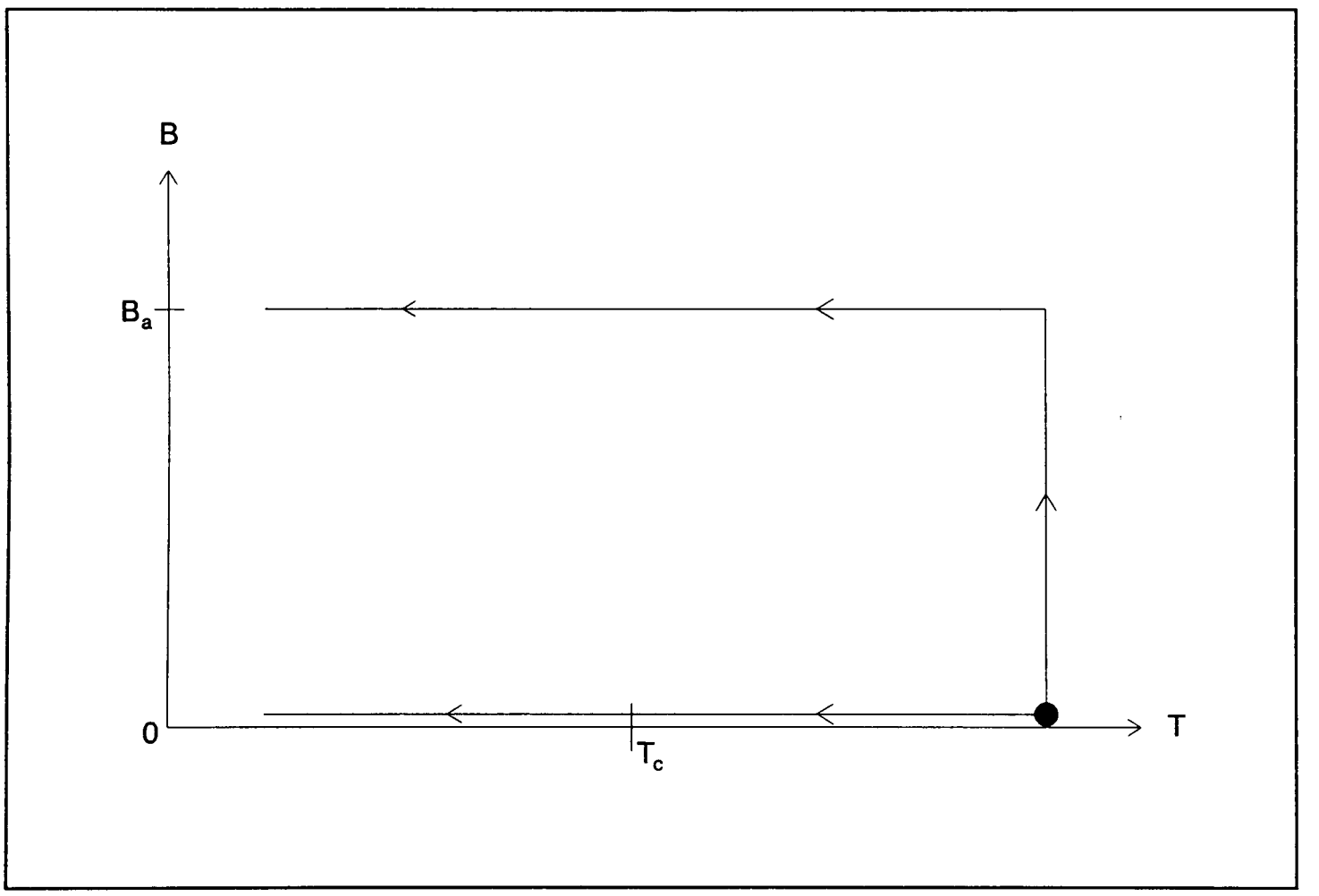

Figure 1.4 Perfect Conductor Interior Flux Density vs Temperature

density in the material remains at B_a *even if the applied field is removed.*

For the superconductor the magnetization depends only on the actual value of applied field and temperature, not on the way they were arrived at. The final state is path *independent* and so a superconductor is in thermodynamic equilibrium [1.19].

On the other hand, the state of magnetization of a perfect conductor depends on the order in which the final conditions of applied magnetic field and temperature were obtained. The final state is path *dependent* and so a perfect conductor cannot be in thermodynamic equilibrium.

1.1.3 The Critical Current Density

A superconductor loses its superconducting property and becomes "normal" if the current density in it exceeds its critical current density (J_c). Much of the fundamental research into HTS has centred upon trying to increase the value of J_c as most applications require high current densities, usually more than 10^4 - 10^5 Acm^{-2}. [1.20].

1.1.4 The Critical Magnetic Field

Superconductivity can also be destroyed if the superconductor lies in too strong a magnetic field. The value of magnetic field at which superconductivity is destroyed is called the critical magnetic field (H_c). However, for many years people working on superconductors had noticed strange effects regarding H_c, but usually put them down to experimental error or impurities in the superconductor. In actual fact, they were

dealing with the inherent properties of a new class of superconductor now known as type II superconductors. For applications the most important difference between type I and II behaviour is shown in Fig. 1.5.

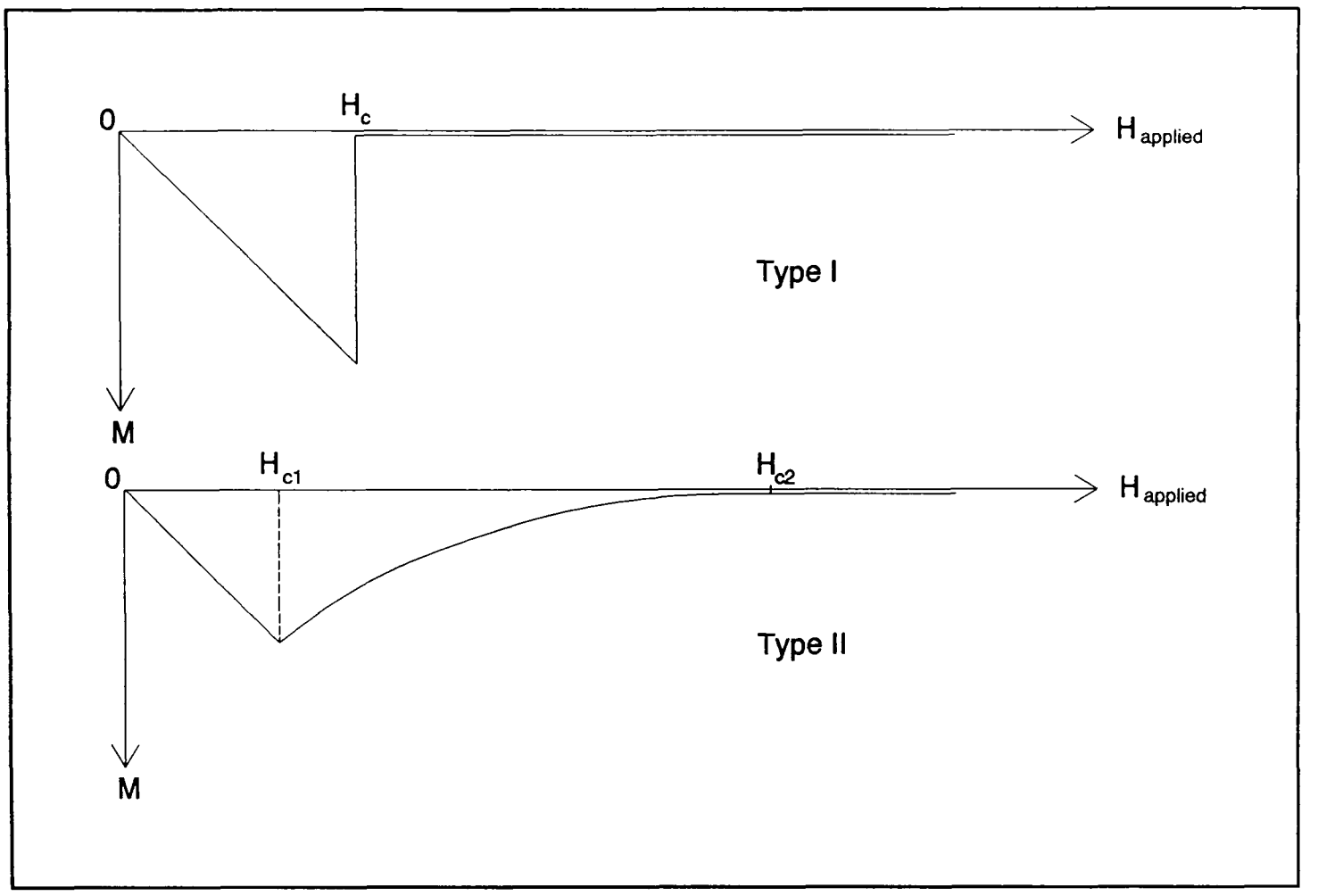

Figure 1.5 Magnetization vs Field for Type I and II Superconductors

The type II superconductor has two critical magnetic fields (H_{c1} and H_{c2}). Up to H_{c1}, the type II behaves exactly as a type I, with magnetization increasing linearly with applied field. However, beyond H_{c1}, the type II goes into the "*mixed state*" [1.21]. As all high temperature superconductors are type II the existence of H_{c2} for high field applications is very useful. A typical value of H_{c2} maybe be in the region of 80-180 T [1.22].

In the mixed state a type II superconductor is penetrated by normal cores. Therefore, we have a structure similar to that shown in Fig. 1.6. The normal cores are

surrounded by circulating shielding currents (to protect the bulk of the superconductor from going normal) and we have (as for a type I) a current flowing on the surface of the superconductor.

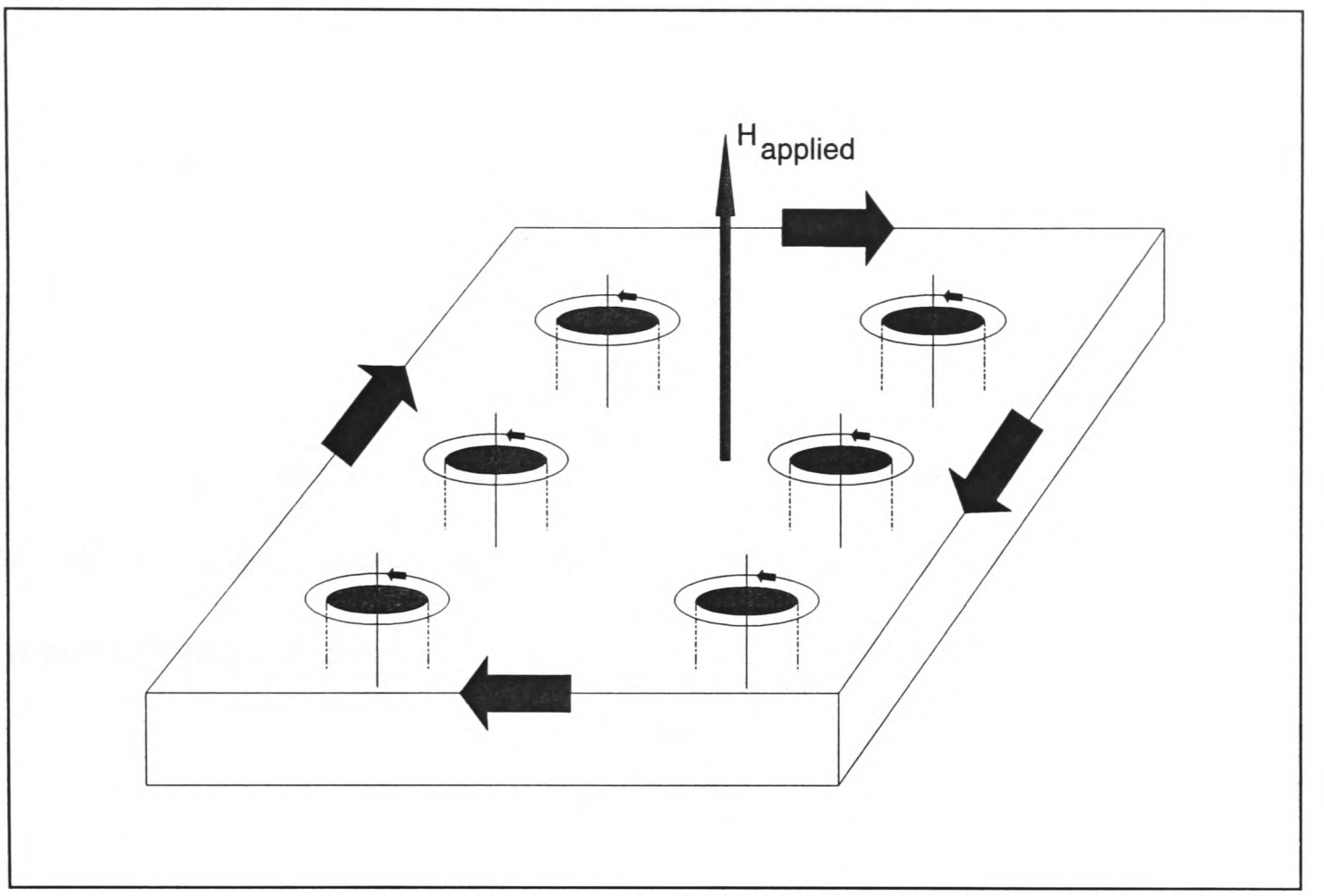

Figure 1.6 The Mixed State

1.1.5 The London Theory

This is a phenomenological theory based upon the assumption that there are two classes of electron: normal and super. The theory does not explain why or how superconductivity occurs, but it does include the Meissner effect [1.23]. Considering the superelectrons, the current density is given by:

$$\underline{J}_S = n_S q \underline{v}_S \tag{1.1}$$

where: n_S = Superelectron number density

q = Charge on the superelectron

$\underline{v}_S$ = Superelectron velocity

But we also have the momentum equation:

$$m\dot{\underline{v}}_S = q\underline{E} \tag{1.2}$$

where: m = Mass of the superelectron

$\underline{E}$ = Electric field

and a dot is used to indicate differentiation with respect to time.

Putting (1.1) in (1.2) gives:

$$\dot{\underline{J}}_S = \frac{n_S q^2}{m}\underline{E} \tag{1.3}$$

Maxwell's equations are now used:

$$\dot{\underline{B}} = -\underline{\nabla} \times \underline{E} \tag{1.4}$$

$$\underline{\nabla} \times \underline{H} = \underline{J} + \dot{\underline{D}}$$

where: $\underline{B}$ = Magnetic flux density

$\underline{H}$ = Magnetic field

$\underline{D}$ = Displacement charge per unit volume

If we assume that the superconductor is non-magnetic (μ_r=1) like other non-ferromagnetic materials and if the fields are varying slowly. That is:

$$\dot{\underline{D}} \ll \underline{J}$$

we obtain (since $\underline{\mathbf{B}} = \mu_o \underline{\mathbf{H}}$):

$$\underline{\nabla} \times \underline{\dot{B}} = \mu_o \underline{J}_S \tag{1.5}$$

where: μ_o = Absolute permeability of free space

Putting (1.3) in (1.4):

$$\underline{\dot{B}} = -\frac{m}{n_S q^2} \underline{\nabla} \times \underline{\dot{J}}_S \tag{1.6}$$

Putting (1.5) in (1.6):

$$\underline{\dot{B}} = -\frac{m}{\mu_o n_S q^2} \underline{\nabla} \times \underline{\nabla} \times \underline{\dot{B}}$$

For convenience (the reason for this is shown later) let:

$$\lambda_L^2 = \frac{m}{\mu_o n_S q^2} \tag{1.7}$$

$$\Rightarrow \quad \underline{\dot{B}} = -\lambda_L^2 \underline{\nabla} \times \underline{\nabla} \times \underline{\dot{B}} \tag{1.8}$$

But we also have the identity:

$$\underline{\nabla} \times \underline{\nabla} \times \underline{\dot{B}} = \underline{\nabla}(\underline{\nabla}.\underline{\dot{B}}) - \nabla^2 \underline{\dot{B}} \tag{1.9}$$

and Maxwell's equation:

$$\underline{\nabla}.\underline{\dot{B}} = \underline{\mathbf{0}} \tag{1.10}$$

Putting (1.9) and (1.10) in (1.8) gives:

$$\dot{\underline{B}} = \lambda_L^2 \nabla^2 \dot{\underline{B}}$$

This has the solution (if taken as a one dimensional problem):

$$\dot{B}(x) = \dot{B}_a e^{-x/\lambda_L} \tag{1.11}$$

where: B_a = Applied magnetic flux density in the z-direction

x = Distance into the superconductor

However:

$$B(0) = B_a \tag{1.12}$$

Therefore, if we integrate (1.11) the constant of integration is zero giving:

$$B(x) = B_a e^{-x/\lambda_L}$$

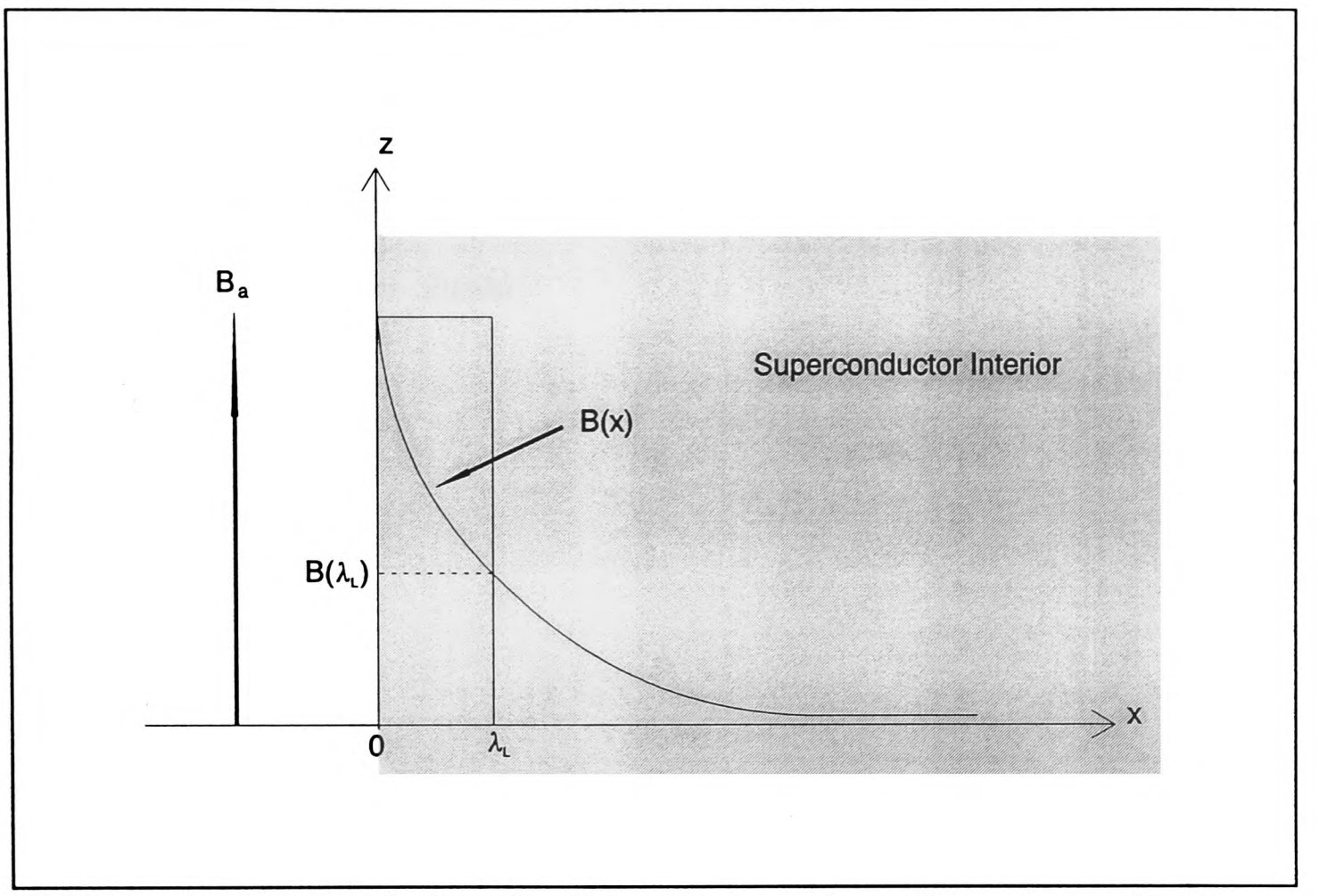

Figure 1.7 Magnetic flux density at the boundary of a superconductor

Fig. 1.7 shows the situation. The distance λ_L is called the London penetration depth and indicates the depth below the surface of the superconductor at which the flux density is 1/e of its value at the surface. For simplification's sake it is often considered that B_a penetrates into the superconductor a distance λ_L after which the flux density drops to zero, since there are equal area under the curves. Using (1.7) and (1.6) we obtain:

$$\underline{\boldsymbol{B}} = -\frac{m}{n_S e^2}\underline{\nabla} \times \underline{\boldsymbol{J}}_S = -\mu_o \lambda_L^2 \underline{\nabla} \times \underline{\boldsymbol{J}}_S \qquad (1.13)$$

and (1.3):

$$\underline{\dot{J}}_S = \frac{n_S e^2}{m}\underline{E} = \frac{1}{\mu_o \lambda_L^2}\underline{E}$$

These two equations have come to be known as the London equations [1.23]. The presence of screening currents is shown as follows. Taking (1.5) and noting that $\underline{\mathbf{B}}$ is in the z-direction only we obtain:

$$\underline{\nabla} \times \underline{B} = \mu_o \underline{J}_s$$

$$\Rightarrow \quad -\frac{\partial B_z}{\partial x} = \mu_o J_y$$

$$J_y = \frac{B_a}{\mu_o \lambda_L} e^{-x/\lambda_L}$$

$$or \qquad J_y = J_a e^{-x/\lambda_L}$$

That is we may consider that a screening current J_a flows on the surface of a superconductor within a depth λ_L, just as we may assume that the magnetic flux penetrates to the same depth.

1.2 Microwave Theory

One of the most important criteria for the design and performance of microwave devices is the surface resistance, R_s [1.24]. A low surface resistance will give low losses and so make a device more efficient. The following shows how R_s is derived for normal and superconductors.

Consider a normal conductor. We have the Maxwell's equation [1.25]:

$$\underline{\nabla} \times \underline{E} = -\dot{\underline{B}}$$

Taking the curl:

$$\underline{\nabla} \times \underline{\nabla} \times \underline{E} = \underline{\nabla}(\underline{\nabla}.\underline{E}) - \nabla^2\underline{E} = -(\underline{\nabla} \times \dot{\underline{B}})$$

Substituting:

$$\underline{B} = \mu\underline{H}$$

and:

$$\underline{\nabla} \times \underline{H} = \underline{J} + \dot{\underline{D}}$$

gives:

$$\underline{\nabla}(\underline{\nabla}.\underline{E}) - \nabla^2\underline{E} = -\mu(\dot{\underline{J}} + \ddot{\underline{D}}) \qquad (1.14)$$

But $\underline{\mathbf{J}}=\sigma\underline{\mathbf{E}}$ and $\underline{\mathbf{D}}=\epsilon\underline{\mathbf{E}}$ which gives:

$$\underline{\nabla}(\underline{\nabla}.\underline{E}) - \nabla^2\underline{E} = -\mu\sigma\dot{\underline{E}} - \mu\epsilon\ddot{\underline{E}}$$

For no free space charge in the volume considered:

$$\underline{\nabla}.\underline{E} = 0$$

$$\Rightarrow \quad \nabla^2\underline{E} = \mu\sigma\dot{\underline{E}} + \mu\epsilon\ddot{\underline{E}} \qquad (1.15)$$

If $\underline{\mathbf{E}}$ is varying slowly enough the second term on the right hand side can be ignored giving:

$$\nabla^2\underline{E} = \mu\sigma\dot{\underline{E}}$$

and if we have a one dimensional variation:

$$\underline{\boldsymbol{E}} = \underline{\boldsymbol{E}}_o e^{-j(\omega t - kz)}$$

we have:

$$\nabla^2\underline{\boldsymbol{E}} + j\omega\mu\sigma\underline{\boldsymbol{E}} = \nabla^2\underline{\boldsymbol{E}} + \left(\frac{2j}{\delta^2}\right)\underline{\boldsymbol{E}} = \underline{\mathbf{0}}$$

where $\delta=\sqrt{(2/\omega\mu\sigma)}$ and is defined as the skin depth. This has the solution:

$$\underline{\boldsymbol{E}} = \underline{\boldsymbol{E}}(0)e^{-\left(\frac{z}{\delta}\right)(1-j)} \tag{1.16}$$

Where $\underline{\mathbf{E}}(0)$=[surface field at z=0]. The definition of R_s is given by the definition of surface impedance:

$$Z_s = \frac{\underline{\boldsymbol{E}}(0)}{\int_0^\infty \underline{\boldsymbol{J}}(x,y,z)\times\underline{\boldsymbol{dn}}} = \frac{\underline{\boldsymbol{E}}(0)}{\sigma\int_0^\infty \underline{\boldsymbol{E}}\times\underline{\boldsymbol{dn}}} \tag{1.17}$$

where $\underline{\mathbf{dn}}$=differential vector normal to the conductor surface. (1.16) in (1.17) gives:

$$Z_s = \frac{\underline{\boldsymbol{E}}(0)}{\sigma\underline{\boldsymbol{E}}(0)\int_0^\infty e^{-\frac{z}{\delta}(1-j)}dz} = \frac{1-j}{\sigma\delta}$$

or substituting for δ:

$$Z_s = (1-j)\left(\frac{\omega\mu}{2\sigma}\right)^{\frac{1}{2}}$$

The real part of Z_s gives the normal conductor surface resistance:

$$R_s^N = \left(\frac{\omega\mu}{2\sigma}\right)^{\frac{1}{2}} = \frac{1}{\sigma\delta} \tag{1.18}$$

For a superconductor we start from equation (1.14), but include an extra term to allow for the effect of the supercurrent:

$$\underline{\nabla}(\underline{\nabla}.\underline{E}) - \nabla^2\underline{E} = -\mu(\underline{\dot{J}} + \underline{\ddot{D}} + \underline{\dot{J}}_S)$$

Going through a similar derivation as for the normal conductor and remembering the London equation:

$$\underline{\dot{J}}_S = \frac{\underline{E}}{\mu\lambda_L^2}$$

we obtain:

$$\nabla^2\underline{E} = \mu\left(\sigma\underline{\dot{E}} + \epsilon\underline{\ddot{E}} + \frac{\underline{E}}{\mu\lambda_L^2}\right) \tag{1.19}$$

If $\underline{\mathbf{E}}$ is varying slowly this becomes:

$$\nabla^2\underline{E} = \underline{E}\left(\frac{1}{\lambda_L^2} - j\omega\mu\sigma\right)$$

This gives a solution of:

$$\underline{E} = \underline{E}(0)e^{-z\left(\frac{1}{\lambda_L^2} - \frac{2j}{\delta^2}\right)^{\frac{1}{2}}}$$

This is similar to the normal conductor solution except an extra $1/\lambda_L^2$ has been added to the exponent. Therefore, the surface impedance is given by:

$$Z_s^S = \frac{1}{\sigma}\sqrt{\frac{1}{\lambda_L^2} - \frac{2j}{\delta^2}}$$
$$= \frac{1}{\sigma\lambda_L}\left[1 - \frac{2j\lambda_L^2}{\delta^2}\right]^{\frac{1}{2}}$$
$$\approx \frac{1}{\sigma\lambda_L}\left[1 - \frac{j\lambda_L^2}{\delta^2}\right]$$

And remembering $\delta^2=(2/\omega\mu\sigma)$:

$$Z_s^S = \frac{1}{\sigma\lambda_L} - \frac{j\omega\mu\lambda_L}{2}$$

The complex conductivity is given by equation (A.6) (Appendix A):

$$\sigma_{eff} = \frac{1}{\omega\mu\lambda_L^2}\left[\frac{\omega\tau}{4}\left(\frac{n_N}{n_S}\right) - j\right]$$

$$\Rightarrow \quad Z_s^S = \frac{\omega\mu\lambda_L\left[\frac{\omega\tau}{4}\left(\frac{n_N}{n_S}\right) + j\right]}{1 + \frac{\omega^2\tau^2}{16}\left(\frac{n_N}{n_S}\right)^2} - \frac{j\omega\mu\lambda_L}{2}$$

Since $\omega\tau<<1$ and $n_N<<n_S$ when $T<T_c$ we have:

$$Z_s^S = \omega\mu\lambda_L\left[\frac{\omega\tau}{4}\left(\frac{n_N}{n_S}\right) + j\right] - \frac{j\omega\mu\lambda_L}{2}$$

Remembering the normal state conductivity=$\sigma_n=ne^2\tau/m$, $\lambda_L^2=m/\mu n_S q^2$ and $q=2e$ gives:

$$\tau = 4\mu\lambda_L^2\sigma_n\left(\frac{n_S}{n}\right)$$

$$\therefore \quad Z_s^S = \omega^2\mu^2\lambda_L^3\sigma_n\left(\frac{n_N}{n}\right) + j\left[\frac{\omega\mu\lambda_L}{2}\right] \tag{1.20}$$

The real part of Z_s^S gives the superconductor surface resistance and so an inspection of (1.18) and (1.20) reveals that:

$$R_s^N \propto \sqrt{\omega} \quad and \quad R_s^S \propto \omega^2$$

Table 1.1 lists some practical investigations to assess the f^n dependence (where $f=\omega/2\pi$) for R_s in superconductors. There is good agreement with the theory.

n	Reference
2	[1.26]
1.9±0.5	[1.27]
2	[1.28]
2.06±0.14	[1.29]
2.0±0.1	[1.30]

Table 1.1 f^n Summary

Therefore, there will be a crossover frequency, f_c, below which the superconducting surface resistance is lower than the normal surface resistance. This is illustrated in Fig. 1.8.

The value of f_c depends on the HTS used but a typical value may be 100 GHz [1.31] at the operating temperature of the HTS used. Below this frequency the lower R_s of superconductors presents lower losses than a normal conductor [1.32]. This is because

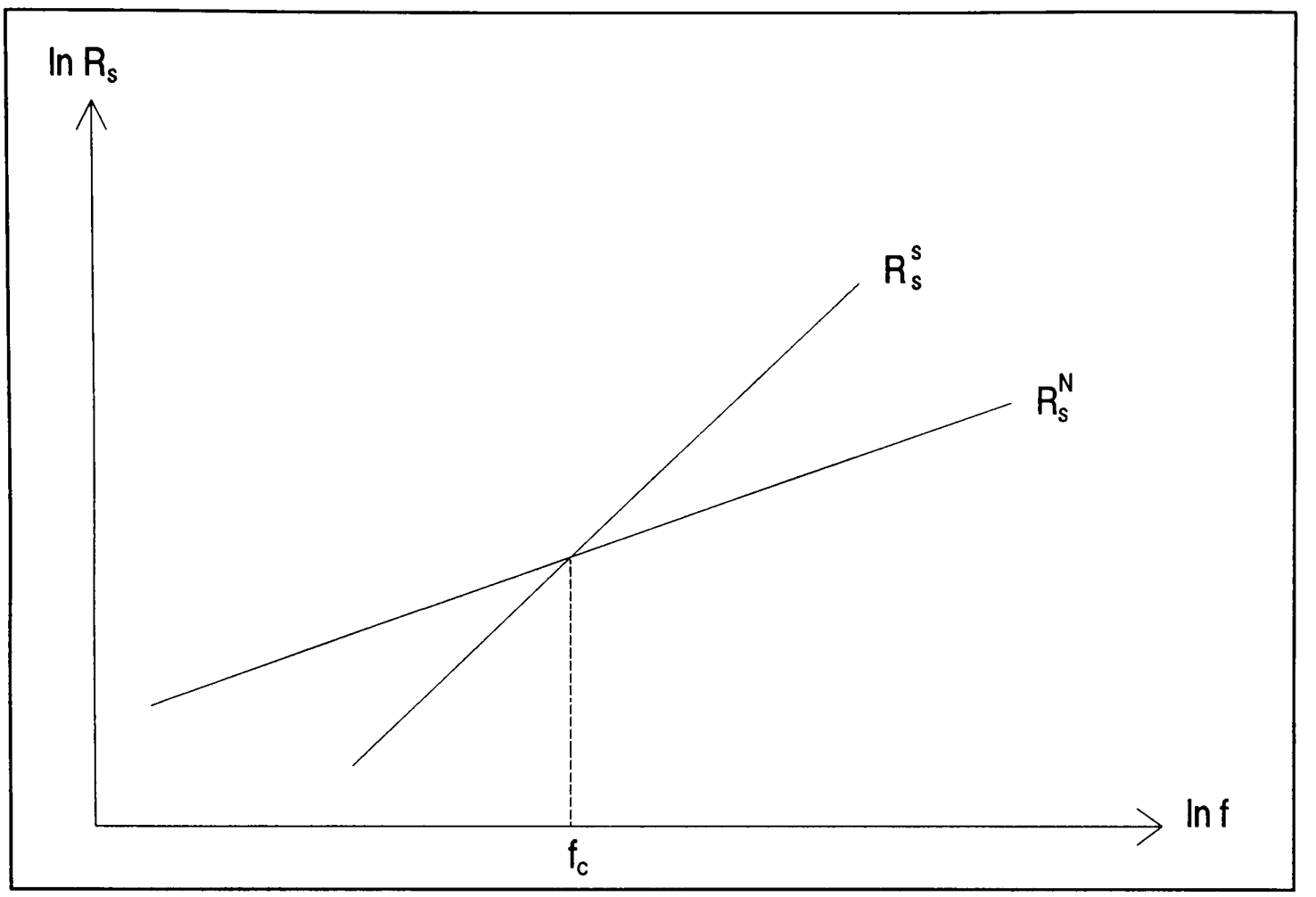

Figure 1.8 Comparison of Normal and Superconducting Surface Resistance

power losses are related to R_s by [1.33]:

$$P_{loss} = \frac{R_s}{2}\int H^2 \, da$$

Let us next consider dispersion in a normal conductor. Returning to equation (1.15) and assuming a one dimensional time varying solution:

$$\underline{\boldsymbol{E}} = \underline{\boldsymbol{E}}_o e^{-j(\omega t - kz)}$$

we have:

$$-k^2 = -j\omega\mu\sigma - \omega^2\mu\epsilon$$

The group and phase velocities are given by:

$$V_g = \frac{\partial \omega}{\partial k} \quad and \quad V_p = \frac{\omega}{k} \qquad (1.21a \text{ and } 1.21b)$$

respectively. It is clear that V_g does not equal V_p and so a normal conductor is dispersive.

Now consider a superconductor. We have equation (1.19) which gives:

$$-k^2 = \frac{1}{\lambda_L^2} - j\omega\mu\sigma - \omega^2\mu\epsilon$$

Substitute the expression for the complex conductivity, equation (A.6) (Appendix A):

$$k^2 = \omega^2\mu\epsilon + \frac{j\omega\mu}{\omega\mu\lambda_L^2}\left[\frac{\omega\tau}{4}\left(\frac{n_N}{n_S}\right) - j\right] - \frac{1}{\lambda_L^2}$$

$$\Rightarrow \quad k^2 = \omega^2\mu\epsilon + \frac{j\omega\tau}{4\lambda_L^2}\left(\frac{n_N}{n_S}\right)$$

$$But \quad \tau = \frac{m\sigma_n}{ne^2} \quad and \quad \lambda_L^2 = \frac{m}{\mu n_S q^2} = \frac{m}{4\mu n_S e^2}$$

$$\Rightarrow \quad k^2 = \mu\epsilon\omega^2 + j\omega\mu\sigma_n\left(\frac{n_N}{n}\right)$$

For a superconductor below about $0.5T_c$:

$$\frac{n_N}{n} \approx 0$$

$$\Rightarrow \quad k^2 = \mu\epsilon\omega^2 \qquad (1.22)$$

From (1.21a) and (1.21b) we find with (1.22) that the group velocity and the phase velocity are equal to:

$$V_g = V_p = \frac{1}{\sqrt{\mu\epsilon}}$$

Hence a superconductor is non-dispersive.

Experimentally, Takemoto et al [1.34] have found "*the attenuation of Y-Ba-Cu-O film on a MgO substrate is approximately 31% lower than gold films at 6.6 GHz and 33% lower at 19.2 GHz for temperatures below 50 K*". Ekholm and McKnight [1.8] have shown that "*YBCO has an attenuation three orders of magnitude better than copper at 10 GHz and maintains a significant advantage to over 100 GHz*" and less distortion in a transmission line.

So, it has been shown that superconductors have less surface resistance than normal conductors below typically 100 GHz, lower attenuation and less dispersion. These factors explain why superconductors are so useful for microwave applications. The low R_s gives less power loss. Low attenuation again gives low power losses along transmission lines leading to more efficient operation. Finally, the low dispersion characteristic suggests that superconductors can be used at higher frequencies than conventional conductors such as copper or gold, perhaps even as high as THz [1.8].

However, superconductors have their disadvantages as well as advantages. The first problem is the need for cooling. The superior performance is only achieved at around liquid nitrogen (<77 K) temperatures for HTS. Secondly, materials manufacturing technology needs to be developed significantly so that consistent quality HTS can be

produced. Thirdly, as explained earlier (section 1.1.4) magnetic fields can destroy superconductivity. Even if low fields are applied they can affect the performance of a device and this may be critical if operating points in a microwave circuit have already been set, although some [1.35] have used field dependence to tune a microwave device in a predictable way. Table 1.2 summarizes the advantages and disadvantages of using HTS for microwave devices.

Advantages	Disadvantages
Lower R_s than conventional materials up to 100 GHz. Lower attenuation. Low dispersion.	HTS require cooling. Materials fabrication techniques need perfecting. Magnetic fields affect performance.

Table 1.2 Advantages and Disadvantages of HTS

1.3 HTS Compounds

There are a number of HTS compounds. This section will compare some of them outlining the advantages and disadvantages of each of them. It will not provide a comprehensive review. Any crystalline material consists of unit cells and those of HTS can be simplified as being rectangular blocks. The typical dimension for the a and b axes is ~3.8 Å and ~30 Å for the c axis [1.36]. Several of these blocks can be lined up together and layered as shown in Fig. 1.9 as a thin film. When there is perfect alignment of these blocks we have perfect epitaxy. However, this is rarely the case and irregularities in the structure cause the R_s of the superconductor to depend

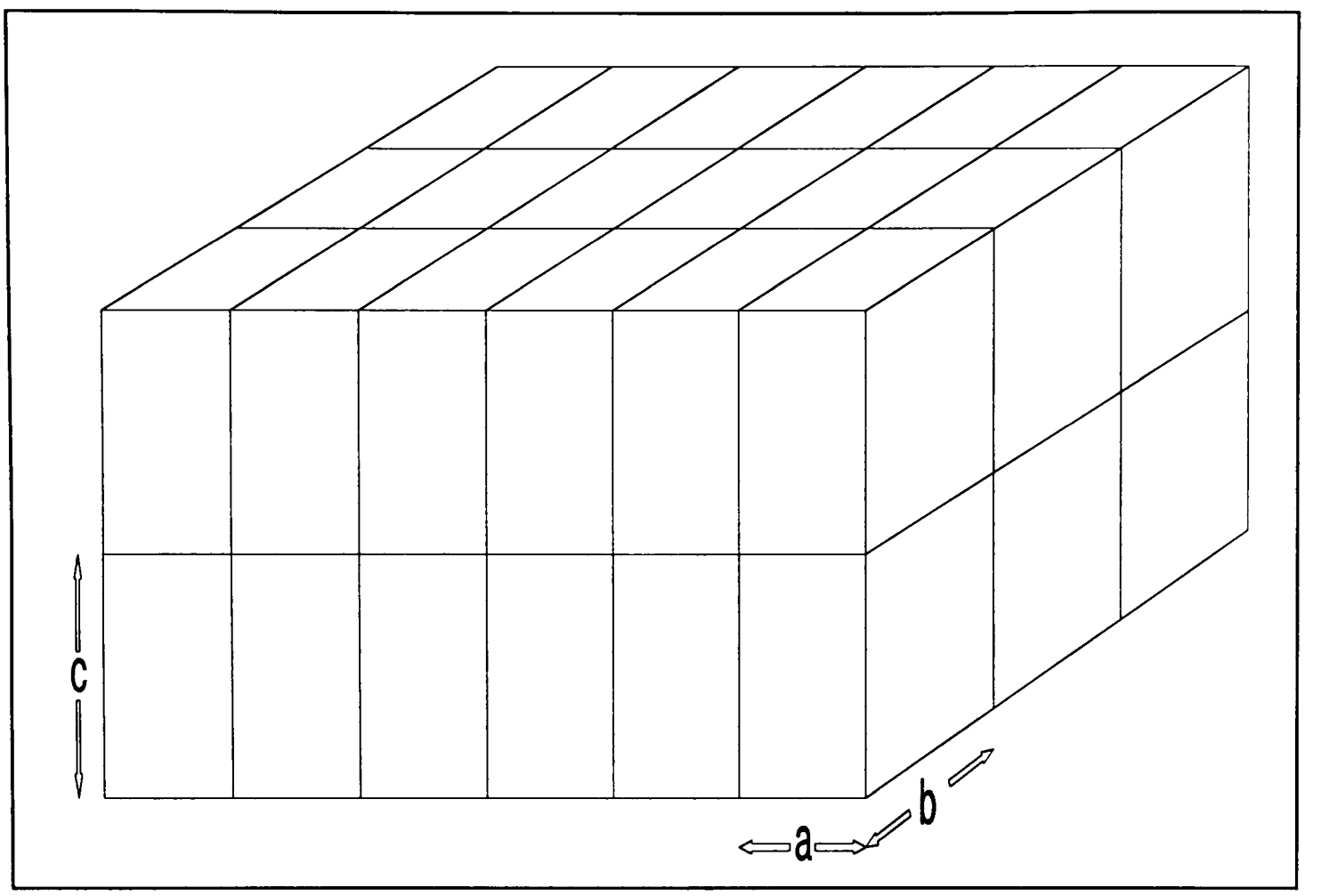

Figure 1.9 Superconductor Unit Cells

on thickness. It has been found [1.37] that the optimum thickness for a thin film is in the region 0.4-1.0 μm. Thinner than this results in the supercurrent exceeding the J_c and thicker than this results in a large amount of disorder in the atomic structure which again increases the R_s.

Table 1.3 reviews some HTS compounds that have been investigated for use in microwave applications.

Compound	Phase	T_c	Reference
YBaCuO (YBCO)	123	93	[1.22]
ErBaCuO (EBCO)	123	92	[1.38]
GdBaCuO (GBCO)	123	92	[1.36]
HgBaCaCuO (HBCCO)	1223	147	[1.39]
BiSrCaCuO (BSCCO)	2212 2223	85 110	[1.40] [1.40]
TlBaCaCuO (TBCCO)	2201 2212 2223	80 110 128	[1.41] [1.42] [1.42]

Table 1.3 HTS Compounds, Phases and T_cs

Key: Y=Yttrium, Er=Erbium, Gd=Gadolinium, Bi=Bismuth, Tl=Thallium, Ba=Barium, Sr=Strontium, Hg=Mercury, Ca=Calcium, Cu=Copper.

A short form is often used for the compounds and phases. For example, $Y_1Ba_2Cu_3O_x$ is repesented by YBCO 123. The BSCCO compound has been found to exhibit very high R_s values [1.43] and is therefore not suitable for microwave applications. HBCCO has the highest T_c, but the compound requires high pressures to form it and so it has not been possible to manufacture it in large areas which would make it of practical use. Specifically, due to the difficult nature of fabrication no R_s values have been published. The other compounds, however, have all demonstrated R_s values of less than 300 $\mu\Omega$ at 10 GHz and 77K [1.36, 1,38, 1.44]. YBCO has been used extensively for making microwave devices [1.45, 1.46], but has a number of disadvantages in terms of its longevity. It has been shown to degrade on exposure to air, CO_2, O_2 and N_2 after periods as short as 16 hours due to a change from a

superconducting to a non-superconducting phase [1.47]. It is also well known that it becomes non-superconducting when exposed to water [1.48]. TBCCO has perhaps the best qualities in terms of R_s, T_c and the ability to be laid down as a thin film. Its R_s has regularly been measured lower than 150 $\mu\Omega$ at 10 GHz and 77K in thin films [1.30] and T_cs routinely exceed 110K [1.42]. These benefits need to be weighed against the small dangers present in dealing with a compound that contains the toxic element thallium.

1.4 Deposition of HTS Thin Films

For thin film deposition there are four main techniques used:

1) Sputtering

2) Laser Ablation

3) Electron-Beam Evaporation (EBE)

4) Chemical Vapour Deposition (CVD)

Sputtering is, perhaps, the crudest method of laying down thin films. It involves abrasing atoms from a target by an inert gas in a dc or rf plasma [1.49]. The substrate is used as an anode and the abrased atoms are deposited onto it. There are problems with sputtering, however. It is difficult to control the stoichiometry of the deposited film. It is dependent upon the composition of the target and the amount of re-sputtering that occurs. These both have important implications for the phase(s) deposited onto the substrate. It has been found [1.4] that a large amount of trial and error is required to find the right target composition so that correct sputtering is

achieved. Advantages of sputtering are its low cost, which is much less then laser ablation and EBE as these require high energy sources [1.50, 1.51] and its ability to deposit large areas of film in excess of 20 cm^2. For laser ablation or EBE the maximum is about one cm^2. This advantage is particularly important for applications of thin films, for instance, microwave systems where a whole circuit could be placed onto a substrate instead of just a filter, say.

Laser ablation creates a plasma, like sputtering, above the substrate within which congruent transport of the elemental species occurs [1.26]. The stoichiometry of the film exactly replicates that of the target used. This makes the process easy to set up, repeat and for a large number of consistent films to be produced in a short time. Only small areas of film can be produced and the technique has the problem of target degradation caused by the laser pitting the target. This can be somewhat overcome by scanning the laser across the surface of the target.

EBE evaporates different target elements onto a substrate's surface. The beams striking each of the targets have to be carefully controlled so that the correct surface stoichiometry is achieved. This is probably the simplest way to deposit films but is very costly due to the difficulty of continuously monitoring the different chemicals used.

In CVD, volatile precursors of the elements required to make the film are passed through a reaction chamber with the substrate and heated over a period of time. The

decomposition of the elements produces the deposition required. This technique shares the problem of sputtering - selection of the correct elements. They must have the right volatility and decomposition temperatures. Just as in sputtering where the composition of the target is crucial.

Two problems that all HTS materials suffer from are weak links and flux flow. Producing single crystal HTS as a thin film on large substrates has proved very difficult and the more usual result is a granular structure [1.52]. If the grains in this structure are too far apart or not aligned correctly then J_c for the superconductor can be drastically affected [1.53]. This is because the inter-grain material is not superconducting and so any supercurrent carried across the gap will be by Josephson tunnelling [1.54]. The supercurrent density across such a junction is given by:

$$J_s = J_c \sin d$$

where: d = Phase difference across the Josephson junction.

and:

$$J_c = \frac{\pi \Delta}{2eR_{NN}}$$

where: Δ = Superconductor energy gap

e = Charge on the electron

R_{NN} = Resistance across the Josephson junction when the superconductor either side of it is in the normal state.

So it can be seen that the higher R_{NN} is (i.e. a very bad impurity) the lower J_c and J_s will be. Hence, weak links cause J_c to be lower then we may want it to be.

The second problem of flux flow becomes apparent when a magnetic field is applied to a superconductor. Providing the applied magnetic field is kept low enough the vortices found in the mixed state are "pinned" in place and do not move. This allows the supercurrent to pass around the vortices. However, when the field is increased, sufficient Lorentz force is generated on each vortex that the pinning force is overcome and they start to flow perpendicular to the supercurrent. This is called "flux flow". The supercurrent's progress is now impeded and there is a loss of superconductivity. Therefore, it is desirable that an HTS has high pinning forces.

1.5 Low Power HTS Applications

HTS superconducting quantum interference devices (SQUIDs) have been used for some time to measure very small magnetic fields in medical patients. They offer the advantage that they can track activity within the body without the need for surgical techniques so making diagnosis cheaper, faster and less painful [1.2]. Typical heart signal levels that can be detected are as small as 10-100 pT peak-to-peak.

Another application of a SQUID is as part of an accelerometer. Mechanical movements can be converted into magnetic signals which are then measured by the SQUID. Very small signals can be measured for vehicular, space and seismological applications [1.55].

Superconductor Josephson junctions have been suggested for use in high speed digital switching and for sensitive detecting or mixing of microwave signals [1.56]. Within the same field of electronics flux flow transistors can be made by using one or several microbridges in which nucleation and motion of high velocity flux vortices can be controlled by a magnetic field generated by a current circulating in a nearby control line, hence controlling a larger current [1.57]. However, early results for these have produced very disappointing current gains of no more than 20.

More promising has been the use of HTS thin films for passive microwave devices. Thin films of HTS are deposited onto substrates. The films are then patterned appropriately to produce different devices such resonators, filters and correlators [1.4, 1.58, 1.59]. Such devices will be reviewed further in chapter 4 demonstrating their value to satellite [1.60, 1.61] and mobile communications.

1.6 Conclusions

This chapter has reviewed the most important superconductor terminology. This has been followed by a discussion of the microwave theory for normal and superconductors. This has shown that HTS has a lower R_s and lower dispersion than normal conductors. It has also described the various HTS compounds that have been discovered outlining their advantages and disadvantages. The chapter has finished with a review of the low power applications of HTS.

1.7 References

[1.1] Bashkirov Y.A. et al (1993) "Design and characterization of a high-T_c superconducting shielded-core transformer". In Freyhardt H.C. (ed.) *Applied Superconductivity 1993 Volume 2*. Germany: DGM Informationsgesellschaft mbH: 919-922.

[1.2] Ter Brake H.J.M. et al (1995) "Operating high-T_c SQUIDs for a multichannel heart scanner in an unshielded environment". In Blank D.H.A. (ed.) *Proceedings of the 2nd Workshop on HTS Applications and New Materials*. Enschede, Netherlands: University of Twente: 154-158.

[1.3] Kale K.S. et al (1996) "TBCCO thin films and passive microwave devices", in In U. Balachandran (ed.) *Proceedings of the TMS Symposium*. Warrendale PA: TMS, in press.

[1.4] Morley S.M. et al (1993) "Synthesis and microwave characterization of DC sputtered Tl-Ba-Ca-Cu-O thin films". *IEEE Transactions on Applied Superconductivity* 3(1): 1753-1756.

[1.5] Du Pont Superconductivity (1993) "25 ns low-loss delay line". *Technical Data Sheet*. Delaware, USA: Du Pont Superconductivity.

[1.6] Khanna A.P.S. et al (1991) "A superconducting resonator stabilized low phase noise oscillator" *Microwave Journal* 34: 127-130.

[1.7] Ashworth S.P. et al (1993) "The technical and economic feasibility of high temperature superconducting power transmission cables". In Freyhardt H.C. (ed.) *Applied Superconductivity 1993 Volume 2*. Germany: DGM Informationsgesellschaft mbH: 879-886.

[1.8] Ekholm E.B., McKnight S.W. (1990) "Attenuation and dispersion for high-T_c superconducting microstrip lines". *IEEE Transactions on Microwave Theory and Techniques* 38(4): 387-395.

[1.9] Mukhanov O.A. (1993) "RSFQ 1024-bit shift register for accusation memory". *IEEE Transactions on Applied Superconductivity* 3(4): 3102-3113.

[1.10] Klein N. et al (1992) "Microwave surface resistance of epitaxial $YBa_2Cu_3O_7$ thin films at 18.7 GHz measured by a dielectric resonator technique". *Journal of Superconductivity* 5(2): 195-201.

[1.11] Schmidt M.S. et al (1991) "Measured performance at 77K of superconducting microstrip resonators and filters". *IEEE Transactions on Microwave theory and Techniques* 39(9): 1475-1479.

[1.12] Williamson M. (1994) "The growth of microsats". *IEE Review* 40(3): 117-120.

[1.13] Onnes H.K. (1911) "The resistance of pure mercury at helium temperatures". *Leiden Comm.*

[1.14] Rose-Innes A.C., Rhoderick E.H. (1969) *Introduction to Superconductivity*, 1st ed. Oxford: Pergamon Press.

[1.15] Dew-Hughes D. (1993) "Superconductivity: Materials and Devices". Lecture Proceedings, Oxford University.

[1.16] Gavaler J.R. (1973) "Superconductivity in Nb-Ge films above 22K". *Applied Physics Letters* 23(8): 480-482.

[1.17] Bednorz J.G., Müller K.A. (1986) "Possible high T_c superconductivity in the Ba-La-Cu-O system". *Zeitschrift für Physik* B64: 189-193.

[1.18] Meissner, Ochsenfeld (1933) *Naturw* 21: 787.

[1.19] Gorter C.J., Casimir H. (1934) "On supraconductivity I". *Physica* 1: 306-320.

[1.20] Ekin J.W. et al (1987) "Evidence for weak link and anisotropy limitations on the transport critical current in bulk polycrystalline $Y_1Ba_2Cu_3O_x$". *Journal of Applied Physics* 62(2): 4821-4828.

[1.21] Abrikosov A.A. (1957) "On the magnetic properties of superconductors of the second group". *Soviet Physics Journal of Experimental and Theoretical Physics* 5(6): 1174-1182.

[1.22] Wu M.K. et al (1987) "Superconductivity at 93K in a new mixed-phase Y-Ba-Cu-O compound system at ambient pressure". *Physical Review Letters* 58(9): 908-910.

[1.23] London F., London H. (1935) "The electromagnetic equations of the supraconductor". *Proceedings of the Royal Society* A149: 71-88.

[1.24] Klopman B.B.G. et al (1993) "The propagation characteristics of wave-guiding structures with very thin superconductors; application to coplanar waveguide $YBa_2Ba_3O_{7-x}$ resonators". *IEEE Transactions on Microwave Theory and Techniques* 41(5): 781-791.

[1.25] Howatson A.M. et al (1990) *Engineering Tables and Data*, 5th ed. London: Chapman and Hall.

[1.26] Chang L.D. et al (1989) "Microwave surface resistance in Tl-based superconducting thin films". *Applied Physics Letters* 55(13): 1357-1359.

[1.27] Martens J.S. et al (1991) "Confocal resonators for measuring the surface resistance of high-temperature superconducting films". *Applied Physics Letters* 58(22): 2543-2545.

[1.28] Delayen J.R. et al (1990) "Measurements of the surface resistance of high-T_c superconductors at high RF fields". *Journal of Superconductivity* 3(3): 243-250.

[1.29] Cooke D.W. et al (1990) "Frequency dependence of the surface resistance in high-temperature superconductors". *Solid State Communications* 73(4): 297-300.

[1.30] Holstein W.L. et al (1993) "Surface resistance of large-area $Tl_2Ba_2CaCu_2O_8$ thin films at microwave and millimeter wave frequencies measured by three noncavity techniques". *Journal of Superconductivity* 6(3): 191-200.

[1.31] Wilker C. et al (1991) "5 GHz high-temperature-superconductor resonators with high Q and low power dependence up to 90K". *IEEE Transactions on Microwave Theory and Techniques* 39(9): 1462-1467.

[1.32] Halbritter J. (1974) "On surface resistance of superconductors". *Zeitschrift für Physik* 266: 209-217.

[1.33] Rubin D.L. et al (1988) "Observation of a narrow superconducting transition at 6 GHz in crystals of $YBa_2Cu_3O_7$". *Physical Review B* 38(10): 6538-6542.

[1.34] Takemoto J.H. et al (1989) "Microstrip ring resonator technique for measuring microwave attenuation in high-T_c superconducting thin films". *IEEE Transactions on Microwave Theory and Techniques* 37(10): 1650-1652.

[1.35] Porjesz T. et al (1993) "Magnetic field controlled superconducting microwave microstrip resonators". *Applied Superconductivity* 1(10-12): 1707-1713.

[1.36] Jenkins A.P. (1994) *Microwave Applications of High Temperature Superconductors*. Unpublished D.Phil. thesis, University of Oxford.

[1.37] Kuhlemann T., Hinken J.H. (1991) "Measurements of the thickness dependence of the surface resistance of laser ablated HTS thin films". *IEEE Transactions on Magnetics* 27(2): 872-875.

[1.38] Takemoto J.H. et al (1991) "Microstrip resonators using two sided metalorganic chemical vapour deposited $\epsilon\nu$-Ba-Cu-O thin films". *Applied Physics Letters* 58(10): 1109-1111.

[1.39] Chu C.W. et al (1993) "Superconductivity above 150K in $HgBa_2Ca_2Cu_3O_{8+\delta}$ at high pressures". *Nature* 365(6444): 323-325.

[1.40] Chu C.W. et al (1988) "Superconductivity up to 114K in the Bi-Al-Ca-Sr-Cu-O compound system without rare earth elements". *Physical Review Letters* 60(10): 941-943.

[1.41] Sheng Z.Z. et al (1988) "Superconductivity at 90K in the Tl-Ba-Ca-Cu-O system". *Physical Review Letters* 60(10): 937-940.

[1.42] Parkin S.S.B. et al (1988) "Tl-Ba-Ca-Cu-O: a new class of crystal structures exhibiting volume superconductivity at up to $\simeq$ 110K". *Physical Review Letters* 61(6): 751-753.

[1.43] Hammer A., Srinivasan G. (1990) "High frequency losses in BSCCO superconductors". *Superconductor Science and Technology* 3: 306-308.

[1.44] Klein N. et al (1989) "Millimetre wave surface resistance of epitaxially grown YBCO thin films". *Applied Physics Letters* 54(8): 757-759.

[1.45] Talisa S.H. et al (1991) "Low- and high-temperature superconducting microwave filters". *IEEE Transactions on Microwave Theory and Techniques* 39(9): 1448-1454.

[1.46] Zhang D. et al (1991) "Quasi-optical millimeter-wave band-pass filters using high-T_c superconductors". *IEEE Transactions on Microwave Theory and Techniques* 39(9): 1493-1497.

[1.47] Russck S.E. (1994) "Surface degradation of YBCO thin films". *Applied Physics Letters* 64(26): 3649-3651.

[1.48] Wada O. et al (1990) "Transmission electron microscopy study of the environmental degradation in $Ba_2YCu_3O_{7-y}$". *Journal of Applied Physics* 68(10): 5283-5288.

[1.49] Gao J. et al (1990) "High critical current density ultrathin $YBa_2Cu_3O_x$ films made by a modified rf-magnetron sputtering technique". *Journal of Apllied Physics* 67(5): 2512-2515.

[1.50] Char K. et al (1990) "Microwave surface resistance of epitaxial $YBa_2Cu_3O_7$ thin films on sapphire". *Applied Physics Letters* 57(4): 409-411.

[1.51] Chaudhari P. et al (1987) "Critical-current measurements in epitaxial films of $YBa_2Cu_3O_{7-x}$ compound". *Physical Review Letters* 58(25): 2684-2686.

[1.52] Yam P. (1993) "Trends in Superconductivity: current events". *Scientific American* 269(6): 84-93.

[1.53] Goldfarb R.B. et al (1987) "Evidence for two superconducting components on oxygen-annealed single phase Y-Ba-Cu-O". *Cryogenics* 27(9): 475-480.

[1.54] Josephson B.D. (1962) "Possible new effects in superconductive tunnelling". *Physics Letters* 1(7): 251-253.

[1.55] Vodel W. et al (1995) "Superconducting accelerometers with dc SQUID", In D. Dew-Hughes (ed.) *Applied Superconductivity 1995 Volume 2.* Bristol: IoP Publishing: 1495-1498.

[1.56] Duzer T.V., Turner C.W. (1981) *Principles of Superconductive Devices and Circuits*. New York, NY: Elsevier: 139.

[1.57] Bernstein P. et al (1995) "Vortex dynamics in superconducting flux flow transistors". In D. Dew-Hughes (ed.) *Applied Superconductivity 1995 Volume 2* Bristol: IoP Publishing: 1661-1664.

[1.58] Jenkins A.P. et al (1993) "Novel on-board processing architectures for satellite spread spectrum communications". In *Proceedings of the Third IEE European Conference on Satellite Communications*. London: IEE: 280-283.

[1.59] Jenkins A.P. et al (1995) "Microstrip bandpass filters fabricated from TBCCO thin films on MgO substrates". In D. Dew-Hughes (ed.) *Applied Superconductivity 1995 Volume 2.* Bristol: IoP Publishing: 1187-1190.

[1.60] Clarke A.C. (1945) "V2 for ionosphere research?". *Wireless World* 51(2): 58.

[1.61] Clarke A.C. (1945) "Extra-terrestrial relays: can rocket stations give world-wide radio coverage?". *Wireless World* 51(10): 305-308.

Chapter 2

Surface Resistance Measurement Techniques

The measurement of the ac surface resistance of high temperature superconductor materials is perhaps the most stringent test of their quality, especially for microwave applications. Such measurements give results which are averaged over the entire surface of the HTS sample and include any non-superconducting inclusions that may be present on the sample surface as a result of the processing. For example, pre-cursor elements can react during the processing to form intermediate compounds such as CuO and BaCuO (these are poor conductors) that will contribute to the rf losses in the system. This is in contrast to dc measurements where a best (or percolative) path may be measured that effectively shorts out the rest of the sample. Hence a high T_c or J_c alone may not be indicative of sample quality, if we also consider homogeneity in the quality definition. Indeed, a detailed study by Edwards et al [2.1] revealed that there is little direct correlation between J_c and R_s for thin films. What can be said is that a film with a very high J_c ($\sim 10^6$ Acm^{-2}) will tend to have a low R_s, but we cannot say how low. Hence, we can use R_s measurements as a very sensitive probe into sample quality, especially since most R_s measurement techniques are non-contacting and non-destructive. This is particularly important if we wish to manufacture devices with such films [2.2-2.4].

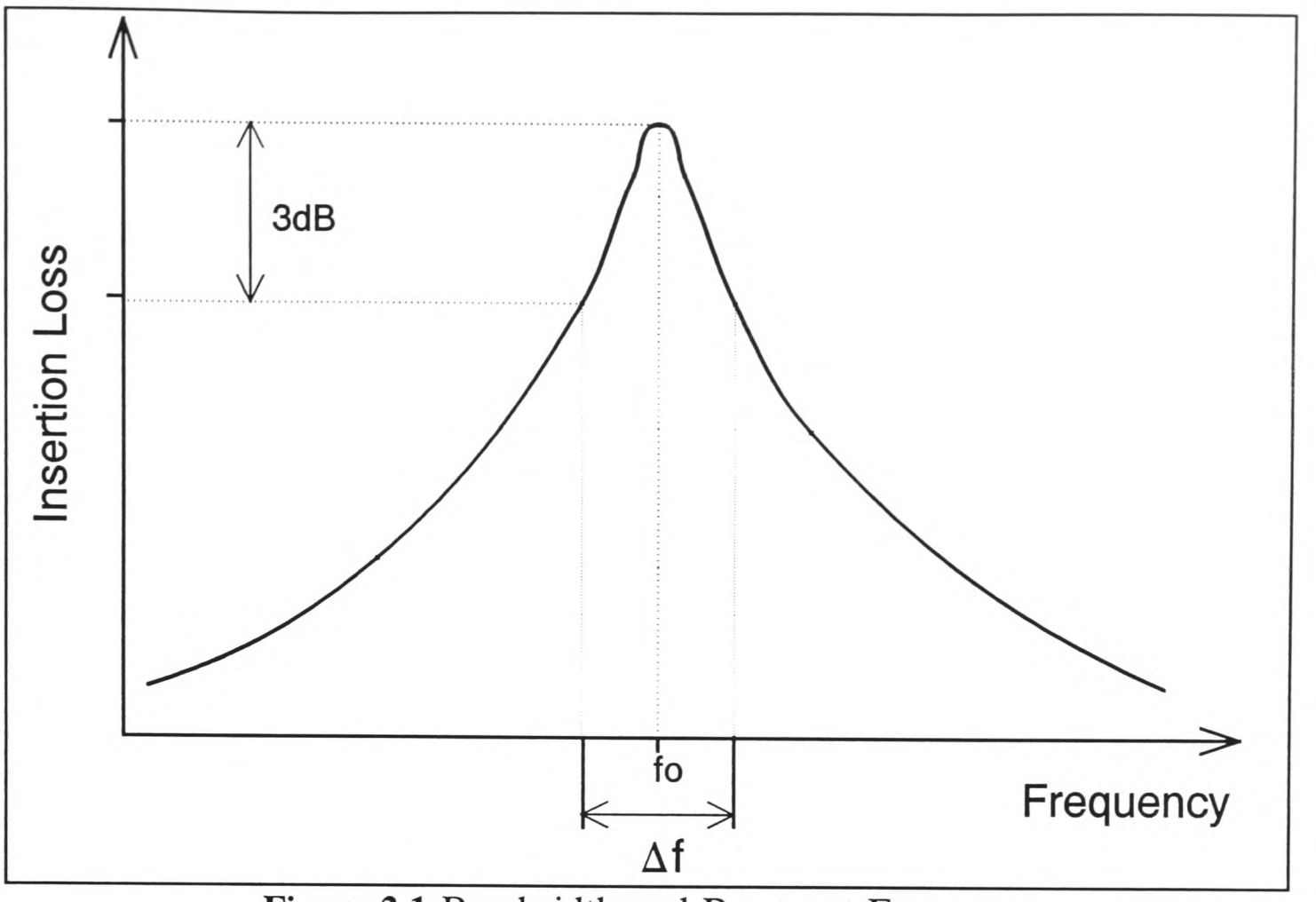

Figure 2.1 Bandwidth and Resonant Frequency

This chapter will present five R_s measurement techniques in detail and some others in lesser detail that have evolved for the testing of HTS films. Most of the techniques employed to determine R_s make use of some form of resonant structure. At resonance, the impedance of a resonator is real and resistive (i.e the reactive parts are zero) and the ohmic losses can be extracted from measuring the quality factor (Q) if we allow for other losses in the system, such as dielectric or radiation losses. A higher Q will indicate a lower R_s. The quality factor is defined as:

$$Q = \omega \frac{\textit{time average stored energy}}{\textit{energy loss per second}} = \frac{f_o}{\Delta f}$$

where f_o is the resonant frequency and Δf is the half power bandwidth (Fig. 2.1.) Finally, R_s can be extracted from the energy losses in the system and a knowledge of the resonator geometry.

2.1 Parallel Plate Resonator

The parallel plate resonator (PPR) R_s measurement technique was developed by Taber [2.5] and can be used to characterize HTS thin films with R_ss as low as 5 $\mu\Omega$ or as high as 1 mΩ [2.5]. Fig. 2.2 shows the arrangement. The resonator is pressed together by a spring mechanism or by a screw placed against one of the substrates.

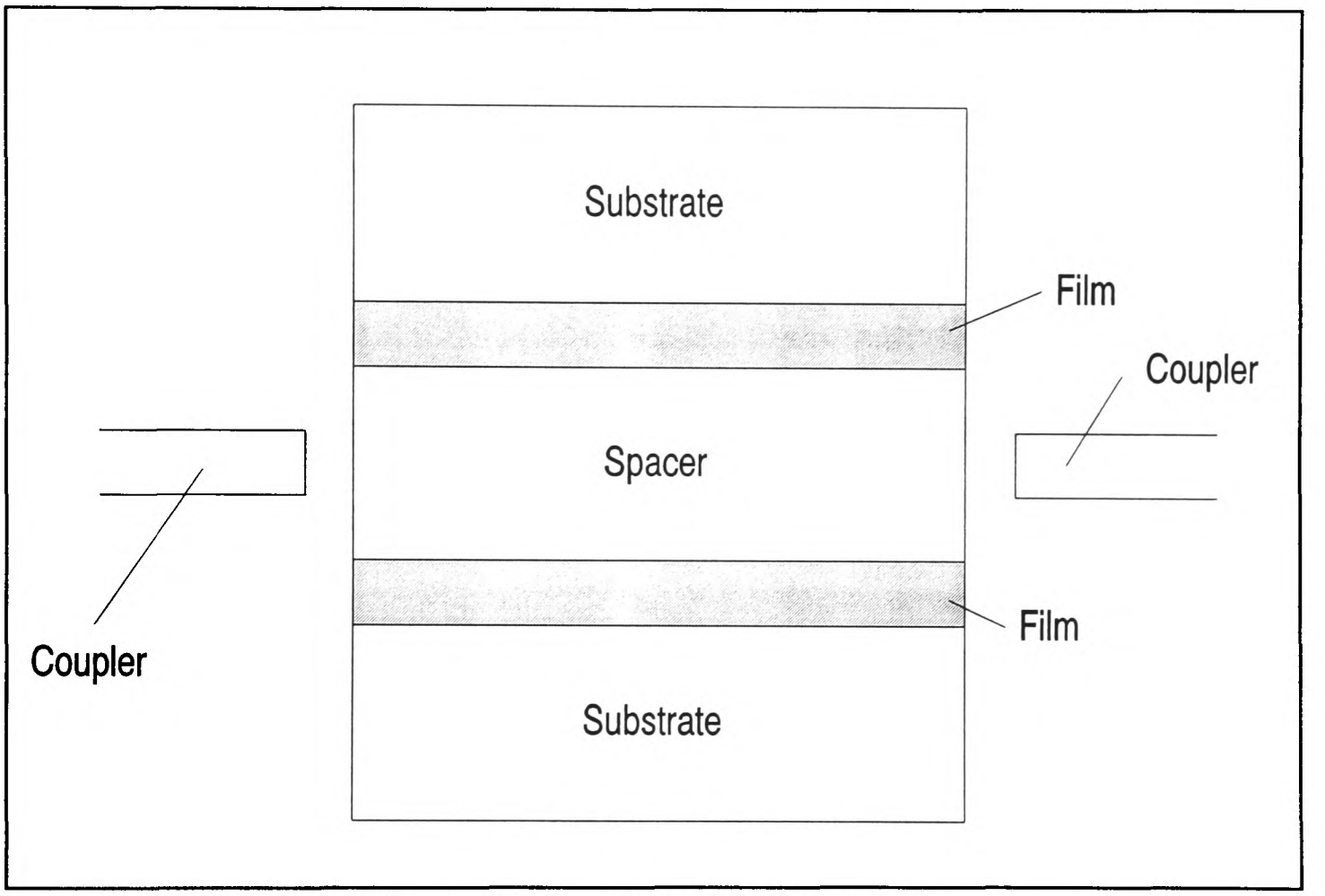

Figure 2.2 Parallel Plate Resonator

It is then placed inside a low surface resistance box (for instance, it may be gold plated). Overall, there will be three loss contributions:

1) dielectric loss in the spacer

2) resistive loss at the superconducting surfaces

3) "radiation" losses at the edges resulting from fringing fields which extend outside the PPR.

Therefore, the surface resistance, R_s is given by [2.5]:

$$\frac{1}{Q} = \tan\delta + \frac{R_s}{\pi \mu_o f s} + \alpha s \qquad (2.1)$$

where: Q=unloaded quality factor

tan δ=loss tangent of the spacer

R_s=average surface resistance of films

μ_o=absolute permeability of free space

f=resonant frequency

s=spacer thickness

α=geometrical constant

Taber [2.5] suggests that if s is of the order of 10 μm then αs becomes small enough to be ignored (however, no evidence of this is given). A more acceptable assumption is that tan δ can be ignored if low loss materials are used (for instance, sapphire which has a tan δ of approximately 10^{-7} at 77 K). Given these assumptions equation (2.1) can be re-written:

$$R_s = \frac{\pi \mu_o f s}{Q}$$

The simplicity of the coupling arrangement can be problematic when measuring R_s values above 1-2 mΩ. This is because the Q value drops correspondingly and so bandwidths are difficult to measure. One way to combat this problem would be to increase the spacing, s. However, as mentioned before (and as shown by equation (2.1)) this will increase the contribution of the αs term and Taber does not go into a sufficient degree of detail to determine how important this really is. Another

problem that may occur is poor coupling to a film that does not go right to the edge of the substrate. This will reduce the Q value giving a higher R_s value than the true value. This problem can also occur if only the edge of the film is poor. Table 2.1 summarizes the advantages and disadvantages.

Advantages	Disadvantages
Very good sensitivity (5 $\mu\Omega$ at 10 GHz) Simple to set up No calibration required	Coupling problems Cursory consideration of radiation losses

Table 2.1 Advantages and Disadvantages of the PPR.

2.2 End Wall Replacement

This is the most well known method of measuring R_s [2.6, 2.7]. One end wall of a cylindrical cavity is replaced with, firstly, a material made from the same material as the rest of the cavity and secondly with HTS. Q and frequency measurements are taken at each stage and from these and geometrical factors the R_s of the superconductor can be found. Fig. 2.3 shows the arrangement.

For a cylindrical cavity manufactured entirely from copper, the relation between Q and R_s is equation (B.65) (Appendix B):

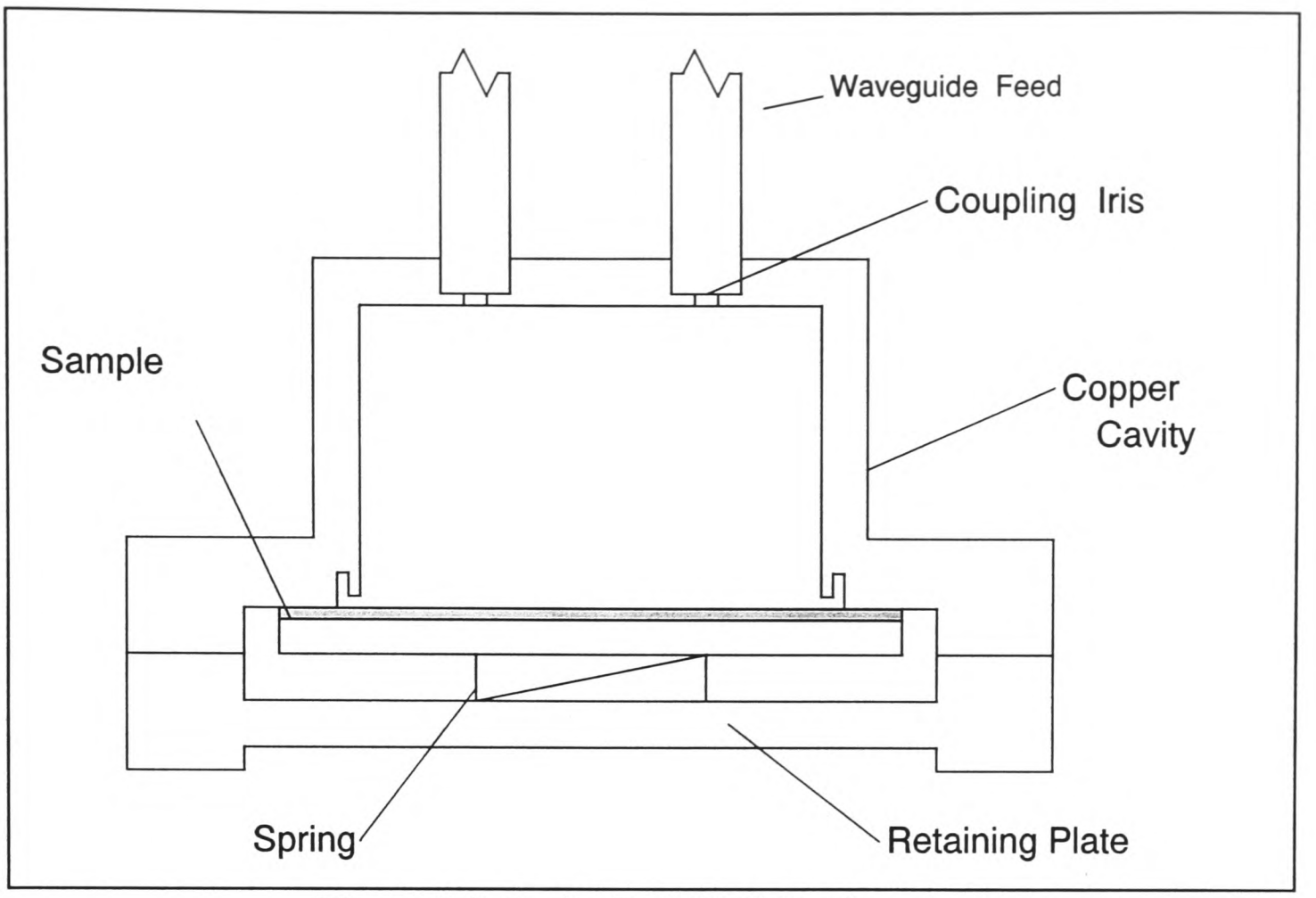

Figure 2.3 Cavity End Wall Replacement

$$Q_{cu} = \sqrt{\frac{\mu_o}{\epsilon_o}} \quad \frac{\left[R_{11}^2 + \left(\frac{\pi a}{d}\right)^2\right]^{\frac{3}{2}}}{2R_{cu}\left[R_{11}^2 + 2\pi^2\left(\frac{a}{d}\right)^3\right]} \tag{2.2}$$

where: a=radius of cavity

d=length of cavity

R_{11}=first root of Bessel function, J_1

R_{cu}=surface resistance of copper

The contribution from one end wall can be separated from the overall Q using the following expression (equation (B.68) (Appendix B)):

$$R_{sc} = R_{cu} - \left[\frac{1}{Q_{cu}} - \frac{1}{Q_{sc}}\right] \frac{F}{2\pi^2 \left(\frac{a}{d}\right)^3} \qquad (2.3)$$

where: R_{sc} = surface resistance of HTS sample

Q_{sc} = measured Q of cavity with HTS sample end wall

$$F = \sqrt{\frac{\mu_o}{\epsilon_o}} \left[R_{11}^2 + \left(\frac{\pi a}{d}\right)^2 \right]^{\frac{3}{2}}$$

Hence measuring Q_{cu} will enable a value for R_{cu} to be derived. Then measuring Q_{sc} and using the previous result a value for the surface resistance of the sample (R_{sc}) can be calculated.

2.3 Partial End Wall Replacement

Essentially, the partial end wall replacement (PEWR) technique involves replacing the central area of an end plate on a cylindrical cavity with the HTS sample to be tested (Fig. 2.4). It thus allows samples that are smaller than the cavity diameter to be measured. The penalty for this is a reduction in sensitivity, a result of the fact that a smaller percentage of the total cavity area has been replaced when compared to complete end wall replacement. However, a larger cavity will allow a lower operating frequency. This is particularly relevant if we consider that most research samples of material that are produced are typically on 10 mm x 10 mm substrates, which would require a cavity operating at frequencies above 50 GHz. Use of the PEWR technique would allow testing of such samples at frequencies between 30-40 GHz, simplifying

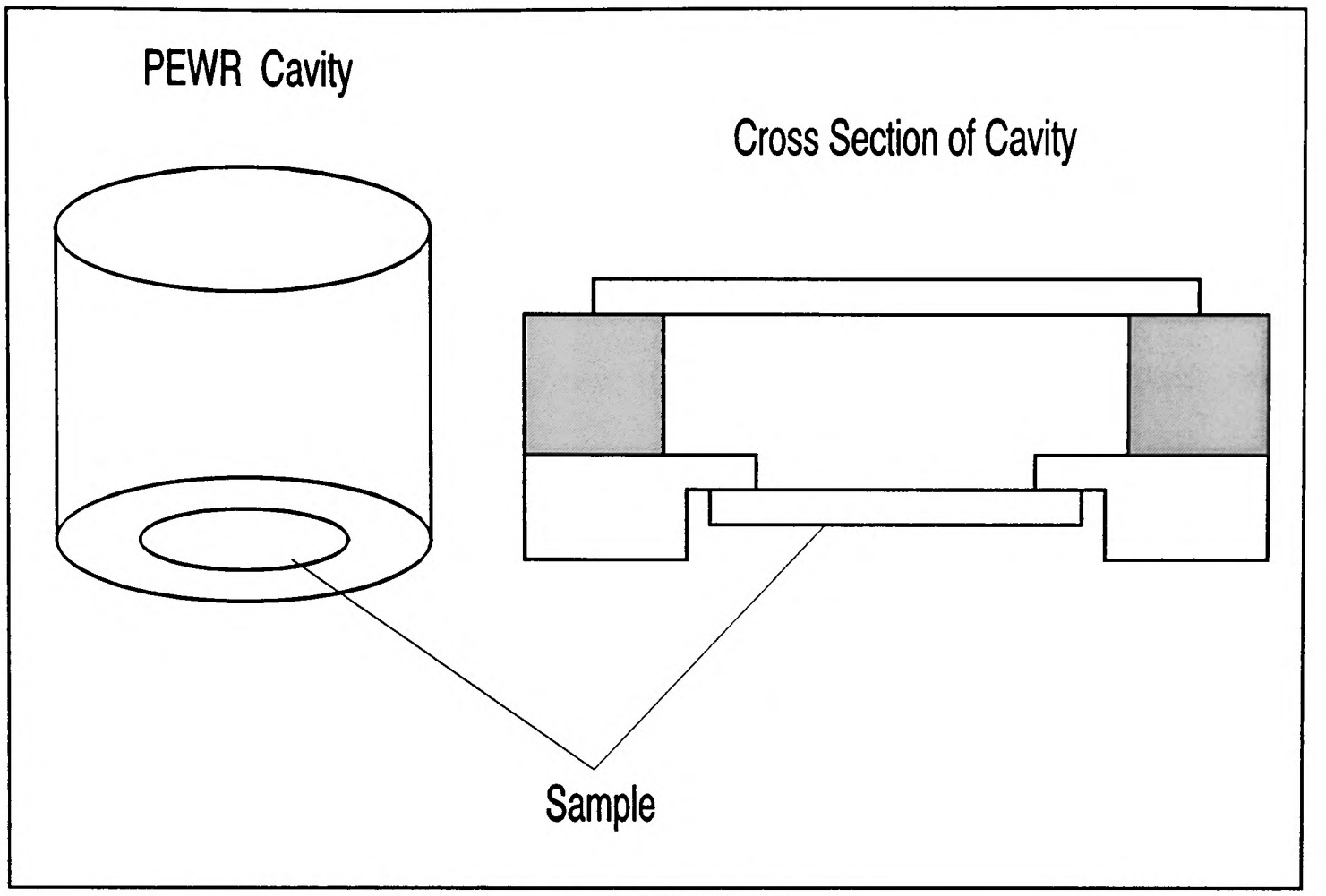

Figure 2.4 PEWR Cavity

the process.

The equations that relate R_s and measured Q values for the PEWR cavity make use of the standard solution for a cylindrical cavity operating in the TE_{011} mode [2.8]. The final result for the superconducting R_s is [2.8]:

$$R_{sc} = R_{cu}\left[1 + \frac{2Q_{cu}[(R_{11})^2 + D]}{DG}\left(\frac{a}{b}\right)^2\left[\frac{1}{Q_{sc}} - \frac{1}{Q_{cu}}\right]\right] \qquad (2.4)$$

where R_{cu} is given by the same expression as for complete end wall replacement:

$$R_{cu} = \sqrt{\frac{\mu_o}{\epsilon_o}} \quad \frac{\left[R_{11}^2 + \left(\frac{\pi a}{d}\right)^2\right]^{\frac{3}{2}}}{2Q_{cu}\left[R_{11}^2 + 2\pi^2\left(\frac{a}{d}\right)^3\right]} \tag{2.5}$$

and

$$D = 2\pi^2\left(\frac{a}{d}\right)^3 \tag{2.6}$$

$$G = \frac{1}{J_0^2(pa)}\left[J_1^2(pb) + J_0^2(pb) - \frac{2J_0(pb)J_1(pb)}{pb}\right] \tag{2.7}$$

$$p = \left[\left(\frac{\omega}{c}\right)^2 - \left(\frac{\pi}{d}\right)^2\right]^{\frac{1}{2}} \tag{2.8}$$

a=cavity radius

b=iris radius

c=speed of light in free space

d=cavity length

The operation of the PEWR cavity is essentially the same as the end wall replacement type. One noticeable difference is that the ring in the end wall (against which the sample is placed) also acts as a mode trap, simplifying the design of the cavity. In addition, the iris against which the sample is placed must be concentric with the circular cavity.

2.4 Microstrip Resonator

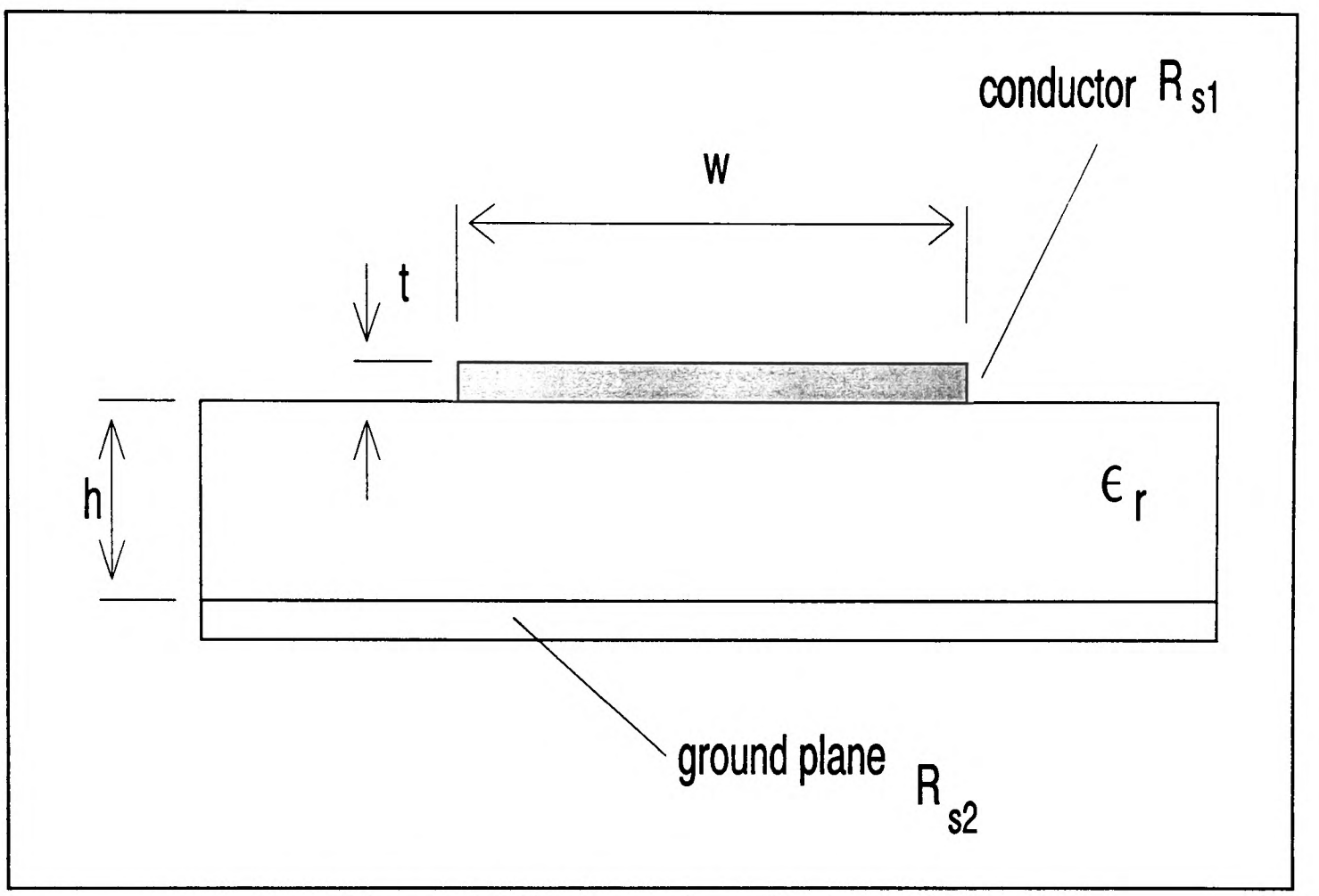

Figure 2.5 Cross section of microstrip.

As the end purpose for a film on a substrate may be a stripline-like device the use of a technique that measures the R_s after the film has been patterned is useful. Such a technique would allow for the measurement of R_s after the patterning of the device and so would be able to say whether the film had been significantly degraded by the patterning process. The microstrip resonator is such a technique. The theory has been developed by Jenkins [2.9]. Fig. 2.5 shows a diagram of a typical microstrip structure.

R_{s1} and R_{s2} refer to the surface resistances of the upper conductor and ground plane respectively. Assuming the case that the ground plane and the upper conductor are

not made of the same material (for instance, the ground plane may be copper and the upper conductor HTS) the surface resistance of the HTS is given by [2.9]:

$$R_{s1} = \frac{64h^3 w_c Z_o \pi^3}{\lambda_g \left(16h^2 - w_c^2\right)(B + 2A)} \left[\frac{1}{Q_{sc}} - \frac{C}{Q_a}\right] \tag{2.9}$$

where:

$$w_c = \frac{t}{\pi}\left[\ln\left(\frac{2h}{t}\right) + 1\right] + w$$

$$Z_o = \frac{120\pi}{\sqrt{\epsilon_{eff}}\left[\frac{w}{h} + 1.393 + 0.667\ln\left(\frac{w}{h} + 1.44\right)\right]}$$

$$\epsilon_{eff} = \frac{\epsilon_r + 1}{2} + \frac{\epsilon_r - 1}{2}\left[1 + \frac{12h}{w}\right]^{-\frac{1}{2}}$$

$$\lambda_g = \frac{c}{f\sqrt{\epsilon_{eff}}}$$

$$A = h\left[\pi + \ln\left(\frac{2h}{t}\right)\right]$$

$$B = \left(w_c\pi - t\right)$$

$$C = \frac{B}{2\,(A + B)}$$

Here, Q_a is the measured unloaded Q from an all metal resonator made of the same metal as the ground plane, with the same dimensions, on the same substrate and Q_{sc} the measured unloaded Q from the HTS/metal resonator at the resonant frequency, f.

2.5 Dielectric Resonator

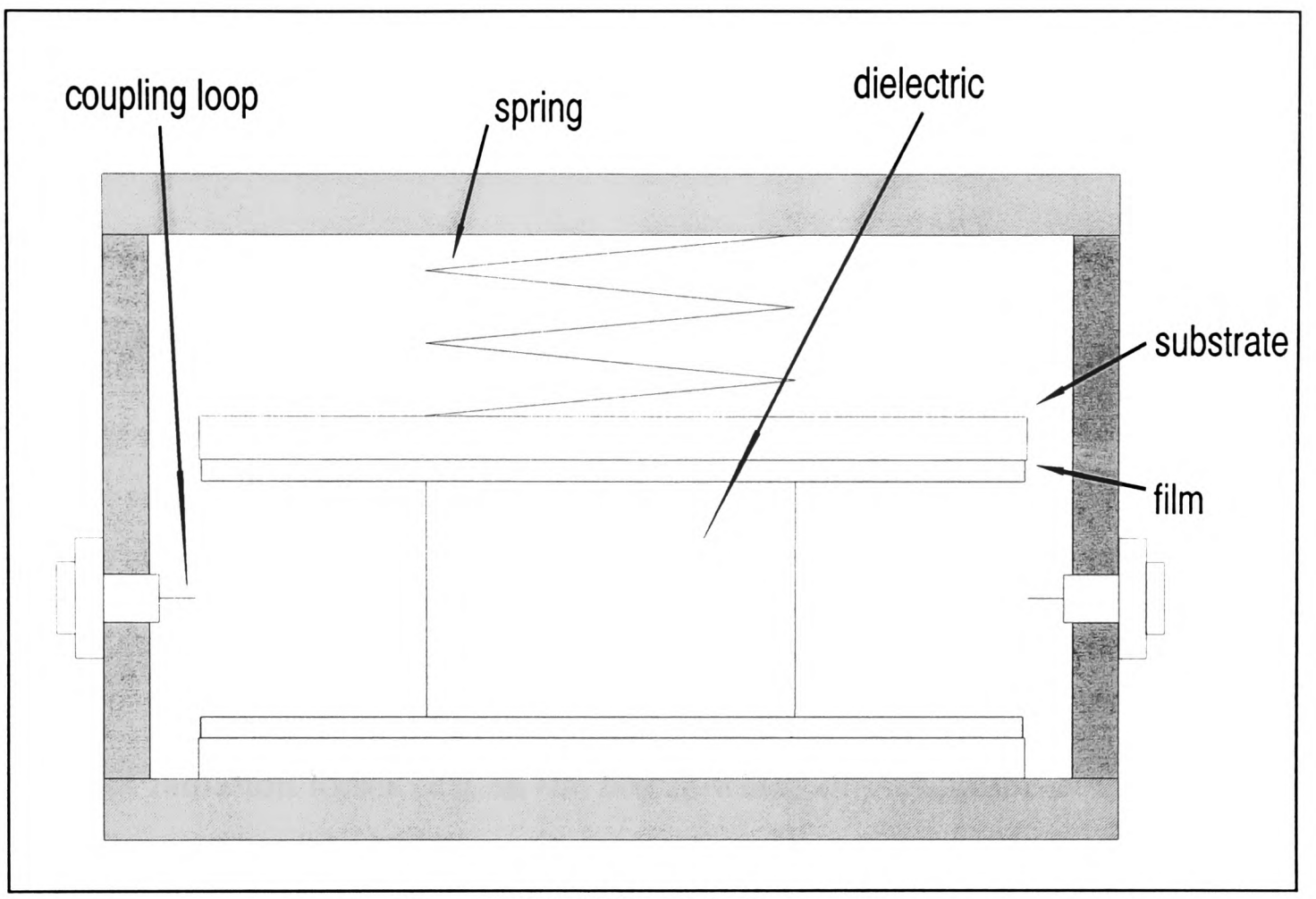

Figure 2.6 Dielectric Resonator

The dielectric resonator (DR) was first used for high Q oscillators [2.10] and measurements of dielectric loss tangents [2.11-2.13] and then adapted for measuring R_s [2.14]. Fig. 2.6 shows a diagram of the set-up. Superconducting disks (radius b) are placed on either side of the dielectric cylinder or puck (radius a). The DR is held together by spring force against the substrates and placed inside a high conductivity box to minimize radiation losses. Microwave energy is coupled into the resonator and the average surface resistance of the two films is extracted from the Q, knowledge of the geometry and the properties of the dielectric used. Unlike the cavity methods it does not require a prior calibration with normal conductor end-plates and so the measurement procedure is simplified and speeded up. However, it only gives the

average R_s of the two films and so to obtain individual results tests need to be performed in a "round robin" fashion with three films or more and the results solved simultaneously.

The two major loss mechanisms in the dielectric resonator are conductor and dielectric loss. The unloaded Q, Q_o, of the system is given by equation (C.34) (Appendix C):

$$\frac{1}{Q_o} = \frac{1}{Q_c} + \frac{1}{Q_d}$$

where: Q_c = superconductor Q

Q_d = dielectric Q

Note that radiation losses (e.g. in the box in which the resonator is held) have been ignored (this assumption is considered in greater detail in the next chapter). For the TE_{011} mode, Q_c and Q_d are given by equations (C.42) and (C.45) (Appendix C) respectively:

$$Q_c = \frac{A}{R_s}$$

$$Q_d = \frac{B}{\tan\delta}$$

where: R_s=HTS surface resistance

tan δ=dielectric loss tangent

A and B are geometrical factors.

The resolution of the technique is typically as good as 10 $\mu\Omega$ at 10 GHz [2.15] with a repeatability as good as 2-3% [2.16].

It is recommended that sapphire is used as the dielectric material in the resonator as it has the lowest tan δ of any known material, especially at cryogenic temperatures [2.10, 2.17], in the region of 10^{-7}. This effectively means that for even the highest quality films ($\sim$250 $\mu\Omega$) the dielectric will not limit the Q of the resonator thereby reducing the sensitivity of the measurement.

2.6 Other Techniques

Other techniques have been used to a lesser degree than those given above to measure the R_s of HTS films. Table 2.2 briefly reviews these other methods against those previously mentioned.

Method	Frequency (GHz)	Resolution (mΩ)	Ref.	Comments
Parallel Plate Resonator	4-12	0.01	[2.5] [2.18] [2.19]	Good resolution. Relies on suitable dielectric spacer. Simple calculation of R_s. Unquantified radiation loss.
Cavity End Wall Replacement	20-110	0.01	[2.7] [2.20] [2.21]	Can be very accurate. Precise derivation of R_s. Requires careful calibration. Wide dynamic range.
Partial End-Wall Replacement	10-100	0.1	[2.8]	Less sensitive than end-wall replacement. Can measure samples smaller than cavity diameter.
Microstrip Resonator	1-10	0.1	[2.9]	Destructive, but able to show effects of patterning.
Dielectric Resonator	5-30	0.01	[2.14] [2.15] [2.16]	Requires accurate dielectric rod. Limited by loss tangent of dielectric.
Cavity Perturbation	1-10	0.3	[2.22] [2.23] [2.24]	Requires LTS host cavity. Expensive. Complicated extraction of R_s
Confocal Resonator	>30	0.1	[2.25] [2.26]	Possible to produce a spatial R_s map. Good spatial resolution requires high frequencies.
Power Transmission	>10	10	[2.27] [2.28]	Requires thin samples and wide dynamic range equipment. Large errors (±30%).

Table 2.2 R_s Measurement Techniques

2.7 Conclusions

This chapter has reviewed some different R_s measurement techniques. This has outlined the advantages and disadvantages of each technique. Some of these methods have been used to take R_s measurements of films made in Oxford and elsewhere and details of these are given in chapter 3.

2.8 References

[2.1] Edwards J.A. et al (1994) "Effects of small changes in composition on the microwave properties of YBCO thin films". *Proceedings of the Microwave Properties and Applications of High Temperature Superconductors Conference*, 19 April. Oxford: University of Oxford.

[2.2] Jenkins A.P. et al (1995) "An HTS microstrip resonator stabilised voltage controlled oscillator". In D. Dew-Hughes (ed.) *Applied Superconductivity 1995 Volume 2*. Bristol: IoP Publishing: 1183-1186.

[2.3] Jenkins A.P. et al (1995) "Microstrip bandpass filters fabricated from TBCCO thin films on MgO substrates". In D. Dew-Hughes (ed.) *Applied Superconductivity 1995 Volume 2*. Bristol: IoP Publishing: 1187-1190.

[2.4] Jenkins A.P. et al (1995) "Subharmonically pumped BSSCO microwave mixers operated at Ka band and 77K". *Superconductor Science and Technology* 8: 613-616.

[2.5] Taber R.C. (1990) "A parallel plate resonator technique for microwave loss measurements on superconductors". *Rev. Sci. Instrum.* 61(8): 2200-2206.

[2.6] Cooke D.W et al (1990) "Microwave surface resistance of $YBa_2Cu_3O_7$ thin films on $LaAlO_3$ substrates". *Journal of Applied Physics* 68(5): 2514-2516.

[2.7] Klein N. et al (1989) "Millimeter wave surface resistance of epitaxially grown $YBa_2Cu_3O_{7-x}$ thin films". *Applied Physics Letters* 54(8): 757-759.

[2.8] Jenkins A.P. et al (1996) "Surface resistance measurement techniques". In A.V. Narlikar (ed.) *Studies in High Temperature Superconductors Vol. 17 (Part I)*. New York, NY: Nova Science Publishers: 179-219.

[2.9] Jenkins A.P. (1994) *Microwave Applications of High Temperature Superconductors*. Unpublished D.Phil. thesis, University of Oxford.

[2.10] Blair D.G., Sanson A.G. (1989) "High Q tunable sapphire loaded cavity resonator for cryogenic operation". *Cryogenics* 29(11): 1045-1049.

[2.11] Kobayashi Y., Tanaka S. (1980) "Resonant modes of a dielectric rod resonator short-circuited at both ends by parallel conducting plates". *IEEE Transactions on Microwave Theory and Techniques* 28(10): 1077-1085.

[2.12] Kobayashi Y., Katoh M. (1985) "Microwave measurement of dielectric properties of low-loss materials by the dielectric rod resonator method". *IEEE Transactions on Microwave Theory and Techniques* 33(7): 586-592.

[2.13] Kobayashi Y., Senju T. (1993) "Resonant modes in shielded uniaxial-anisotropic dielectric rod resonators". *IEEE Transactions on Microwave Theory and Techniques* 41(12): 2198-2205.

[2.14] LLopis O., Graffeuil J. (1990) "Microwave characterization of high T_c superconductors with a dielectric resonator". *Journal of the Less-Common Metals* 164 & 165: 1248-1251.

[2.15] Holstein W.L. et al (1993) "Surface resistance of large-area $Tl_2Ba_2CaCu_2O_8$ thin films at microwave and millimeter wave frequencies measured by three noncavity techniques". *Journal of Superconductivity* 6(3): 191-200.

[2.16] Wilker C. et al (1993) "A sapphire resonator for microwave characterization of superconducting thin films". *IEEE Transactions on Applied Superconductivity* 3(1): 1457-1460.

[2.17] Braginsky V.B., Ilchenko V.S. (1987) "Experimental observations of fundamental microwave absorption in high-quality dielectric crystals". *Physics Letters* A: 300-305.

[2.18] Napoli L.S., Hughes J.J. (1971) "A simple technique for accurate determination of the microwave dielectric constant for microwave integrated circuits". *IEEE Transactions on Microwave Theory and Techniques* 19: 664-665.

[2.19] Basovich A.Y. et al (1992) "Parallel plate resonator of variable spacer thickness for accurate measurements of surface impedance of HTS films". *Journal of Superconductivity* 5(6): 497-501.

[2.20] Miranda F.A. et al (1990) "Microwave surface resistance of laser ablated YBCO films". *Applied Physics Letters* 57(10): 1058-1060.

[2.21] Asano H. et al (1991) "Microwave properties of EuBaCuO". *Applied Physics Letters* 58(25): 2981-2983.

[2.22] Chang L.D. et al (1989) "Microwave surface resistance in Tl-based HTS thin films". *Applied Physics Letters* 55(13): 1357-1359.

[2.23] Hammond R.B. (1990) "Epitaxial TBCCO thin films with low 9.5 GHz R_s at high power and above 77K". *Applied Physics Letters* 57(8): 825-827.

[2.24] Delayen J.R. et al (1990) "Apparatus for measurement of surface resistance versus RF magnetic field of HTS". *Rev. Sci. Instrum.* 61(8): 2207-2210.

[2.25] Boyd G., Gordon J. (1991) "Confocal multimode resonator for millimetre through optical wavelength masers". *Bell System Technical Journal* March: 488-507.

[2.26] Martens J.S. et al (1991) "Confocal resonators for measuring the surface resistance of HTS films". *Applied Physics Letters* 58(22): 2543-2545.

[2.27] Wu P.H., Min Q. (1992) "Calculations of the microwave conductivity of high-T_c superconducting thin films from power transmission measurements". *Journal of Applied Physics* 71(11): 5550-5553.

[2.28] Kobrin P.H. et al (1990) "Millimeter wave complex conductivity of some epitaxial YBCO films". *Physical Review B* 42(10): 6259-6263.

Chapter 3

Surface Resistance Measurements

This chapter reviews measurements made using some of the techniques described in the last chapter. Both thick and thin films were tested. HTS films were, in some cases, tested using different techniques to compare and contrast results. Films reported on in this chapter were produced by S.M. Morley, A.P. Bramley, B.J. Glassey, L.Y. Su of the Materials Department, Oxford University, J.D. O'Connor and S. Huang of the Engineering Science Department, Oxford University and by the commercial company, NKT of Denmark.

The chapter begins with a review of substrate materials that have been used with thin films and the reasons for choosing them. This is followed by a summary of the types of film tested by various techniques. R_s results obtained by the PPR, microstrip resonator, end wall replacement, PEWR and DR techniques are given together with an analysis of the results and how each of the methods was set-up for optimum performance. In the particular case of the DR, radiation losses in the metallic walls of its enclosure are considered in some detail as this has been somewhat neglected in the past.

3.1 Substrate and Film Review

For thin films, different substrates have been used that have both good microwave and material properties, with the ultimate aim of producing high performance stripline-like devices. For good microwave performance a low dielectric constant (ϵ_r) is required to keep devices of a reasonable size. In addition, a very low loss tangent (tan δ) ensures that the substrate does not limit performance even when the HTS R_s is very low. Other desirable properties include low cost and high mechanical strength.

$LaAlO_3$ is widely used as a substrate because of its excellent lattice match with TBCCO [3.1, 3.2]. However, there is a 2% unpredictability in ϵ_r due to twinning [3.3]. $LaAlO_3$ has a tan δ of 10^{-4} at 77K and a ϵ_r of 23.5-24.5 at microwave frequencies [3.3-3.5]. The high ϵ_r can sometimes cause problems with some commercial microwave modelling packages as they have been designed for use with dielectric constants less than 10 [3.6, 3.7]. In addition, $LaAlO_3$ is expensive to produce and this increases the cost of integrated systems.

MgO is a low cost substrate with excellent dielectric properties: ϵ_r=9.6-10 at 77K and tan $\delta=10^{-5}$ at 77K and 10 GHz [3.3]. Compared to $LaAlO_3$ it has a larger mismatch with TBCCO films of 9.4% [3.3, 3.8] and the hygroscopic nature of the substrate may affect its surface quality.

The final substrate used at Oxford is sapphire. For the microwave engineer sapphire offers many advantages as it combines the lowest tan δ, less than 10^{-6}, at 10 GHz and 77K with a low ϵ_r of 9.32 in the basal plane and 11.6 along the c-axis [3.3]. It has excellent mechanical strength and is available in the form of cheap, large area wafers and so is capable of being used for integrated circuits. However, it suffers from a large lattice mismatch (9.8%) with TBCCO which can be overcome by the use of buffer layers [3.9]. The buffer layers reduce the rate of change of strain in the lattice structure helping the film retain its superconducting properties [3.10]. A common buffer layer is CeO_2 and the following sections report on the R_s values of TBCCO on CeO_2-buffered sapphire as well as on the other substrates mentioned above. Table 3.1 reviews the different types of films tested.

Compound	Substrate	T_c(K)	J_c(Acm^{-2})	Ref.
$Tl_2Ba_2CaCu_2O_8$	1cm x 1cm, 2" diameter $LaAlO_3$	107	$7x10^6$	[3.10]
$Tl_{1-x}Pb_xBa_2Ca_2Cu_3O_x$	1cm x 1cm $LaAlO_3$	103	-	[3.11]
$Tl_2Ba_2Ca_2Cu_3O_x$	2cm x 2cm, 4" diameter MgO	122	$1.5x10^5$	[3.12]
$Tl_2Ba_2CaCu_2O_8$	1cm x 1cm CeO_2-buffered sapphire	101.6	$1.25x10^5$	[3.10, 3.13]
$YBa_2Cu_3O_x$	1cm x 1cm, 2" diameter CeO_2-buffered sapphire	-	-	-
Sprayed $Tl_2Ba_2Ca_2Cu_3O_x$	1" zirconia	-	$3x10^4$	[3.14]
$Bi_2Sr_2CaCu_2O_y$	1" silver	-	$1.7x10^4$	[3.15]

Table 3.1 Film Summary

Wherever possible Table 3.1 gives T_c and J_c values reported in a reference (where exact processing conditions are described) for the different types of film. The following summarizes the different processes used for producing the films.

The first four types of film given were sputtered and the annealed using an ex-situ process with anneal temperatures in the range 720-855°C. Some $Tl_2Ba_2CaCu_2O_8$ (Tl(2212)) films were annealed in argon atmospheres to reduce the anneal temperature which is especially useful for thin films on CeO_2-buffered sapphire as then the formation of reaction layers, which degrade the quality of these films, is eliminated [3.9]. R_s results have also been obtained for $Tl_2Ba_2Ca_2Cu_3O_x$ (Tl(2223)) films on both sides of MgO substrates. For microwave applications there is considerable benefit in having both sides of the substrate coated with HTS films since the low R_s of the ground plane and the conductor compared to normal metals leads to improved device performance. Double-sided film deposition over large area substrates will become increasingly desirable for satellite applications of HTS microwave devices as entire sub-systems can then be integrated onto a single substrate.

The YBCO films tested were provided by NKT who did not supply the processing conditions. The sprayed TBCCO thick films were tested to provide an indication as to whether they may be useful for microwave cavities as spray techniques are not restricted to planar surfaces like thin films [3.16]. Finally, the BSCCO thick films were tested [3.15].

3.2 Parallel Plate Resonator Results

3.2.1 Results

A parallel plate resonator (PPR) constructed by A.P. Jenkins [3.17] was used to measure the R_s of the films reported on in this section. The PPR was first tested with substrates with a 10 μm silver coating evaporated onto them together with a 510 μm $LaAlO_3$ spacer. This spacer was chosen as the loss tangent of $LaAlO_3$ was low enough to be considered negligible in the calculations for R_s and the thickness of the spacer provided Q values during the measurement of reasonable size (in the 100s). The R_s value obtained was 24 mΩ scaled to 10 GHz (using a $f^{0.5}$ scaling) and 77K. This compares to a theoretical value of 11 mΩ [3.18]. The discrepancy can be explained by the poor quality of the evaporated edges of the substrate where the silver was peeling slightly. Further details of why this has a major effect are given in the next section. Table 3.2 shows the results for HTS films tested using the PPR technique. A f^2 scaling has been used to scale the results to 10 GHz as the resonant frequency of the PPR was typically 3.5 GHz. The error in the results given is $\pm 1\%$ as this was found to be the variation in the unloaded Q during testing.

Film	R_s at 10 GHz and 77K (mΩ)
La88	67.7
La89	61.2
La90	59.9
La91*	166
La92*	48.0
La93	484
La94*	436
La95	44.0
La96	91.0
La97	138
La98	220
La99	24.1
La100	44.1
La102	123
La103	DNS
LaR7	257
LaR12	DNS
LaR21	DNS
LaR26	678
LaR28	459
BPB17	DNS
BPB18	127

Table 3.2 PPR Results

DNS = Did not superconduct

* La91, La92 and La94 were also tested after re-annealing them in an oxygen atmosphere to investigate the effect on R_s. The results for this were 883 mΩ, 82.0 mΩ and 351 mΩ respectively. Therefore, oxygenation degraded the R_s for the first two and did not produce a significant improvement for La94.

3.2.2 Analysis

The results obtained for the HTS films suggests that they are not of a very high quality given that an R_s as low as 130 $\mu\Omega$ has been achieved at the same frequency, same temperature and using the same technique [3.19]. However, these high quality films were cut out from larger substrates and so there would be complete HTS film coverage of the sections cut. The films given in Table 3.2 were directly sputtered onto 1cm square substrates held in place by clamps along their edges leading to no coverage in this region. As the electric field is at a maximum at the edge of the substrate, decaying sinusoidally to zero at the centre, then rising once more to a maximum at the opposite edge [3.20] any losses here will have a detrimental effect upon the R_s value obtained as then the stored energy and so Q is reduced.

A related issue is the accuracy of the orientation of the films in relation to the spacer between them. Ideally, all edges line up exactly and this was kept consistent through the whole series of "round robin" tests. Although every attempt was made to make sure this was the case it is a tentative possibility that even a small error in the alignment may be enough to change the boundary conditions and so alter the R_s obtained. As the focus of this work was upon producing working devices, as opposed to refining R_s measurement techniques, this possibility was outside the scope of the work described here, but warrants further investigation.

3.3 Microstrip Resonator Results

3.3.1 Mask Design

Figure 3.1 shows the various masks designs used as patterns for making HTS resonators on 1cm square MgO or $LaAlO_3$ substrates. The meander line was used with MgO as it has a ϵ_r of 9.8 which would have led to a resonant frequency above the 6 GHz maximum of the network analyzer used if a linear design was patterned. This is because a higher ϵ_r leads to a lower resonant frequency for the same length of line. Later on a 40 GHz network analyzer was purchased which overcame this problem. The linear design was used with $LaAlO_3$ which has a ϵ_r of 24.

Initially, designs where the lines went right up to the edge of the substrate were used. However, given the evidence from the parallel plate resonator measurements it was apparent that the low film quality at the edges of substrates was degrading the quality factors that could be achieved. Hence, it was decided to move to a new design which had coupling gaps which isolated the resonant structure from the low quality film (marked "After" in Fig. 3.1). The line width determined previously [3.17] was 0.5mm which gave a 50 Ω line on MgO and 30 Ω on $LaAlO_3$. The coupling gaps were optimized previously [3.17] (0.3mm for MgO and 0.2mm for $LaAlO_3$) to give an insertion loss greater than 20 dB so that the resonators were lightly coupled. This makes measurements easier and more accurate as small insertion losses are difficult to measure.

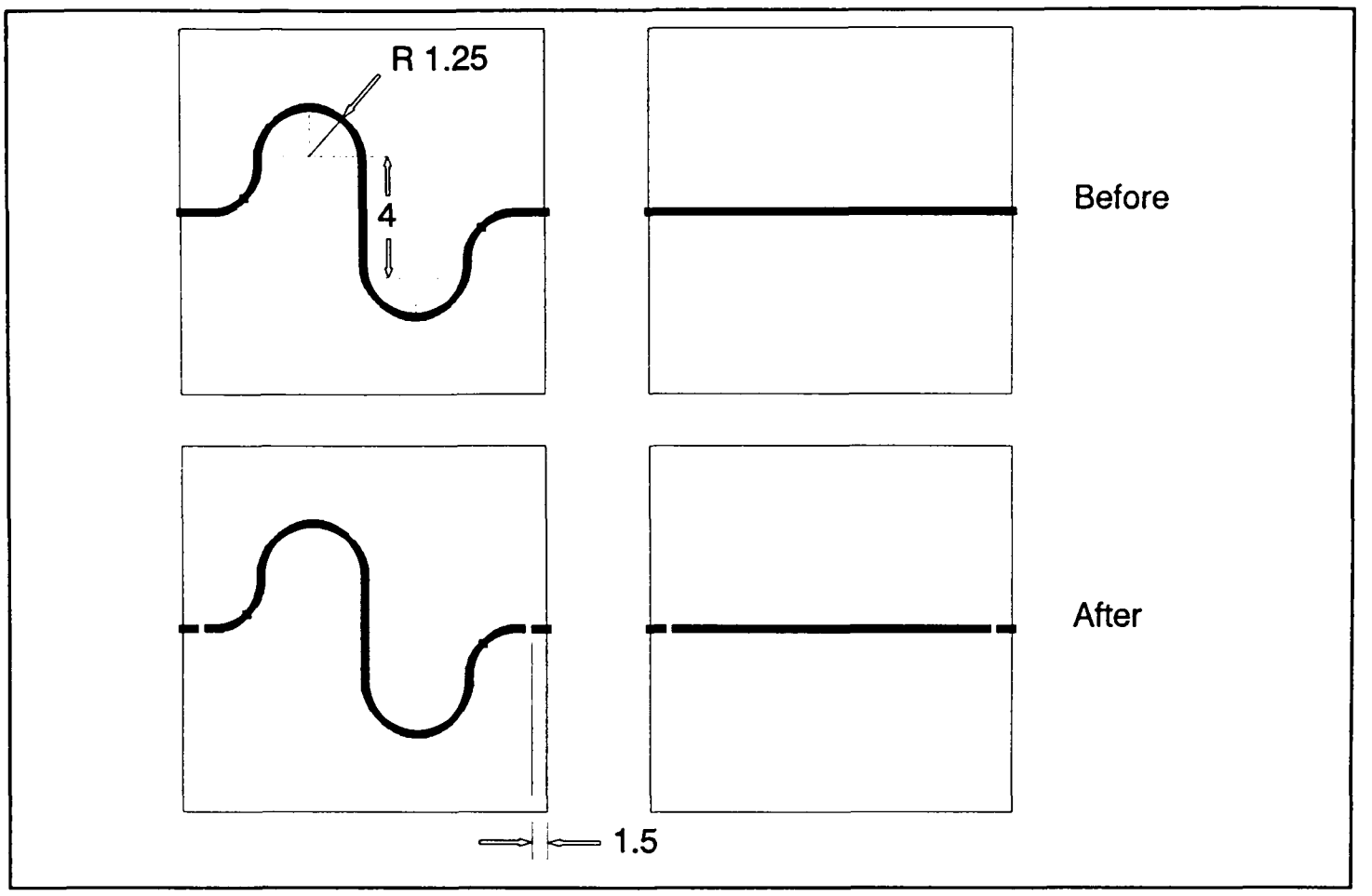

Figure 3.1 Mask Designs (dimensions in mm)

3.3.2 Results

Equation (2.9) from section 2.4 was used to determine the R_s from the unloaded Q and the resonant frequency with values of h=0.5mm, t=1 μm, w=0.5mm. A silver resonator was constructed which gave a value for Q_a of 300 (found to be consistent for the power ranges used). This reduces the equation to:

$$R_{sl} = 1.20\times10^{-9} f_o \left[\frac{1}{Q_{sc}} - \frac{0.12}{Q_a} \right]$$

Table 3.3 summarizes the results of the resonators tested.

Sample	Mask Type	f_o (GHz)	P_{in} (dBm)	Q_{sc}	R_s at 10GHz ±7% (mΩ)
La56	L	2.33, 2.60*	-20, -50*	101, 570*	489, 62.5*
La57	M	2.10, 2.64*	0,0*	52, 77*	1076, 572*
La67A	L	5.22	-50	55	409
La67B	L	5.20	-30	43	527
La68	M	1.78, 2.57*	-20, -50*	124, 140*	517, 315*
La73	M	1.70, 2.64*	-10, -30*	20, 21*	3501, 2146*
La77	L	6.48	-30	68	265
JDMGO16	M	3.68, 3.81*	-50, -50*	625, 233*	39.1, 123*
La90	L	5.96 5.95 5.96	0 -20 -40	87 89 94	223 219 206
ABTM24	L	8.00 8.00 8.00	0 -20 -40	222 397 484	61.6 31.8 25.0
ABTM31	L	7.70 7.70 7.70 7.70	0 -20 -40 -60	166 325 461 532	87.6 41.7 27.6 23.1
ABTM33	L	8.39 8.40 8.40	0 -20 -40	215 335 390	60.8 36.9 30.9
ABTM35	L	8.24 8.30 8.30	0 -20 -40	148 244 355	92.6 53.5 34.9
ABTM37	L	8.04 8.04 8.04	0 -20 -40	360 525 544	35.5 22.5 21.5

Table 3.3 Microstrip Resonator Results

Key: * Two results indicate a resonator patterned without coupling gaps and then with gaps.
L Linear Resonator Mask
M Meander Line Resonator Mask

3.3.3 Analysis

The ±7% error bounds have been calculated using the Q_{sc}=625 result for JDMGO16 as this has the highest Q and so will be most sensitive to errors in measurement. The power level for this measurement was very low (-50 dBm) and so there was an observed ±5% error in the Q measurement. This leads to the following calculation:

$$\begin{aligned} R_{s1} &= 1.20\times10^{-9} f_o \left[\frac{1}{Q_{sc}} - \frac{0.12}{Q_a}\right] \\ &= 1.20\times10^{-9}\times3.68\times10^{9}\times\left[\frac{1}{625\pm5\%} - \frac{0.12}{300}\right] \\ &= 5.3\times10^{-3}\pm7\% \end{aligned}$$

The results clearly show that resonators re-patterned with coupling gaps have better performance. This together with the evidence from the parallel plate resonator suggests that the edges of films should be avoided for making devices. The only exception to this is JDMGO16 (HTS on a MgO substrate) and this result may have been affected by accidental water exposure to the sample.

Films on $LaAlO_3$ (e.g. La57) did not have particular good performance compared to the silver test sample, but the ABTM films on MgO show improvement in their Qs over a similar silver resonator. This in turn gives a lower R_s figure in the final column in which a frequency squared scaling has been used.

The result for La90 can be compared to that obtained by the PPR. With the latter measurement a value of 59.9 mΩ is obtained, but from the resonator result the R_s is

just over 200 mΩ. The discrepancy between these results can be explained by the degradation of the film during the etching process. Martens et al [3.21] have shown that etching solutions and photoresist can degrade HTS thin films by as much as 100% due to initially superconducting parts of the film going normal. The etch used for the resonators given in Table 3.3 was $FeCl_3$ which has a very short etch time of around 10 seconds for HTS thin films. Given the harshness of the etch and exposure to photoresist during the patterning process the increase in R_s can be accounted for.

3.4 End Wall Replacement Results

3.4.1 Results

The R_s measurements of sprayed TBCCO and BSCCO HTS samples were carried out using the TE_{011} mode of a 20 GHz copper cavity. A cavity calibration was first carried out with an all copper cavity and then one end wall was replaced with the HTS sample. From the differences in the measured Q, the resonant frequency and geometrical information the R_s of the sample can be determined. In order that samples placed in the cavity should not be degraded by water vapour, the cavity was evacuated prior to immersion in liquid nitrogen and during the cool down and warm up process.

For a cavity of radius 10.9mm, length of 13.5mm and given that the first root of the Bessel function J_1 is 3.83, equations (2.2) and (2.3) from section 2.2 become:

$$R_{cu} = \frac{729}{Q_{cu}}$$

$$R_{sc} = R_{cu} - 3518.5\left[\frac{1}{Q_{cu}} - \frac{1}{Q_{sc}}\right]$$

The results for the TBCCO and BSSCO films tested at 77K are given in Table 3.4.

Sample	P_{in} (dBm)	Q_{sc}	f_o (GHz)	R_s at 10 GHz (mΩ)±8.0%
CD01	-10	646	20.116	1330
CD02	-10 -30	39,297 40,990	20.089 20.089	3.6 2.7
CD08	-10	1,258	20.091	668
EMA1	-10 -30 -50	23,318 23,767 24,519	20.089 20.089 20.089	18.3 17.6 16.4

Table 3.4 End Wall Replacement R_s Results

3.4.2 Analysis

Films with a CD prefix were TBCCO and EMA1 is the BSCCO film and f_o is the measured resonant frequency. A frequency-squared scaling was used to scale the results to 10 GHz. When CD01 and CD02 were tested the all-copper cavity Q_{cu} was measured as 37,225 (not power dependent). For CD08, Q_{cu} was measured as 33,177 (again not power dependent). Finally, when EMA1 was tested Q_{cu} was measured as 36,163 (again not power dependent). The variations can be explained by the differing degrees of cleanliness of the cavity (e.g. if it had been polished recently Q_{cu} was higher).

The error in the R_s results was obtained by assuming a 1% variation (this was the observed fluctuation) in the measured Q_{sc} for the lowest power measurement of CD02. This will be the most sensitive to any errors as it has the lowest R_s. The maximum error is found as follows:

$$R_{sc} = \left(1.958\times10^{-2} - 3518.5\times\left[\frac{1}{37{,}225} - \frac{1}{40{,}990\pm1\%}\right]\right)\times\left(\frac{10}{20.089}\right)^2 = 2.7\times10^{-3}\pm8\%$$

The R_s of the TBCCO films are not consistent, but CD02 has a very good R_s for a sprayed thick film. In fact, CD02 represents the second best R_s value obtained in the world (the best value also being obtained in Oxford [3.16]) for a thick film.

EMA1 has a R_s that is slightly greater than the copper calibration performed with this cavity. The calibration gave a result of 14.2 mΩ at 10 GHz assuming a $f^{0.5}$ scaling for a normal conductor. Other groups have also found that the R_s of BSCCO is poor and that its main benefit is the high current densities it can handle [3.22].

The results for CD02 and EMA1 show a distinct power dependency for R_s. This is due to parts of the HTS film deposited going normal due to the current passing through these exceeding the local J_c [3.14].

3.5 Partial End Wall Replacement Results

3.5.1 Results

A partial end wall replacement cavity [3.20] was constructed from copper as outlined in section 2.3. Equations (2.4)-(2.8) from section 2.3 are used to determine the HTS R_s of various films. The cavity dimensions used were as follows:

a=cavity radius=5.59mm

b=iris radius=4.5mm

d=cavity length=6.8mm

s=step height=0.3mm

In order to allow for the step between the copper cavity and the film the cavity length is adjusted using:

$$d' = d + \left(\frac{b}{a}\right)^2 s$$

The resonant frequency was found to be 39.30 GHz and Q_{cu} was 22,366 at 80K. This gives (at 39.30 GHz):

$$R_{sc} = 3.270\times10^{-2}\times\left(1 + 120{,}127.03\times\left[\frac{1}{Q_{sc}} - \frac{1}{22{,}366}\right]\right)$$

The limiting unloaded Q of the cavity was found to be 27,483 (i.e. the Q that would be obtained if a notional film of zero surface resistance was placed on the iris end). The resonant frequency is very close to the maximum operating frequency of 40 GHz of the HP8510B network analyzer used in the measurement set-up. By selecting as

high a frequency as possible the unloaded Q obtained is lowered (due to a larger R_s at higher frequencies) which makes measurement easier and more accurate. Table 3.5 gives the results for 1cm and 2cm square films tested (a f^2 scaling has been used to scale the R_s results from 39.3 GHz to 10 GHz).

Sample	Temperature (K)	Q_{sc}	R_s at 39.3 GHz (mΩ)	R_s at 10 GHz (mΩ)
BLa15	80	26,153	9.4	0.6±14.9%
LaR26	80	21,833	36.9	2.4±4.9%
LaR33	80	12,372	172.5	11.2±1.8%
BPB25	80	21,567	39.0	2.5±4.6%
ABRCE25	80	20,867	45.1	2.9±4.2%
ABRCE34	80	6,725	435.1	28.2±1.4%
ABRCE36	80	16,323	96.8	6.3±2.5%
ABRCE48	80	13,295	150.8	9.8±1.9%
ABTM43A	80	23,506	24.9	1.6±6.4%
ABTM43B	80	24,252	20.2	1.3±7.4%
ABTM73A	80	24,275	20.1	1.3±7.5%
ABTM73B	80	18,543	65.8	4.3±3.0%
ABTM83A	80	26,330	8.5	0.6±16.5%
ABTM83B	80	2,299	1434.4	92.9±1.1%
A398A	80	4,504	718.9	46.5±1.2%
A398C	80	8,445	317.9	20.6±1.5%
A398H	Did	not	super-	conduct
A398L	80	13,584	144.6	9.4±2.0%

Table 3.5 PEWR Results

3.5.2 Analysis

BLa15 is Tl(2212) on 2cm square $LaAlO_3$ and has a very low R_s close to the lowest achieved in TBCCO of 130 $\mu\Omega$ at 77K and 10 GHz [3.23]. As the sample is 2cm square the PEWR cavity was used in complete end wall replacement mode. That is a copper piece was placed over the iris end and the HTS sample replaced the other end. In this case the complete end wall replacement equations (2.2) and (2.3) from section 2.2 can be used which gives:

$$R_{sc} = 3.270\times10^{-2} - \left[\frac{1}{22{,}366} - \frac{1}{Q_{sc}}\right]\times 3591.78$$

The limiting Q is this operational mode is 28,085.

The errors in Table 4.5 are calculated on the basis that there was an observed $\pm 1\%$ error in the measured Q_{sc}. Hence, due to the nature of the equations used to find R_{sc} the higher the Q_{sc} obtained the greater the error.

The LaR films have been produced on 1cm square $LaAlO_3$ using the low temperature argon anneal described earlier. The result for LaR26 is promising and has helped with the processing of the ABRCE films which are Tl(2212) on 1cm square CeO_2-buffered sapphire using the same low temperature anneal to prevent the formation of $BaCeO_3$ between the HTS film and the CeO_2 buffer layer on the sapphire [3.9].

BPB25 is a Pb doped Tl(1223) film on 1cm square $LaAlO_3$ with again a promising R_s result.

The ABTM films were double-sided Tl(2223) on 2cm square MgO. The A and B tagged at the end of the sample name indicating the side of the film tested. ABTM43 (Fig. 3.2) demonstrates that near equal values for R_s can be obtained for both sides of the substrate, but the result for ABTM73 (Fig. 3.3) shows that this process needs to be controlled very tightly or else consistency is lost.

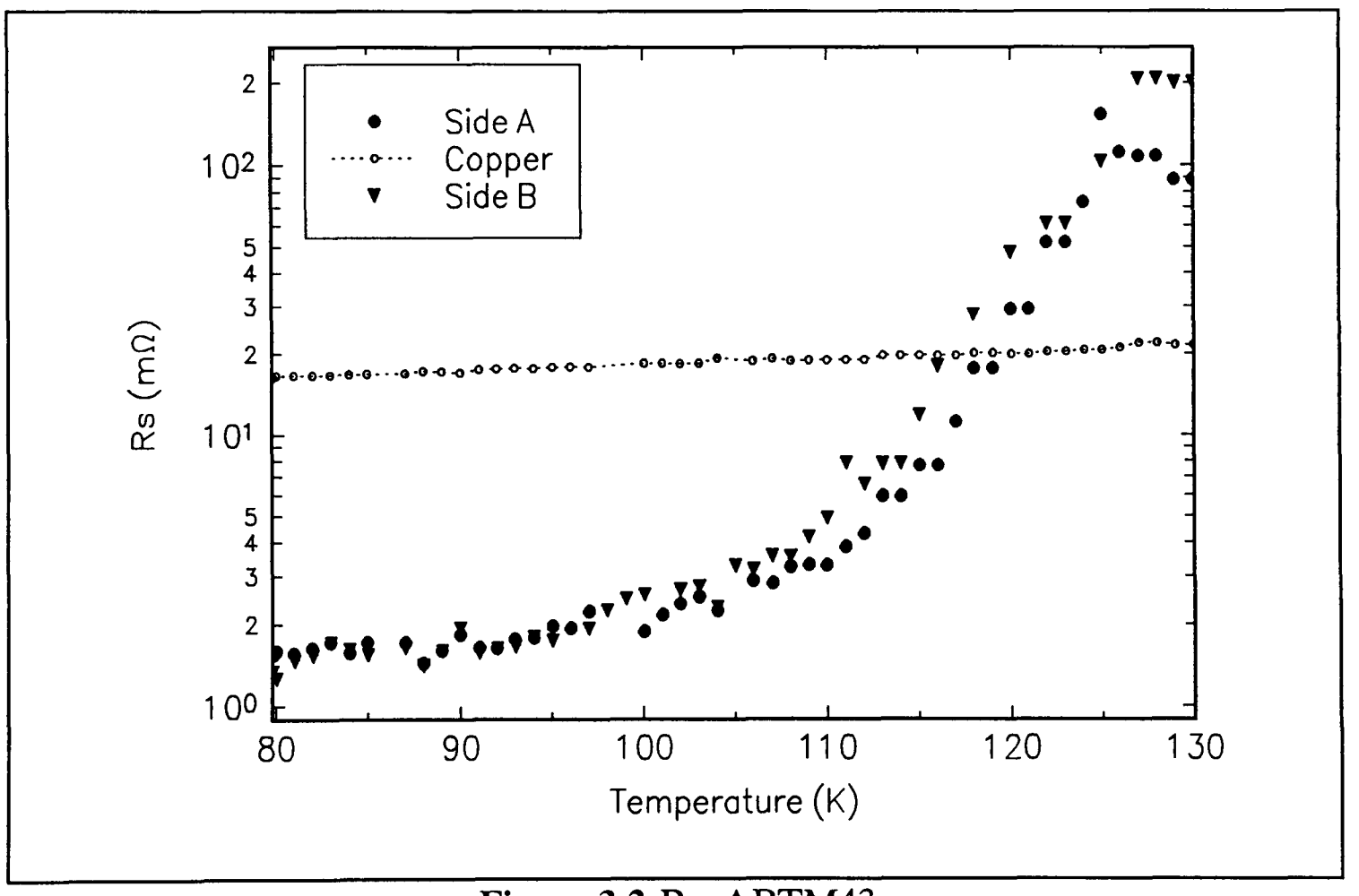

Figure 3.2 R_s: ABTM43

The final films tested were supplied by NKT, Denmark. These were YBCO deposited onto 1cm square CeO_2-buffered sapphire. The samples tested had been cut from a two inch diameter substrate and the figures demonstrate the inhomogeneity that has occurred during processing leading to a wide range of R_s values and even a particular

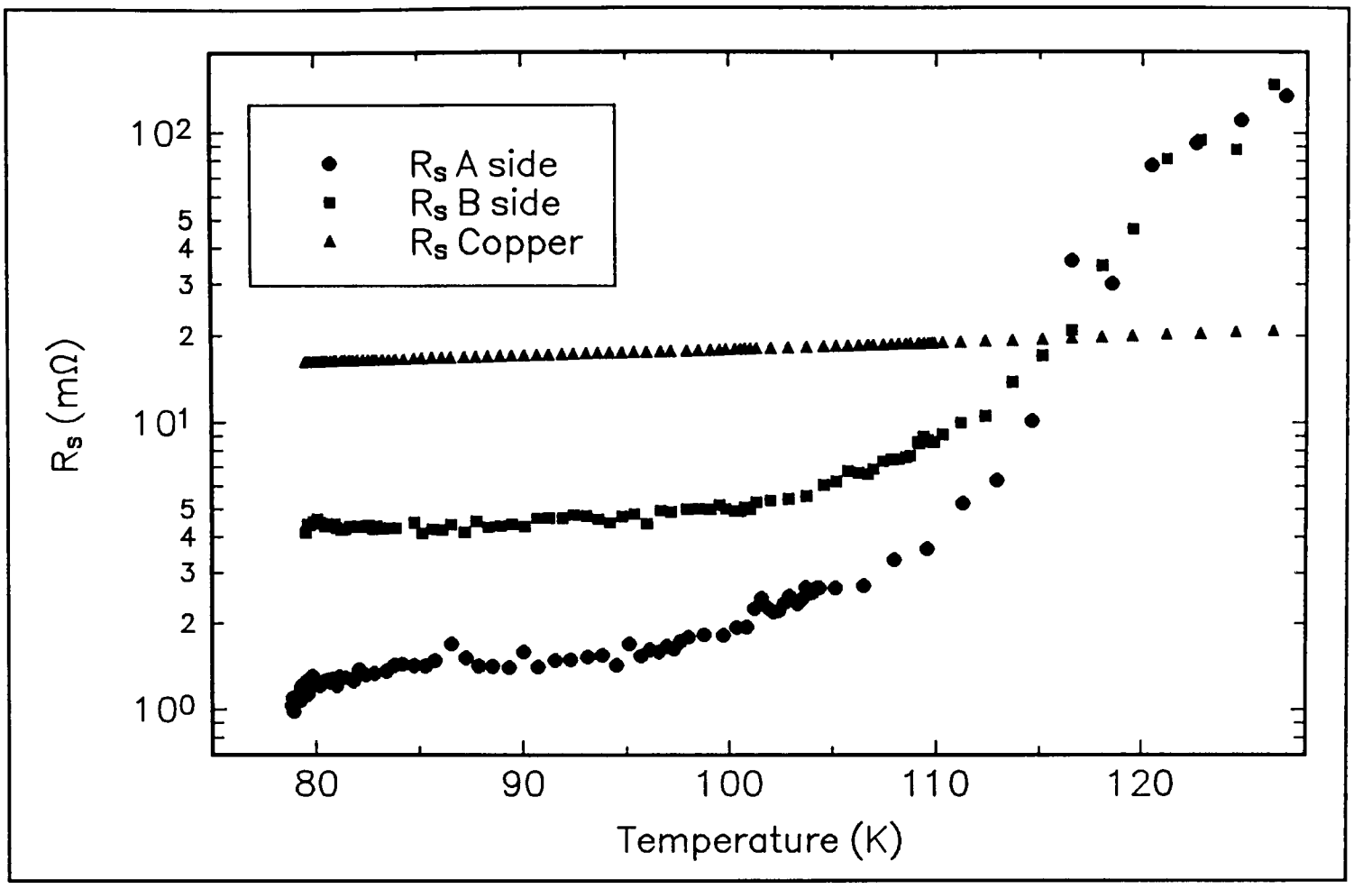

Figure 3.3 R_s: ABTM73

1cm square sample (A398H) that did not superconduct. This sample was also tested as a complete two inch diameter sample with a dielectric resonator and this is described in the next section. Fig. 3.4 shows SEM photographs of samples A398C and A398H with very similar microstructures. Therefore, it would seem that, in this instance, there is little correlation between the R_s of a film and its microstructure. This result is in agreement with a more detailed study performed by Edwards et al [3.24].

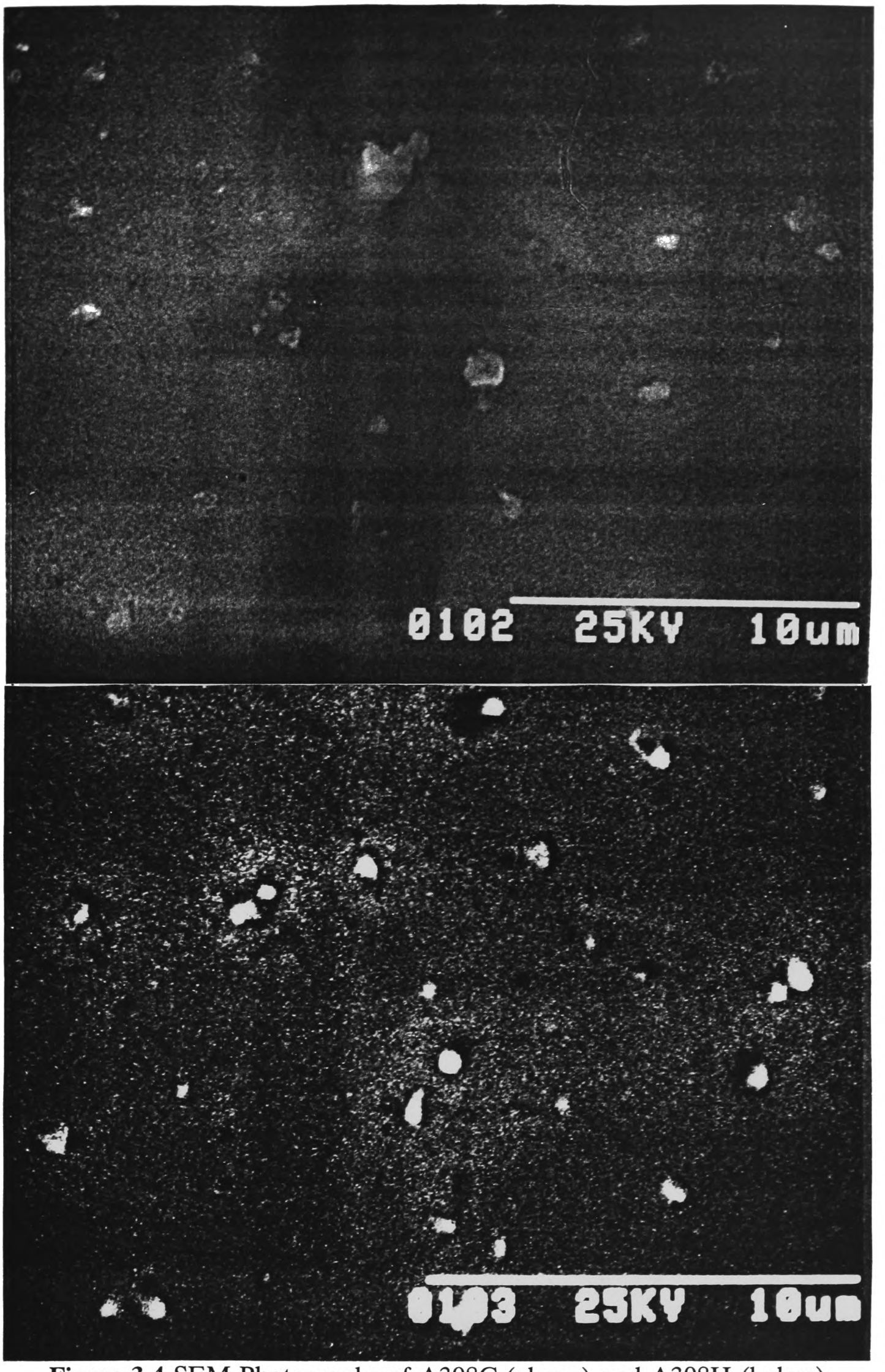

Figure 3.4 SEM Photographs of A398C (above) and A398H (below)

3.6 Dielectric Resonator Results

3.6.1 Theory

Before investigating the practical uses of a dielectric resonator (DR) it is worth considering the theory behind the operation of the device. Much of the theory associated with the DR has been developed by Kobayashi and his co-workers [3.25-3.27] and the DR has been used since the 1960s as a device for measuring dielectric constants [3.28-3.30]. However, Shen and his co-workers at Du Pont first suggested the use of the DR for measuring the R_s of superconducting films [3.31]. Both Kobayashi and his co-workers and Shen and his co-workers consider the device as standing on its own and do not consider the effect that a box enclosure may have on its operation (e.g. the effect on the Q). Although the DR has been used in practical situations where it is contained in usually a metallic box the theory regarding its operation under these circumstances has been somewhat neglected. Before using the DR for measuring the R_s of superconducting films or as the basis for a low phase noise oscillator it was decided to determine whether the theory could be improved upon.

The TE_{011} mode is often used for the operation of a DR [3.31] as it has a high Q and can be isolated easily from other modes by careful adjustments of the coupling loops. Use of a high Q mode also allows for the DR to be used as the resonant element in

oscillators. For this mode equations (C.17), (C.18), (C.21) and (C.22) from Appendix C, given below, can be solved simultaneously to find the resonant frequency.

$$\beta^2 = k^2\epsilon_r - \xi_1^2 = k^2 + \xi_2^2$$

$$k = \frac{2\pi}{\lambda} = \frac{2\pi f}{c} = 2\pi f\sqrt{\epsilon_o\mu_o}$$

$$\frac{J_1(\xi_1 a)K_o(\xi_2 a)}{\xi_1 a} + \frac{K_1(\xi_2 a)J_o(\xi_1 a)}{\xi_2 a} = 0$$

$$\beta = \frac{\pi}{d}$$

The unloaded Q of the DR is given by equation (C.34) (Appendix C):

$$\frac{1}{Q} = \frac{1}{Q_c} + \frac{1}{Q_d} + \frac{1}{Q_r}$$

where: Q_c = the superconductor Q due to the superconducting endplates

Q_d = the dielectric Q due to losses in the dielectric

Q_r = the radiation Q due to losses in the box walls.

In the particular case of Q_r it has been assumed that energy is absorbed by the box walls only and that none of the energy is reflected back into the TE_{011} mode. This places a worst case scenario upon the radiation Q which then helps to determine the effect the box walls have upon the DR's unloaded Q.

Computer programs were written (Appendix D) to determine the resonant frequency, R (The ratio of energy stored outside the dielectric to that stored inside it. A definition is given in Appendix C.) and Q_r.

3.6.2 5.58 GHz Dielectric Resonator

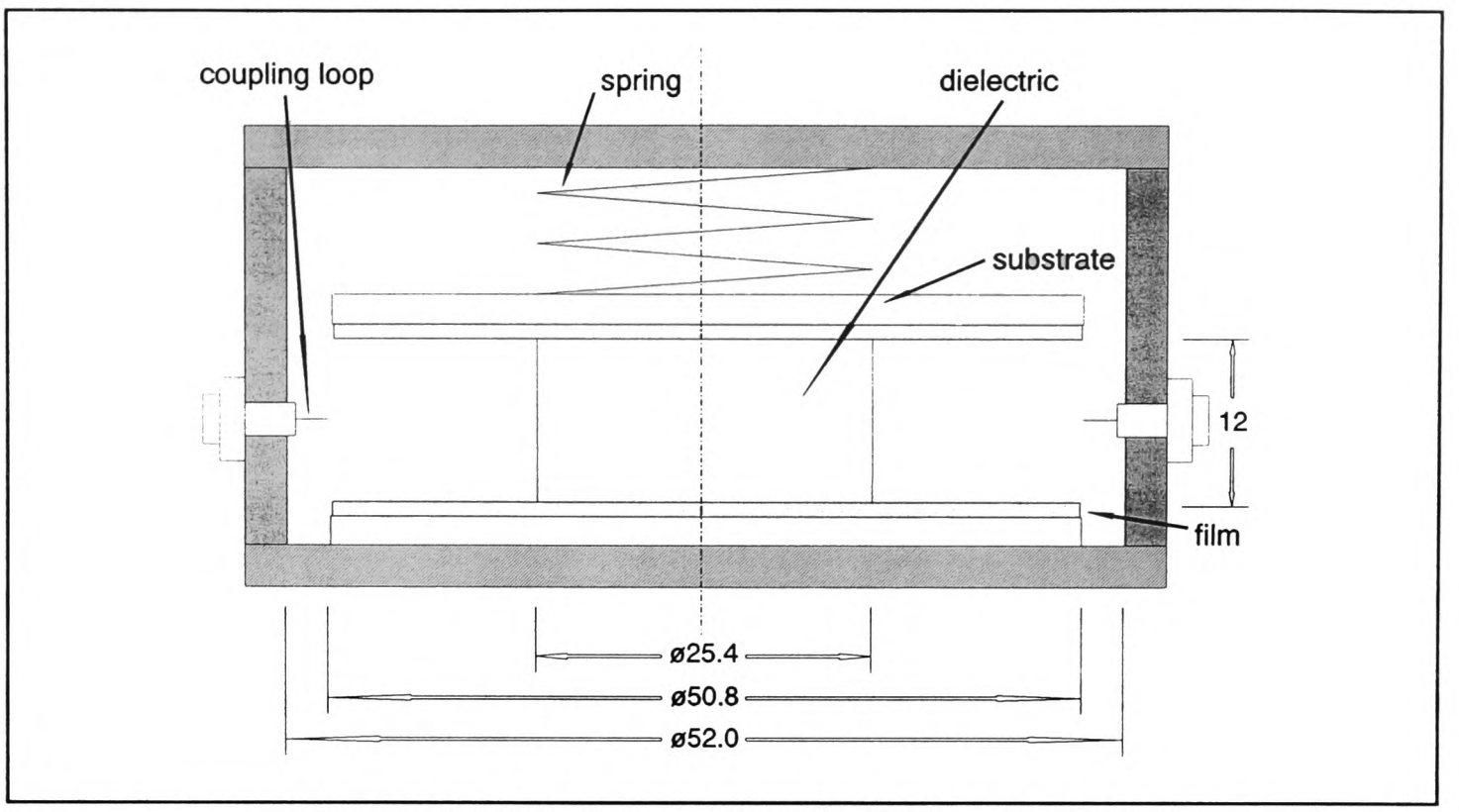

Figure 3.5 DR Schematic (dimensions in mm)

In order to test the accuracy of the computer predictions a DR was constructed with dimensions as shown in Fig. 3.5. The dielectric used was sapphire as this has the lowest tan δ of any known substance ($< 10^{-7}$ at 10 GHz and 77K [3.3]) which means that the effects of losses in the dielectric can be considered negligible. Fig. 3.6 shows a picture of the actual device.

From the picture can be seen a white PTFE ring in the top plate which is pressed against a raised triangular cross-section part of the box middle. The differences in the coefficients of expansion between PTFE and brass means that an effective hermetic seal is achieved. This means that the whole assembly can be placed directly in liquid nitrogen speeding up the testing sequence. A schematic is shown in Fig. 3.7. Similar

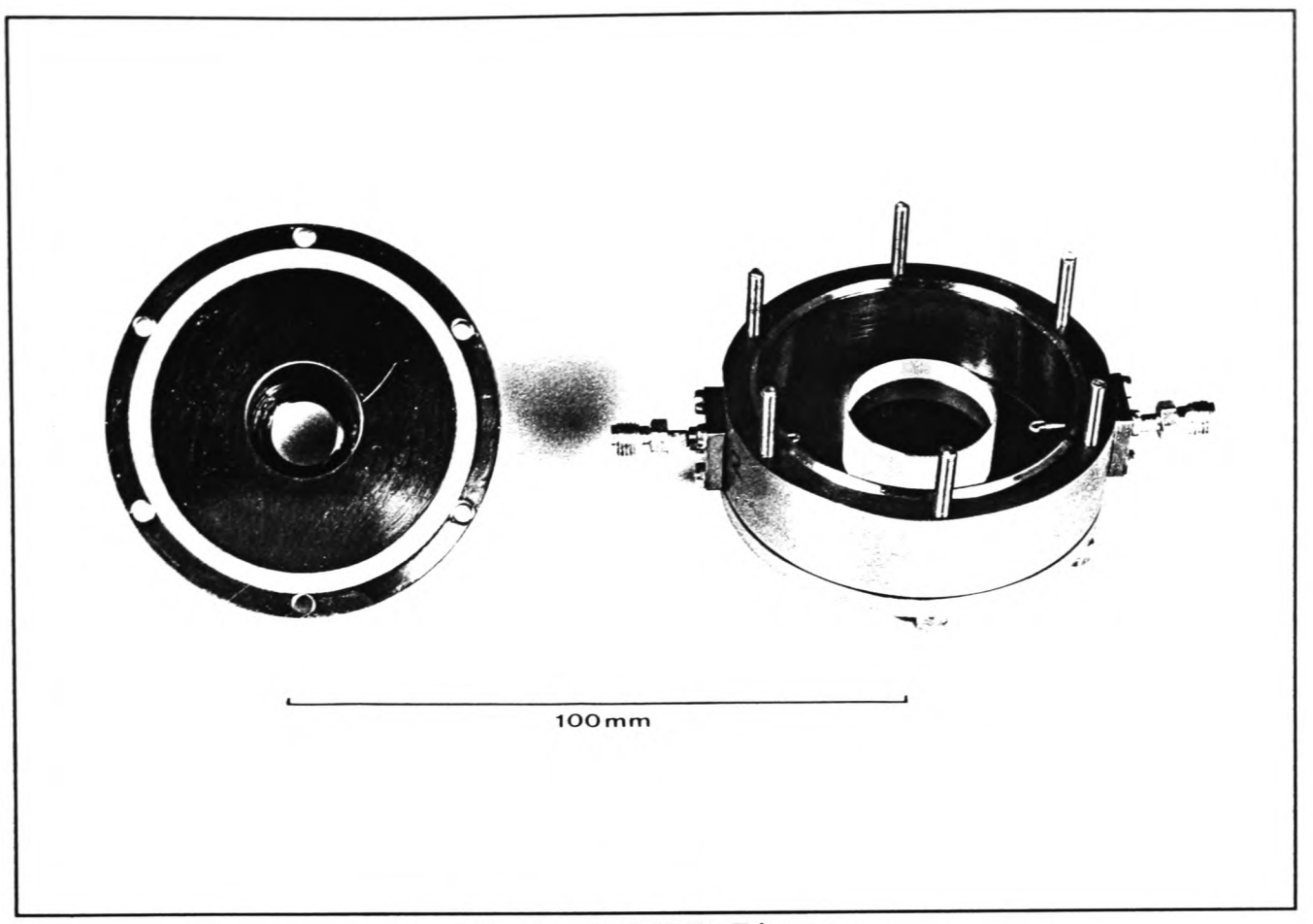

Figure 3.6 DR Picture

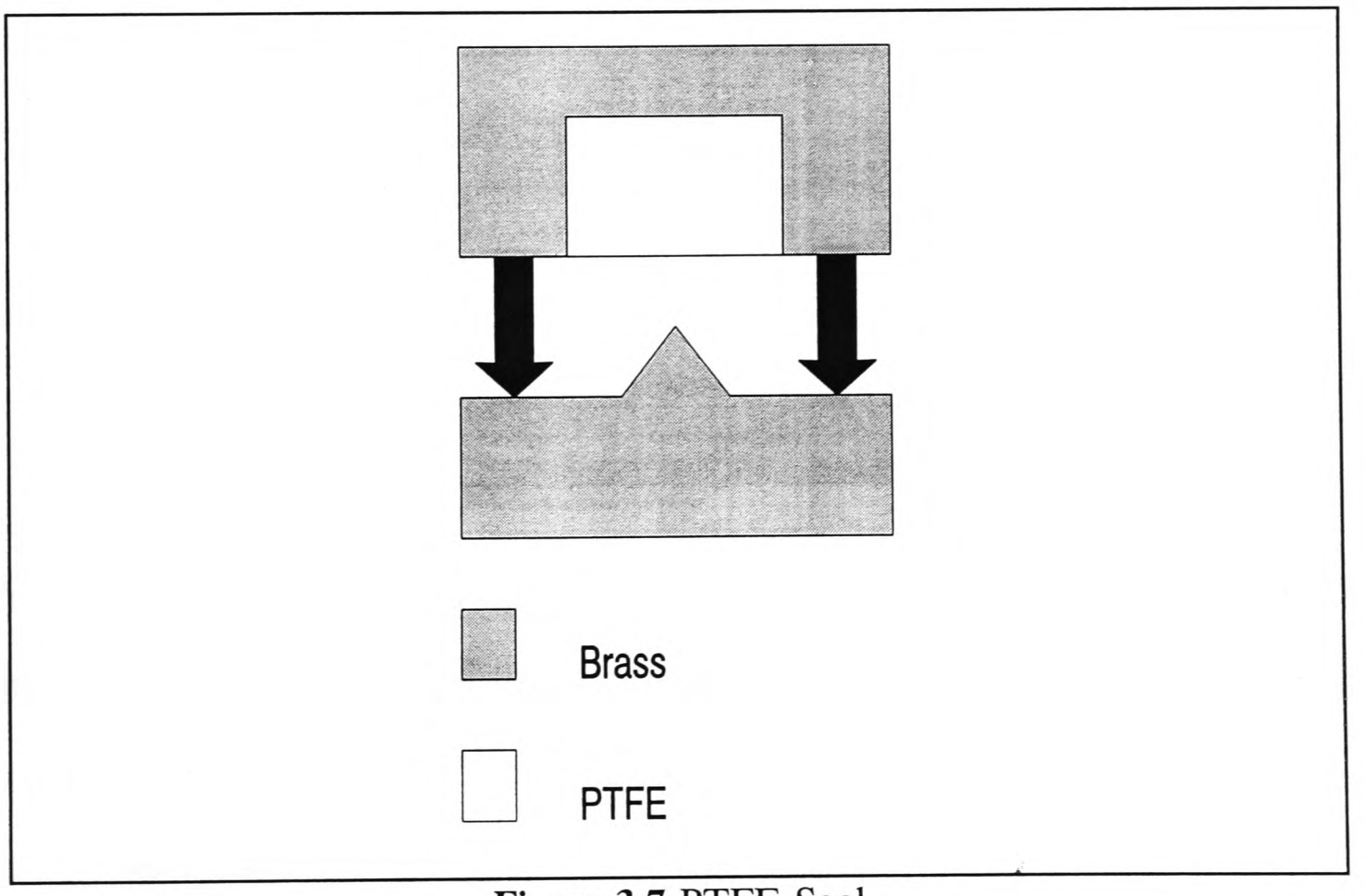

Figure 3.7 PTFE Seal

seals have been used to prevent liquid nitrogen leaking in around the SMA connectors (these were designed by Shri S.V. Kale).

The results from the computer predictions (Appendix D) are given below.

Resonant Frequency: 5.549 GHz

R: 0.0154

Q_r: 2.13×10^{11}

In comparison, the resonant frequency of the constructed DR was found to be 5.578 GHz at 77K. The frequency agreement is within 0.5% and the inaccuracy was caused by polishing errors and thermal contraction of the puck. To calculate Q_r it has been assumed that the R_s of the brass box walls is 38.8 mΩ at 5.549 GHz [3.32] and the radius of the box walls is 26mm. The result for R indicates that only a small amount of energy is present outside the dielectric. This suggests that the mode was trapped well within the sapphire [3.25]. Also for a tan δ of 10^{-7} the dielectric Q is:

$$Q_d = \frac{1 + R}{\tan\delta} = \frac{1 + 0.0154}{10^{-7}} = 1.0154 \times 10^7$$

The highest DR unloaded Q reported is 1.4×10^7 at 5.552 GHz and 4.2K [3.31]. This implies that for most situations the radiation Q (Q_r) can be ignored and for only the highest quality films does the loss tangent of the sapphire need to be included in the calculations for the DR unloaded Q. Hence:

$$\frac{1}{Q} \approx \frac{1}{Q_c}$$

In conclusion, the above analysis has compared theoretical and practical measurements of a DR and has given particular consideration to losses in the box walls which has been overlooked in the past.

3.6.2.1 Results

Before using the DR to test superconducting films it was used to find the R_s of two copper plates in order to prove its accuracy. For a sapphire puck of radius 12.7mm, length 12mm, R=0.0154 and ϵ_r=9.32 equation (C.42) (Appendix C) becomes:

$$R_s = 1.255\times10^{-27}\left(\frac{f^3}{Q_o}\right)$$

For copper, Q_o was measured as 17,439 at 80K and 5.578 GHz which gives the R_s as 12.49 mΩ which scales to 16.7 mΩ at 10 GHz (using a $f^{0.5}$ scaling). The plates were then tested in a 10 GHz end wall replacement cavity which gave a average R_s of 17.0 mΩ at the same temperature. These values are in good agreement. Table 3.6 gives the R_s results for films tested using the DR at 77K. At 0 dB attenuation, the input power is -10 dBm.

Film	R_s scaled to 10 GHz, 77K (mΩ)	Attenuation (dB)
A394	6.13±4.0% 4.64±8.2% 4.37±14.0%	0 20 40
A398	19.55±4.0% 16.56±8.2% 16.11±14.0%	0 20 40
LaB5	117±4.0%	0
LaB6	14.55±4.0% 15.04±8.2% 14.45±14.0%	0 20 40
LaB7	84±4.0%	0
LaB8	12.73±4.0% 13.04±8.2% 13.55±14.0%	0 20 40
LaB9	5.81±4.0%	0

Table 3.6 Film Results

During the measurements it was found that the insertion loss varied by ±0.2 dB at 0 dB attenuation, ±0.9 dB at 20 dB attenuation and ±1.5 dB at 40 dB attenuation. This occurred because at higher attenuations the total insertion loss measured (including the attenuation) is larger and so the error will be larger. The loaded Q for all attenuations was found to vary by ±500. This leads to the errors shown above. The resonant frequency in all the tests was found to be 5.578 GHz. To illustrate how the values above were obtained the following example is given for A394, A398 and LaB6. Table 3.7 shows the measurements obtained for these films.

Sample Combination	Insertion Loss (dB)±0.2	Loaded Q±500	Q_o (upper) Q_o (nominal) Q_o (lower)	Average R_s (10 GHz) (mΩ)
A394, A398	6.30	28,100	56,684 54,476 52,387	12.84 (-3.8%, +4.0%)
A398, LaB6	14.4	33,233	41,880 41,034 40,202	17.05 (-2.0%, +2.1%)
A394, LaB6	9.56	45,160	69,225 67,672 66,172	10.34 (-2.2%, 2.3%)

Table 3.7 R_s Measurement Example

The relationship between loaded Q (Q_L) and unloaded Q (Q_o) is:

$$Q_o = \frac{Q_L}{1 - 10^{-IL/20}}$$

where: IL=insertion loss (dB)

The R_s values in the final column can then be used to solve simultaneously for the individual R_s values for A394, A398 and LaB6 giving the results in Table 3.6. The largest R_s error in Table 3.7 is +4.0% and this has therefore been used as the error for all the measurements. Similar calculations for the other power levels give maximum errors of 8.2% at 20 dB attenuation and 14.0% at 40 dB attenuation.

Films A394 and A398 are YBCO on CeO_2-buffered sapphire. The others are Tl(2212) on $LaAlO_3$. Film A398 was returned to NKT who then cut it into four 1 cm square pieces. These were then tested using the PEWR technique (the results for

these are given in section 3.5.1). Using the PEWR and DR results it is possible to investigate the relationship between R_s and frequency. Table 3.8 summarizes this.

Sample	T (K)	R_s (mΩ)	f (GHz)	Relation
A398 (2" wafer)	77	5.02±0.70	5.578	-
A398A (1cm x 1cm)	80	785.3±3.0	39.3	2.59±0.07
A398C (1cm x 1cm)	80	345.8±3.0	39.3	2.17±0.07
A398H (1cm x 1cm)	Did	not	super-	conduct
A398L (1cm x 1cm)	80	155.7±3.0	39.3	1.76±0.07

Table 3.8 DR/PEWR Comparison

The relation column shows the $R_s \propto f^n$ relation. The average is n=2.17±0.07.

3.6.3 23 and 24.75 GHz Dielectric Resonators

Having confirmed the operation of a 5.58 GHz DR a smaller DR was constructed for testing 1 cm square films. Mode charts provided by Kobayashi and Tanaka [3.25] were used as a first approximation to find suitable dimensions for the sapphire puck to be used. This meant that the TE_{011} mode would be isolated as much as possible from other modes within the sapphire and a resonant frequency that was below 40 GHz was obtained so that a 40 GHz network analyzer could be used. The dimensions chosen were 4 mm diameter and 4 mm length. Using the computer predictions once again the following values were obtained:

Resonant frequency: 24.429 GHz

R = 0.0610

$$Q_r = 7.6328 \times 10^{11}$$

The Q_r value is based upon a box wall radius of 4.5 mm and the box was made of brass as before. Fig. 3.8 shows a picture of the device.

This device did not make use of the PTFE sealing rings used for the larger DR. Instead it was placed inside a hermetically sealed stainless steel vacuum jacket. This has SMA connectors mounted at the top and can be submerged in liquid nitrogen for cooling. Fig. 3.9 shows the arrangement. Due to the larger thermal mass and no direct contact between the DR and the liquid nitrogen the lowest temperature that can be achieved with this set-up is approximately 79K.

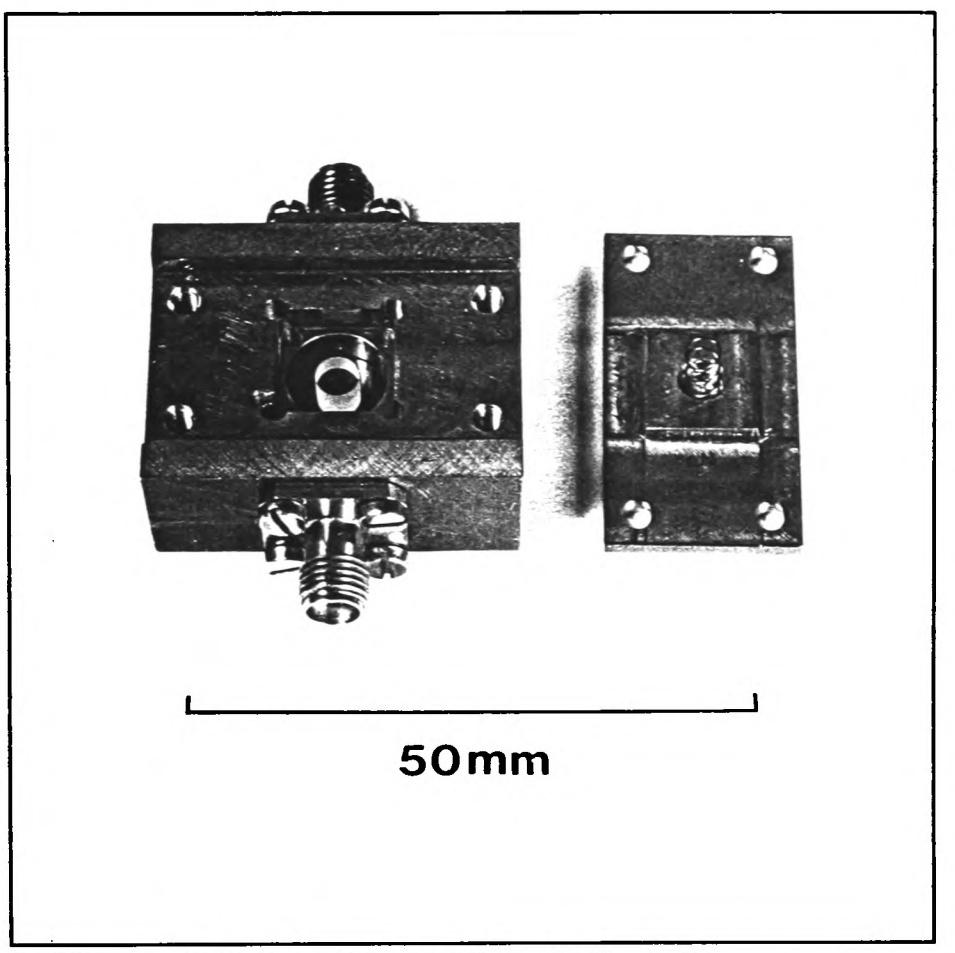

Figure 3.8 Small sapphire dielectric resonator

The temperature of the DR was measured using a commercial silicon diode (IN4148) that had been calibrated in a cryostat. The voltage across the diode was measured with a constant current passing through it and this was converted into a temperature reading. The DR's Q and temperature were monitored with a HPIB control and a PC.

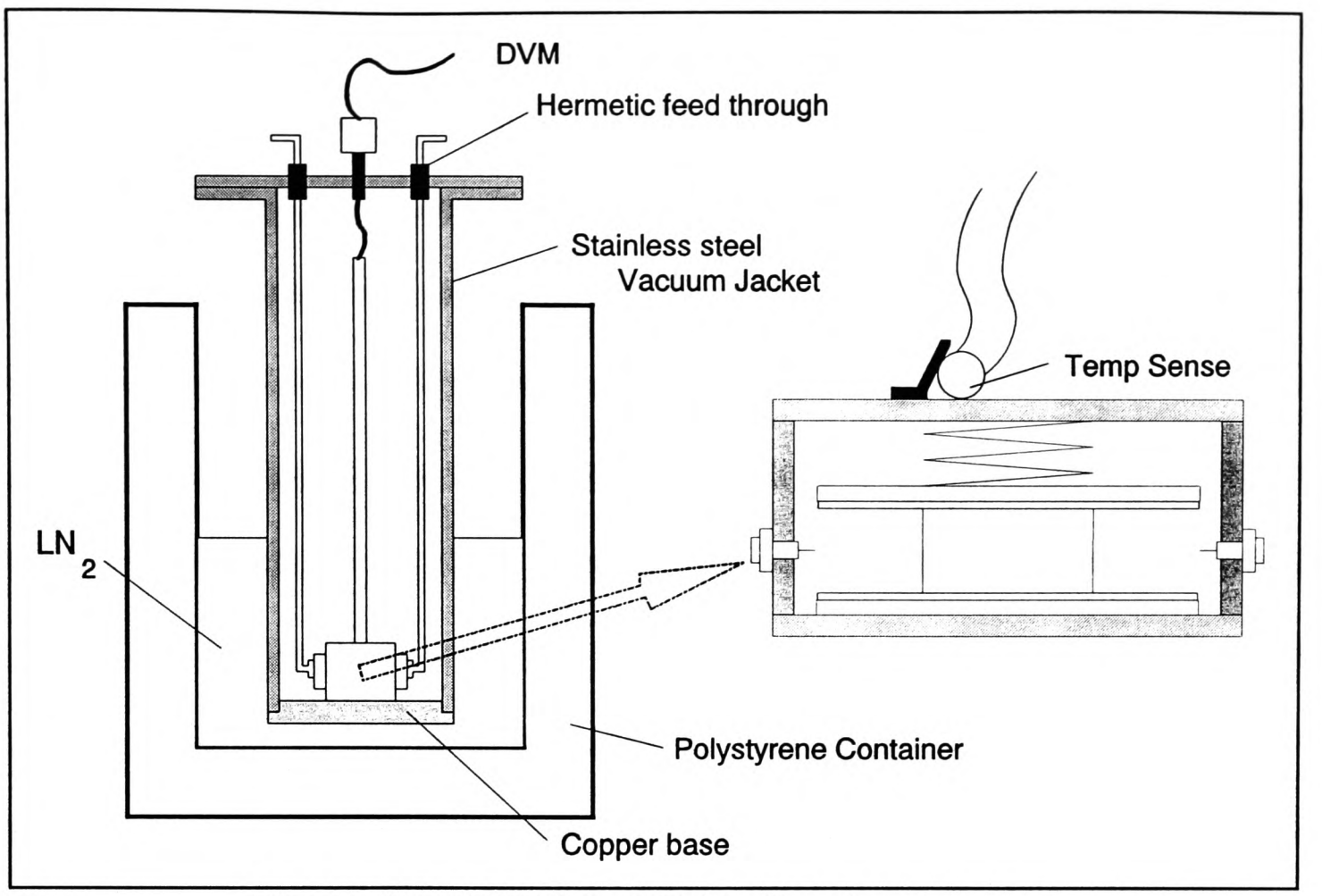

Figure 3.9 24.75 GHz DR Cooling Arrangement

3.6.3.1 Results

After an initial test of this DR with two 1cm square copper pieces (which gave an R_s of 14.0 mΩ at 80K and scaled to 10 GHz) two HTS films, La99 and La100 (Tl(2212) on $LaAlO_3$), were tested. The results are given in Table 3.9.

Temperature (K)	80.0
Resonant Frequency (GHz)	24.753
Insertion Loss (dB)	21.5
Loaded Q	83322
Unloaded Q	90991±1.0%
Average R_s (mΩ)	5.59±1.0%

Table 3.9 La99, La100 R_s Results

The discrepancy between the theoretical and measured resonant frequencies is 1.3% due to inaccuracies in the polishing and thermal contraction of the puck. These films were also tested by the Physics Department, Bergische University, Wuppertal, Germany in an 87 GHz full end wall replacement cavity. The results obtained at 80K were 16.627 mΩ and 14.854 mΩ for La99 and La100 respectively giving an average R_s of 15.74 mΩ at 87 GHz. Taken with the DR results above this would imply a frequency scaling for R_s of 0.82 which is highly divergent with the usual f^2 scaling found in superconductors. Using this scaling the Wuppertal results would produce an average R_s at 24.753 GHz of only 1.27 mΩ ($15.74x(24.753/87)^2=1.27$). This suggested that perhaps the tan δ of sapphire should not be ignored in the calculation for R_s when using the DR.

At the same time as the 4 mm length sapphire puck, two $LaAlO_3$ pucks were obtained to investigate the operation of a DR using a different dielectric. The dimensions chosen were 1.75mm length x 4mm diameter and 3.5mm length x 4mm diameter. The computer predictions were again used to find their frequency of operation, R and Q_r giving:

Resonant frequency: 23.129 GHz

$R = 0.0046$

$Q_r = 5.15x10^{13}$

The Q_r value assumes a box wall radius of 4.5mm and that these walls are made of brass. The 1.75mm length puck operates in the TE_{011} mode and the 3.5mm length puck in the TE_{012} mode. By doubling the length of the puck the conductor Q, Q_c is

doubled as we have twice the stored energy, but surface area of the films remains constant giving the same film losses. Q_d remains the same and so it is possible to determine tan δ for the dielectric used as well as the average R_s. That is:

$$\frac{1}{Q_1} = \frac{1}{Q_c} + \frac{1}{Q_d}$$

$$\frac{1}{Q_2} = \frac{1}{2Q_c} + \frac{1}{Q_d}$$

$$\Rightarrow \quad \frac{1}{Q_d} = \frac{2}{Q_2} - \frac{1}{Q_1} = \frac{\tan\delta}{1 + R}$$

where: Q_1 = unloaded Q from 1.75mm puck DR

Q_2 = unloaded Q from 3.5mm puck DR

The results for La99 and La100 tested in these two DRs are given in Table 3.10.

Length (mm)	1.75	3.5
Temperature (K)	80	80
Resonant Frequency (GHz)	22.854	23.226
Insertion Loss (dB)	12.6	15.1
Loaded Q	36685	43826
Unloaded Q	47877±1%	53223±1%

Table 3.10 $LaAlO_3$ DR R_s Results

The discrepancy in the resonant frequency compared to the theoretical value is 1.2% and 0.4% for the 1.75mm and 3.5mm length pucks respectively due to polishing errors and thermal contraction. For the purposes of calculation, an average frequency was taken of 23.04 GHz. The value for tan δ for $LaAlO_3$ obtained was $1.68\text{x}10^{-5}$±3.7% at 80K and 23.04 GHz (the error bound is due to the ±1% variation in the unloaded Q measurements). Assuming that tan $\delta \propto f$ [3.3] then this scales to

7.28×10^{-6} at 10 GHz. This value can be contrasted with the values given in Table 3.11 (all measured at 77K except for the experimental result which was measured at 80K, as described above).

tan δ	Frequency (GHz)	tan δ at 10 GHz	Reference
1.68×10^{-5}	23.04	7.28×10^{-6}	Experimental
0.76×10^{-5}	10	7.6×10^{-6}	[3.5]
10^{-4} 9×10^{-6} 5×10^{-6}	18 18 18	55.6×10^{-6} 5×10^{-6} 2.78×10^{-6}	[3.4]

Table 3.11 $LaAlO_3$ tan δ Values

As can be seen the tan δ of $LaAlO_3$ can vary depending on the supplier [3.4], but is generally of the order 10^{-6} at 10 GHz and 80K.

Having found the loss tangent for the $LaAlO_3$, the average R_s obtained for the two films is given by:

$$\frac{1}{Q_1} - \frac{1}{Q_2} = \frac{1}{2Q_c}$$

Substituting equation (C.42) (Appendix C):

$$\frac{1}{Q_1} - \frac{1}{Q_2} = \frac{1}{2}\left[\frac{R_s}{240\pi^2\epsilon_r}\left(\frac{c}{df}\right)^3 \frac{1 + \epsilon_r R}{1 + R}\right]$$

For the 1.75mm and 3.5mm pucks with ϵ_r=24 and f=23.04 GHz this gives:

$$R_s = 249.73 \times \left[\frac{1}{47{,}877 \pm 1\%} - \frac{1}{53{,}223 \pm 1\%} \right] = 5.24 \times 10^{-4}\ \Omega \pm 18.9\%$$

Using the Wuppertal results once again (15.74 mΩ at 87 GHz and 80K) this gives a frequency scaling in the range 2.43-2.72. This is much more in line with other scaling measurements performed by other groups [3.33-3.36]. Using the 2.43-2.72 scaling range, the R_s is in the range 54-69 $\mu\Omega$ at 10 GHz.

3.6.4 Analysis

For all the DRs constructed it was found that the box walls do not affect the performance of the device. Radiation Qs were very much larger then the unloaded Qs measured during R_s testing. However, the calculation of radiation Q was deemed necessary as this part of the DR theory was somewhat neglected in the past. It also served the purpose of showing that the construction was done in a rigorous fashion.

However, the dielectric Q was found to affect the performance of the sapphire DRs. Sapphire is not as low loss as reported by some researchers [3.19, 3.37-3.39] and tan δ needs to be considered in the R_s calculations unless it is known that the puck has come from a reliable supplier with a loss tangent less than around 10^{-7}.

Using two pucks to measure R_s overcomes the loss tangent problem to some extent, but even then inaccuracies in the R_s value become larger as the unloaded Q reaches

the limiting Q of the DR. For instance, for the $LaAlO_3$ DRs the limiting Q is given by:

$$Q_{limit} = \frac{1 + R}{\tan\delta} = \frac{1 + 0.0046}{1.68\times10^{-5}} = 59{,}798$$

The values for unloaded Q from Table 3.10 are 47,877 and 53,223 which are close to Q_{limit} and hence we have a $\pm$18.9% error in the R_s.

Using the average R_s of La99 and La100 of 0.524 mΩ at 23.04 GHz and 80K it is possible to estimate the tan δ of sapphire. Using a frequency scaling factor of 2.56 (the nominal value of the 2.43-2.72 range given above) we obtain a R_s of 0.630 mΩ at 24.753 GHz. Therefore tan δ is given by:

$$\frac{1}{Q_o} = \frac{R_s}{240\pi^2\epsilon_r}\left(\frac{\lambda}{d}\right)^3\frac{1 + \epsilon_r R}{1 + R} + \frac{\tan\delta}{1 + R}$$

$$\frac{1}{90991} = 1.173\times10^{-6}\pm18.9\% + \frac{\tan\delta}{1.0610}$$

$$\tan\delta = 1.04\times10^{-5}\pm2.4\%$$

Assuming tan $\delta \propto$ f this scales to $2.3\text{x}10^{-6}\pm2.4\%$ at 5.58 GHz. This value could be used to adjust the R_s values in Table 3.6, but one would have to assume that the loss tangent of the 5.58 GHz puck is the same as that for the 24.753 GHz puck. Secondly, as the value of (1+R)/tan δ is an order of magnitude higher than any of the unloaded Qs measured during testing with the 5.58 GHz DR there will only be a maximum of 10% error in the results in Table 3.6. However, for films with lower R_s values higher quality sapphire will need to be used.

3.7 Conclusions

This chapter has presented practical results from the different methods used to measure the R_s of superconducting films. The parallel plate resonator was shown to be a technique that requires careful set-up in order to achieve consistency in results and that it exaggerates the effects of low quality film at the edges of substrates.

The end wall replacement method is well known and was found to be reliable in measuring R_s. It was particularly useful for testing TBCCO thick films deposited onto zirconia substrates. One of these samples (CD02) had a R_s of 2.7 mΩ at 10 GHz and 77K which is one of the lowest R_s values to be recorded in the world for a thick film.

The microstrip resonator method was, like the parallel plate resonator, found to depend critically upon the quality of film edges. The major advantage of using this technique to measure R_s is that it gives an indication of what might be expected from a film that is going to be used to make a device. The other tests described are useful as non-destructive quality assurance.

The PEWR method has the major advantage that it is able to test small size films at fairly low frequencies obviating the need for expensive test equipment. However, its accuracy degrades as the unloaded Q of the cavity approaches the limiting Q. Films having a R_s of around 500 $\mu\Omega$ at 10 GHz have error bounds of around $\pm$20%.

The dielectric resonator is an accurate method for measuring R_s providing that high quality dielectrics can be found. DRs have been constructed to test two inch and 1cm square samples showing that the technique is adaptable to different sample sizes and frequencies. A 5.58 GHz DR together with the PEWR technique has been used to investigate the relationship between R_s and frequency. This has obtained the result that $R_s \propto f^{2.17\pm0.07}$ which is in line with other research [3.33-3.36]. Further work may consider the possibility of using higher resonant frequency DRs so that the difference in scaling for tan δ and R_s against frequency works in favour of more accurate results and tan δ can be considered negligible. The results obtained using sapphire pucks are somewhat anomalous and this has been investigated by use of $LaAlO_3$ puck DRs and it has been concluded that this effect can be put down to the poor tan δ of sapphire.

3.8 References

[3.1] Werder D.J., Liou S.H. (1991) "Epitaxial $Tl_2Ba_2Ca_2Cu_3O_{10}$ on (0,0,1) $LaAlO_3$ substrates". *Physica C* 179: 430-436.

[3.2] Subramanian M.A. et al (1988) "Crystal structure of the high-temperature superconductor $Tl_2Ba_2CaCu_2O_8$". *Nature* 332(31): 420-422.

[3.3] Hollmann E.K. et al (1994) "Substrates for high-T_c superconductor microwave integrated circuits". *Superconductor Science and Technology* 6(1): 1-13.

[3.4] Krupka J. et al (1994) "Dielectric properties of single crystals of Al_2O_3, $LaAlO_3$, $NdGaO_3$, $SrTiO_3$ and MgO at cryogenic temperatures". *IEEE Transactions on Microwave Theory and Techniques* 42(10): 1886-1890.

[3.5] Konaka T. et al (1991) "Relative permittivity and dielectric loss tangent of substrate materials for high-T_c superconducting film". *Journal of Superconductivity* 4(4): 283-288.

[3.6] York R.A., Compton R.C. (1990) "Experimental evaluation of existing CAD models for microstrip dispersion". *IEEE Transactions on Microwave Theory and Techniques* 38(3): 327-328.

[3.7] Macdonald P. et al (1994) "HTS microstrip matching networks and filters". *IEEE Transactions on Microwave Theory and Techniques* 42(3): 523-525.

[3.8] Toradi C.C. et al (1988) "Crystal structure of $Tl_2Ba_2Ca_2Cu_3O_{10}$, a 125K superconductor". *Science* 240: 631-633.

[3.9] Kale K.S. et al (1996) "TBCCO thin films and passive microwave devices". In U. Balachandran (ed.) *Proceedings of the TMS Annual Meeting, Anaheim, CA, USA, February*. Warrendale, PA: TMS, in press.

[3.10] O'Connor J.D. et al (1996) "Low temperature processing of superconducting $Tl_2Ba_2Ca_1Cu_2O_x$ films on CeO_2 buffered sapphire". *Applied Physics Letters* 69(1): 115-117.

[3.11] Glassey B.J. (1995) *Synthesis of chromium and lead doped thallium based superconducting thin films*. Unpublished Fourth Year Dissertation, University of Oxford.

[3.12] Nabatame T. et al (1990) "Properties of $Tl_2Ba_2Ca_2Cu_3O_{10}$ thin films with a critical temperature of 122 K prepared by excimer laser ablation". *Japanese Journal of Applied Physics* 29(10): L183-L185.

[3.13] Bramley A.P. et al (1995) "Buffer layer film interaction in the growth of $Tl_2Ba_2CaCu_2O_x$ films on CeO_2-buffered sapphire". *Applied Physics Letters* 66(4): 517-518.

[3.14] Su L.Y. et al (1995) "Superconducting and microwave properties of spray pyrolized $Tl_2Ba_2Ca_2Cu_3O_x$ films on 1 inch polycrystalline zirconia disks". *Applied Physics Letters* 66(12): 1542-1544.

[3.15] Huang S. et al (1995) "Highly reproducible high critical current density in partial-melt $Bi_2Sr_2CaCu_2O_y$/Ag tapes fabricated by electrophoretic deposition". *Superconductor Science and Technology* 8(1): 32-40.

[3.16] Jenkins A.P. et al (1995) "Microwave surface resistance measurements of air-atomised spray deposited Tl-Ba-Ca-Cu-O thick films". *IEEE Transactions on Applied Superconductivity* 5(2): 1095-1098.

[3.17] Jenkins A.P. (1994) *Microwave Applications of High-Temperature Superconductors*. Unpublished D.Phil. thesis, University of Oxford.

[3.18] Matula R.A. (1979) *Journal of Physical Chemistry Reference Data* 8: 1147.

[3.19] Holstein W.L. et al (1993) "Surface resistance of large area $Tl_2Ba_2CaCu_2O_8$ thin films at microwave and millimeter wave frequencies measured by three noncavity techniques". *Journal of Superconductivity* 6(3): 191-200.

[3.20] Jenkins A.P. et al (1996) "Surface resistance measurement techniques". In A.V. Narlikar (ed.) *Studies in High Temperature Superconductors* Vol. 17 (Part I). New York, NY: Nova Science Publishers: 179-219.

[3.21] Martens J.S. et al (1991) "The effects of processing sequences on the microwave surface resistance of TlBaCaCuO". *Journal of Applied Physics* 69(12): 8268-8271.

[3.22] Bohn C.L. et al (1989) "Radio frequency surface resistance of large area Bi-Sr-Ca-Cu-O thick films on Ag plates". *Applied Physics Letters* 55(3): 304-306.

[3.23] Holstein W.L. et al (1992) " $Tl_2Ba_2CaCu_2O_8$ films with very low microwave surface resistance up to 95 K". *Applied Physics Letters* 60(16): 2014-2016.

[3.24] Edwards J.A. et al (1994) "Effects of small changes in composition on the microwave properties of YBCO thin films". *Proceedings of the Microwave Properties and Applications of High Temperature Superconductors Conference*, 19 April. Oxford: University of Oxford.

[3.25] Kobayashi Y., Tanaka S. (1980) "Resonant modes of a dielectric rod resonator short-circuited at both ends by parallel conducting plates". *IEEE Transactions on Microwave Theory and Techniques* 28(10): 1077-1085.

[3.26] Kobayashi Y., Katoh M. (1985) "Microwave measurements of dielectric properties of low-loss materials by the dielectric rod resonator method". *IEEE Transactions on Microwave Theory and Techniques* 33(7): 596-592.

[3.27] Kobayashi Y., Senju T. (1993) "Resonant modes in shielded uniaxial-anisotropic dielectric rod resonators". *IEEE Transactions on Microwave Theory and Techniques* 41(12): 2198-2205.

[3.28] Cohn S.B., Kelly K.C. (1966) "Microwave measurement of high-dielectric constant materials". *IEEE Transactions on Microwave Theory and Techniques* 14(9): 406-410.

[3.29] Hakki B.W., Coleman P.D. (1960) "A dielectric resonator method of measuring inductive capacities in the millimeter range". *IRE Transactions on Microwave Theory and Techniques* 8(4): 402-410.

[3.30] Snitzer E. (1961) "Cylindrical dielectric waveguide modes". *Journal of the Optical Society of America* 51(5): 491-498.

[3.31] Shen Z. et al (1992) "High T_c superconductor-sapphire microwave resonator with extremely high Q-values up to 90K". *IEEE Transactions on Microwave Theory and Techniques* 40(12): 2424-2432.

[3.32] Howatson A.M. et al (1990) *Engineering Tables and Data*, 5th ed. London: Chapman and Hall.

[3.33] Chang L.D. et al (1989) "Microwave surface resistance in Tl-based superconducting thin films". *Applied Physics Letters* 55(13): 1357-1359.

[3.34] Martens J.S. et al (1991) "Confocal resonators for measuring the surface resistance of high-temperature superconducting films". *Applied Physics Letters* 58(22): 2543-2545.

[3.35] Delayen J.R. et al (1990) "Measurements of surface resistance of high-T_c superconductors at high RF fields". *Journal of Superconductivity* 3(3): 243-250.

[3.36] Cooke D.W. et al (1990) "Frequency dependence of the surface resistance in high-temperature superconductors". *Solid State Communications* 73(4): 297-300.

[3.37] Braginsky V.B. et al (1987) "Experimental observation of fundamental microwave absorption in high-quality dielectric crystals". *Physics Letters A* 120(6): 300-305.

[3.38] Blair D.G., Sanson A.M. (1989) "High Q tunable sapphire loaded cavity resonator for cryogenic operation". *Cryogenics* 29(11): 1045-1049.

[3.39] Klein N. et al (1992) "Microwave surface resistance of epitaxial $YBa_2Cu_3O_7$ thin films at 18.7 GHz measured by a dielectric resonator technique". *Journal of Superconductivity* 5(2): 195-201.

Chapter 4

Microwave Applications

Conventionally, passive microwave devices, such as resonators, filters, delay lines and mixers, that require high Qs and/or low losses used in satellites are manufactured from either normal metal waveguide or coaxial elements. Low losses from these components come about because the stored energy is proportional to volume, the dissipated energy to surface area and:

$$Q = 2\pi f \frac{time\ average\ stored\ energy}{energy\ loss\ per\ second}$$

where: f=resonant frequency of device.

Therefore, there is an advantage in having larger components. However, this is in direct contradiction to keeping the weight and volume of satellites to a minimum. Hence, there has been much interest in the use of HTS thin films deposited onto substrates which can then be patterned into devices that perform to the same level, or better, than their waveguide or coaxial counterparts [4.1-4.3]. The low R_s of HTS compared to normal metals makes such advances possible. Fig 4.1. shows a block diagram of a typical satellite front end. This diagram will be referred to in the course of this chapter.

HTS does have an extra weight penalty added to its implementation in satellites and this is the cooling required. Research has been done into the possibility of

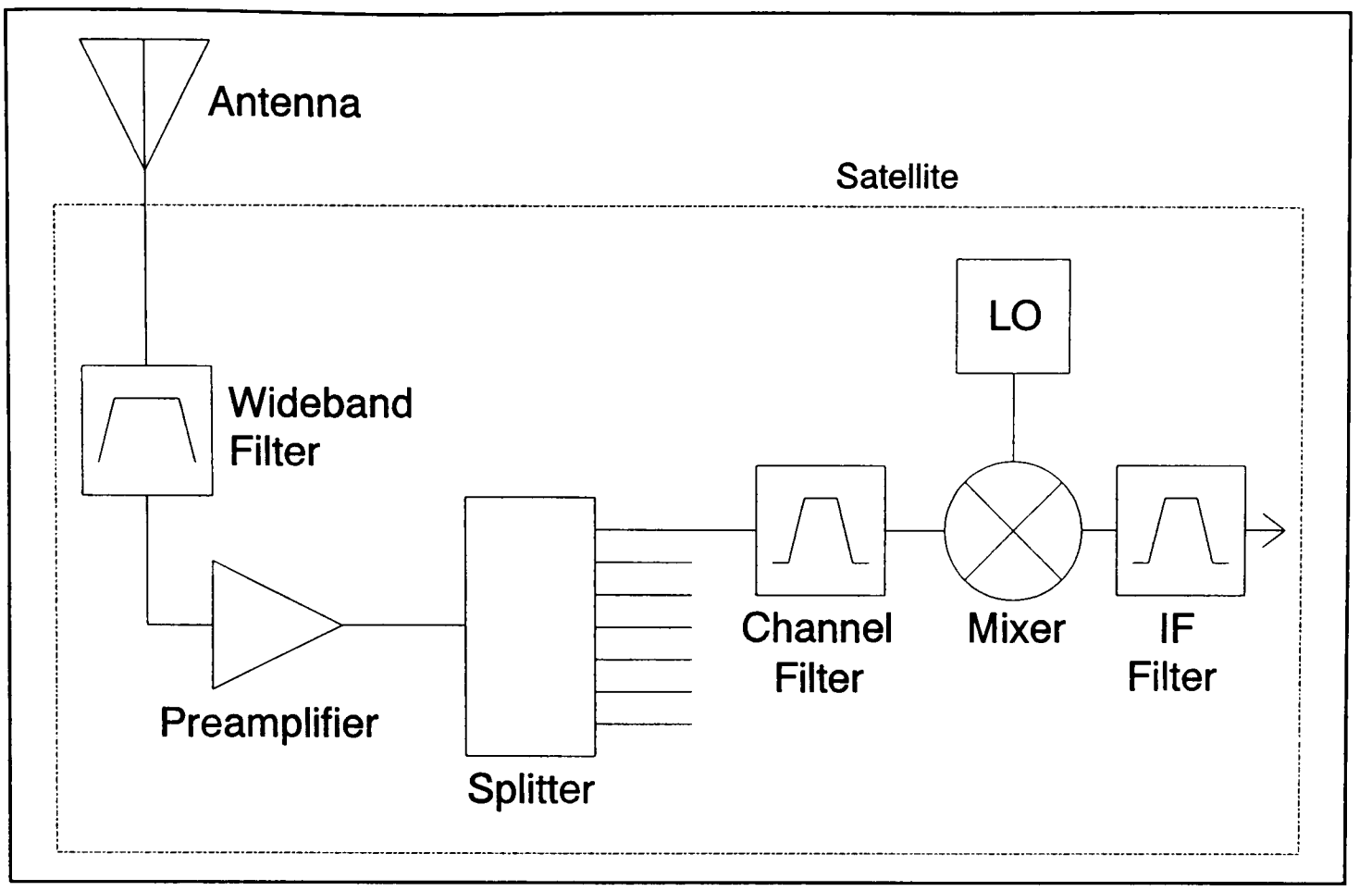

Figure 4.1 Satellite Front End

implementing this using liquid cryogens, but this has been unacceptable to microwave systems engineers who demand cooling with high reliability. This has meant the development of compact closed cycle coolers [4.4]. Despite this extra weight, at a systems level, there are financial benefits to using HTS over conventional technology [4.5].

Even more recent has been the suggestion that HTS technology be used for wireless communications, which is the fastest growing area of the communication industry [4.5]. HTS devices that may find use here are ultra-high performance filters and low-noise figure receiver front ends [4.6]. These would be used in base stations situated across a country and would again require reliable coolers that would operate with minimal maintenance. With the R_s scaling with the square of the frequency for HTS

and mobile communications typically operating at frequencies an order of magnitude lower than for satellites there are even more performance enhancing opportunities for mobile than satellite communications [4.7].

This chapter will examine the many uses of HTS for microwave devices that have been suggested and built by research and commercial groups around the world. It will be seen that these devices are already producing performance enhancements over conventional technology.

4.1 Device Geometries

As the lowest R_s values have been achieved in thin films deposited onto substrates such as MgO, $LaAlO_3$ or sapphire with good microwave properties, rather than thick films, the greatest performance enhancements may be expected from devices patterned from these thin films. In addition, thick films, although allowing for non-planar deposition - holding out the possibility of HTS cavities to replace normal metal cavities to produce high Qs - would not deliver the significant volume savings possible with the use of thin films. Another advantage of thin films is the opportunity to integrate passive devices with active semiconductor components on the same substrate. The well known, accurate and easy patterning methods used in the semiconductor industry can then be exploited to produce hybrid devices. There are a number of geometries that may be used with thin films on substrates (Fig. 4.2).

All these geometries can be regarded as variations on a theme and as effectively being unfolded coaxial transmission lines. Coplanar waveguide (marked Coplanar in Fig. 4.2) is the simplest geometry as it only requires the deposition of a single layer on a substrate. It is composed of a main upper conductor line in the centre and ground planes on either side. However, it suffers from the most radiation losses. In this respect, Stripline is much better as it has two dielectric layers to confine the propagating wave, but this adds to the cost and volume of a device. Microstrip is perhaps the optimum geometry and is a good compromise between Coplanar and Stripline as it has a ground plane below which helps to confine the wave, but at the

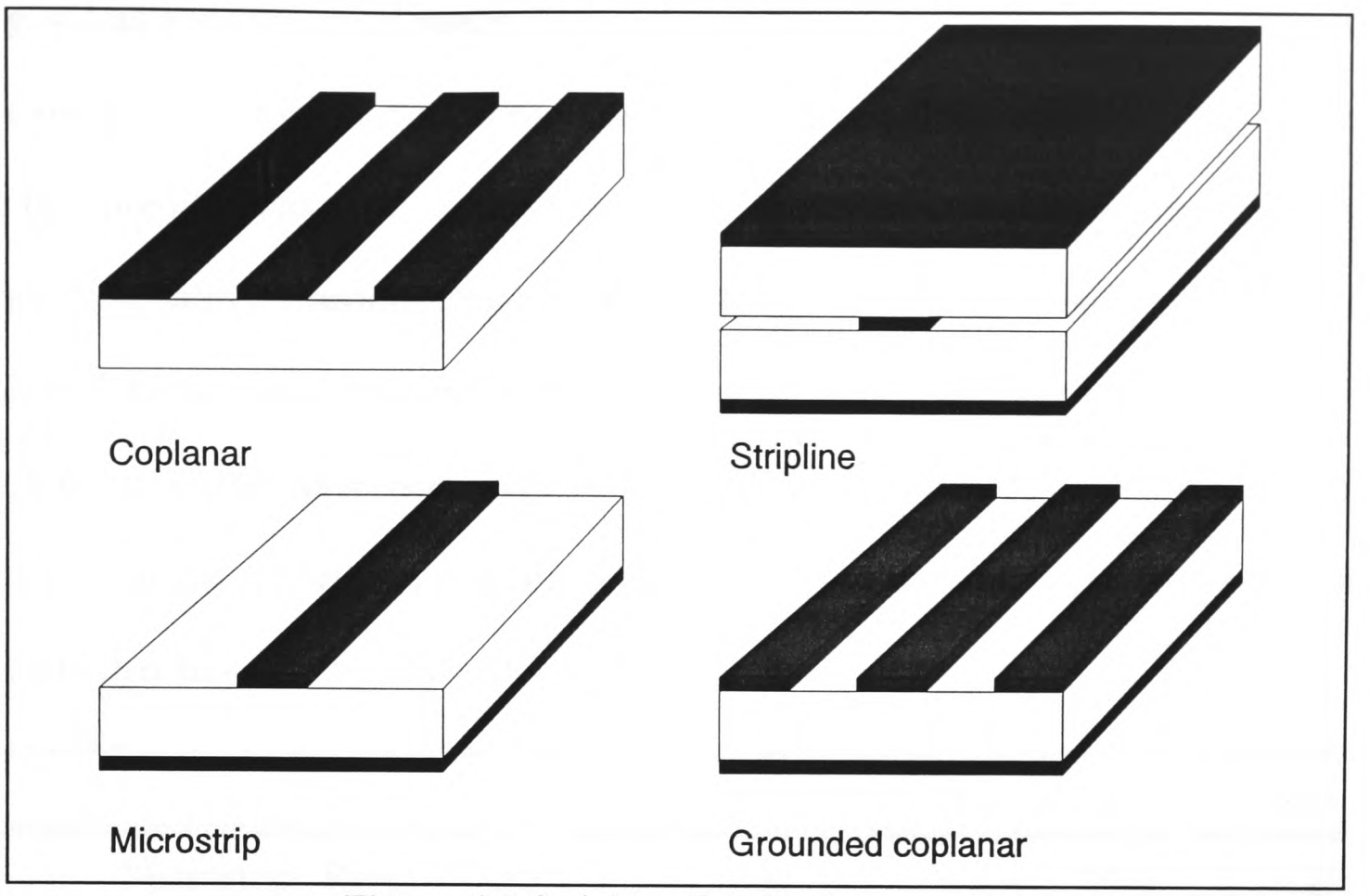

Figure 4.2 Stripline Family Geometries

same time does not require extra dielectric material. Finally, Grounded Coplanar waveguide reduces radiation losses in the Coplanar geometry, but is harder to fabricate than Microstrip as the gaps between the main line and the upper ground planes need to be controlled as well as the width of the main line.

4.2 Resonators

Resonators are a fundamental building block for oscillators and are the easiest components to construct using a stripline family geometry. For instance, in microstrip they will simply be made from a length of line patterned onto the top of the substrate with the length defining the resonant frequency and the width the characteristic impedance. They could be used, for instance, in the local oscillator (LO) shown in

Fig. 4.1 as a stabilizing element. The higher the Q of the resonator used to stabilize the oscillator, the lower the phase noise [4.8]. This in turn improves the performance of the satellite electronics as a whole. There are a number of ways to use HTS to make resonators. Previous chapters have already mentioned that Qs as high as 10^6 can be achieved with dielectric resonators [4.9]. Microstrip resonators with loaded Qs as high as 20,000 have been achieved at 5 GHz and 77K [4.10]. This is 50 times better than its copper equivalent at the same temperature. Table 4.1 lists some results that have been achieved.

Type	Q	T (K)	f_o (GHz)	Ref.
Microstrip, Ring, YBCO	90	50	19.2	[4.11]
Microstrip, Ring, YBCO	80	50	6.6	[4.11]
Microstrip, Linear, TBCCO	20,000 (loaded)	90	5	[4.10]
Co-planar Waveguide, Linear, YBCO	1625	77	5	[4.12]
Co-planar Waveguide, Linear, Nb	8150	4	5	[4.12]
Microstrip, Ring, YBCO	550	77	6	[4.13]
Microstrip, Ring, TBCCO	1000	77	12	[4.14]
Microstrip, Linear, YBCO	2800	77	13.3	[4.15]
Dielectric, YBCO plates	$1.3x10^5$	77	11.6	[4.16]
Dielectric, TBCCO plates	$3x10^6$	80	5.55	[4.9]

Table 4.1 Resonator Results

Unless stated the Q values given are unloaded. The last two results are for dielectric resonators with YBCO and TBCCO end-plates respectively. An LTS Nb coplanar waveguide result has also been given. As can be seen the best microstrip resonator

has a Q more than two times the value for the Nb resonator. Therefore, HTS can even improve upon the performance of LTS.

It has also been found that resonators can be tuned by the application of a magnetic field which is an effect that can be used as the basis of a low phase noise voltage controlled oscillator [4.17, 4.18].

4.3 Filters

With the rapid growth in wireless and satellite communications there has been a considerable desire to make better use of the available spectrum of radio frequencies. One area which has raised the interest of commercial customers is HTS high-performance filters [4.5]. Fig. 4.1 shows the possible uses of filters within a rf receiver in a satellite. As can be seen there are three points where an HTS filter may be of use. As one of the advantages of HTS is low losses they have been used for the wideband and channel filter elements where this requirement is most important [4.6, 4.19].

Zhang et al [4.20] have reported a 75% improvement in the quality factor of a 92 GHz centre frequency bandpass filter compared to a similar filter realized in gold. Qs higher than 15,000 have been obtained for TBCCO microstrip filters operating at a centre frequency of 4.66 GHz and at 77K [4.21]. Table 4.2 reviews some research results.

Type	Insertion Loss (dB)	f_o (GHz)	Ref.
M, YBCO, 4P, 1.5% BPF	<1	9	[4.19]
M, YBCO, 3P, 4% BPF	3.6	10	[4.22]
S, TBCCO, 5P, 2.6% BPF	0.1	2.3	[4.23]
M, YBCO, 4P, 2% BPF	<1	13	[4.6]
M, YBCO, 4P, 10% BPF	0.6	13	[4.6]

Table 4.2 Filter Review

Key: M=microstrip
S=stripline
P=poles
BPF=Band Pass Filter. A percentage indicates the proportion of the centre frequency (f_o) that is the bandwidth.

Not only do HTS filters provide the benefit of higher Qs, but they are smaller and lighter than their equivalent copper cavity implementations. For example, a four pole, 9 GHz centre frequency, 1.5% bandwidth bandpass filter built by Talisa et al [4.19] utilized thin films of HTS deposited onto a $LaAlO_3$ substrate 16mm long by 5mm wide. This had an insertion loss of less than 1 dB.

The similar performance copper cavity would be around 150mm long and 50mm in diameter. The space and weight savings are dramatic for satellite applications. The copper equivalent can handle higher powers, but for satellite front ends this is not a pertinent advantage.

A schematic of a microstrip coupled line filter is shown in Fig. 4.3. It consists of four pairs of coupled lines and two feed lines on the extreme left and right sides of the diagram. Each line pair has a different width and spacing and these two parameters

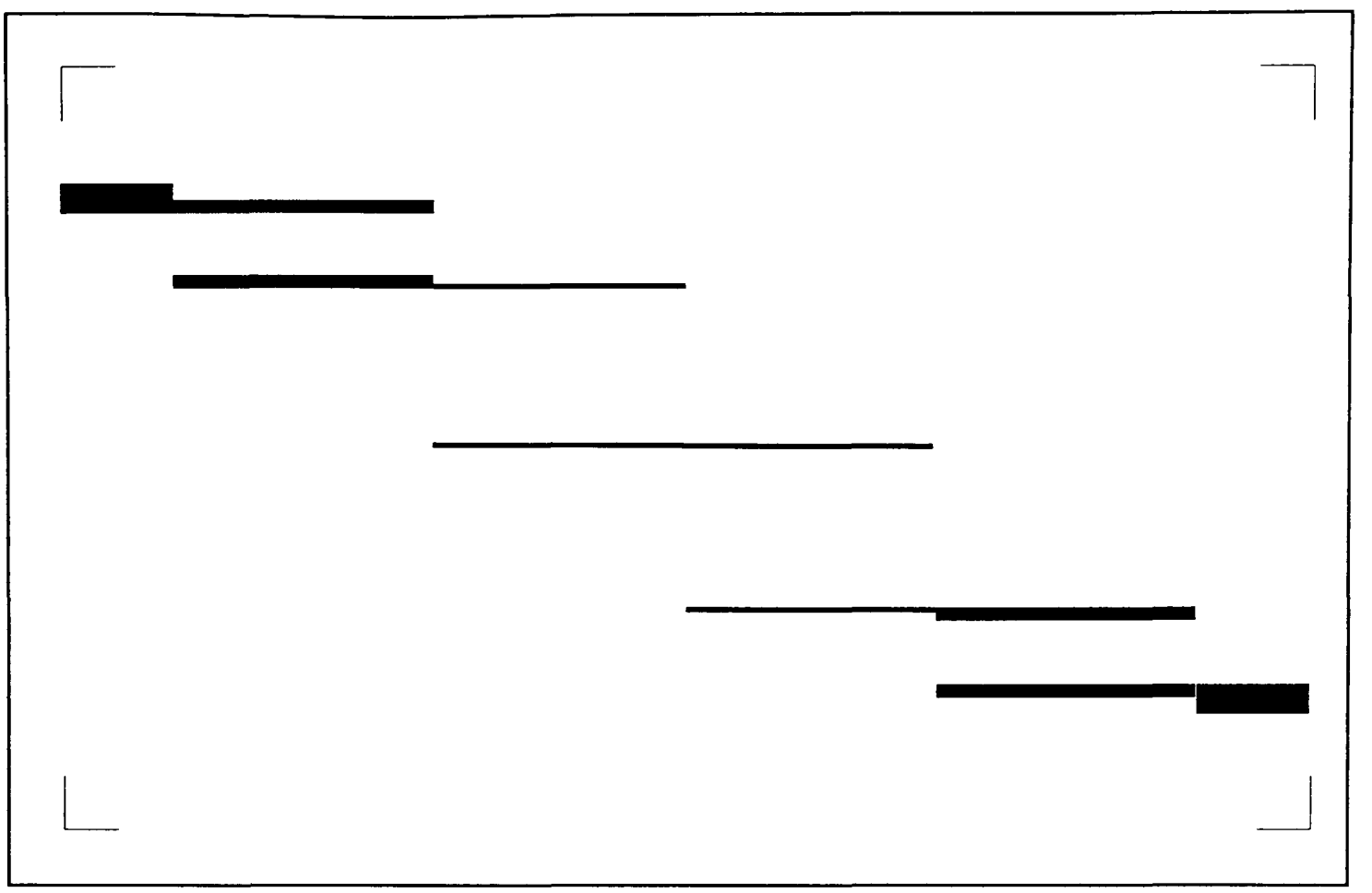

Figure 4.3 Schematic of a 3-pole microstrip filter

define the impedances of a coupled pair. The complete circuit may be regarded as a cascade of parallel and series inductor-capacitor resonant circuits that define the passband of the filter. The lengths of the coupled lines define the centre frequency. This particular filter has three poles. Typical dimensions for a 6 GHz centre frequency, 1% bandwidth bandpass filter on MgO might be:

Line length ~5mm

Line width ~0.3mm

Line spacing ~2mm

Thin films cannot be deposited onto curved surfaces and so it is not possible to make HTS cavity filters by this technique. However, thick films can be spray pyrolized onto curved surfaces and so HTS cavity filters can be made that have walls with a lower R_s than copper or silver and so deliver better performance [4.24]. The difficulty in

this case is the precise control over the spraying technique in order to ensure accurate cavity dimensions.

4.4 Delay Lines

The low R_s of HTS is used to particular advantage for delay lines. For a low loss delay line a coaxial geometry needs to be used with conventional conductors. For typical delays of around 10 ns lengths of about 10m are required. In HTS this can be reduced to 1m or even less in a microstrip geometry which makes use of a dielectric with a high ϵ_r (for instance, $LaAlO_3$) saving space and weight, but still delivering the same low insertion loss. This means that a complete delay line can be built onto a two inch diameter substrate, for example. Table 4.3 reviews some results for HTS delay lines tested at 77K.

Insertion Loss (dB)	Delay (ns)	Loss/Delay (dB/ns)	Reference
2	5	0.4	[4.25]
-	2.9	-	[4.26]
1.5	8.9	0.17	[4.27]
7.5	25	0.3	[4.28]
3	9	0.3	[4.29]

Table 4.3 Delay Line Results

Commercially, the delay line with 25 ns delay [4.28] has the most significance as this item can be bought on the open market and is produced by Du Pont. This demonstrates that HTS devices have real selling potential.

4.5 Mixers

HTS mixers can be made by exploiting deliberately made irregularities such as weak links [4.30] and are usable at frequencies greater than 100 GHz because of the large band gap in HTS [4.31]. The irregularities in HTS create a non-linear I-V characteristic and this is the source of the mixing in much the same way as a diode may be used for heterodyne mixing [4.32].

YBCO, BSCCO and TBCCO mixers have been made operating at rf frequencies greater than 20 GHz [4.31, 4.33-4.36]. A conversion loss of 9 dB and a noise temperature of ~1000K have been measured [4.37, 4.38], which compares favourably with figures of 6 dB and 7900K for a GaAs FET implementation of a similar device [4.39]. Table 4.4 reviews some results.

Material	Frequency (GHz)	IF Signal-to-Noise (dB)	Insertion Loss (dB)	Reference
TBCCO	61	40	-	[4.33]
TBCCO	55, 94	60	-	[4.34]
YBCO	24	-	-	[4.35]
YBCO	25, 55, 110	-	-	[4.37]
YBCO	20	-	8, 32	[4.38]
YBCO	20	20	8	[4.39]

Table 4.4 HTS Mixer Results

4.6 Other Devices

Other more specialized devices have been made or suggested to be made from HTS. These include chirp filters [4.40] and correlators [4.41]. The latter are particularly useful for satellite systems that use spread spectrum techniques and are an adaption of delay line design.

Others have looked at creating hybrid systems using HTS and semiconductor technology. An oscillator that uses an HTS resonator as its stabilizing element in combination with GaAs MESFETs at room temperature has been developed [4.42]. Jenkins et al [4.17] have gone one step further and operated the whole oscillator at 77K improving the performance further with the reduction of the noise from the active devices. This oscillator has also been made tunable by the application of a magnetic field.

Macdonald et al [4.6] have demonstrated HTS matching networks which can be used to match the input impedance of a transistor to a source impedance for example. The use of HTS reduces the noise figure in such networks and this has particular application in satellite front ends where a low noise figure has considerable benefit. They [4.6] found that the noise figure was 0.21 dB less than for the equivalent gold network and when integrated with a HTS filter operating at 12 GHz the overall improvement over a similar gold set-up was 1.3 to 1.4 dB.

Researchers have looked to see if it is possible to produce active devices in HTS. This would provide considerable advantages. Firstly, it would lead to the possibility of solely HTS circuits that would not require semiconductor active elements. Secondly, it would lead to performance enhancements by the combination of the best of semiconductor technology integrated with HTS producing excellent hybrid devices. However, problems do remain. Current research [4.43-4.45] has only produced very small current gains for HTS three-terminal devices of around 20. Another problem is that it has not been possible to find a substrate that provides a good match with HTS and has sufficiently good semiconductor qualities so that truly integrated circuits can be made on a single substrate. This in itself would be a significant advance. Further research is required in this area.

4.7 Conclusions

This chapter has reviewed the different types of devices that have already been made from HTS. Many of them have shown considerable performance enhancement over conventional technology especially for satellite applications. Devices are already commercially available demonstrating that HTS has a real use in the communications field.

4.8 References

[4.1] Belohoubek E. et al (1993) "High temperature superconducting components for microwave systems". *Applied Superconductivity* 1(10-12): 1555-1573.

[4.2] Denlinger E. et al (1992) "Superconducting nonreciprocal devices for microwave systems". *IEEE Microwave and Guided Wave Letters* 2(11): 449-451.

[4.3] Liang G. et al (1994) "High-temperature superconductive devices on sapphire". *IEEE Transactions on Microwave Theory and Techniques* 42(1): 34-40.

[4.4] Kyoya M. et al (1994) "Development of two stage, small Stirling cycle cooler for temperatures below 20K," *Cryogenics* 34(5): 431-434

[4.5] Rolfes M. (1995) "Superconductors: the wireless industry comes of age". *Superconductor Industry* 8(4): 24-30, 56.

[4.6] Macdonald P. et al (1994) "HTS microstrip matching networks and filters". *IEEE Transactions on Microwave Theory and Techniques* 42(3): 523-525.

[4.7] Edwards D.J. (1995) (Private Communication).

[4.8] Tobar M.E., Blair D.G. (1994) "Phase noise analysis of the sapphire loaded superconducting niobium cavity oscillator". *IEEE Transactions on Microwave Theory and Techniques* 42(2): 344-347.

[4.9] Shen Z. et al (1992) "High T_c superconductor-sapphire microwave resonator with extremely high Q-values up to 90K". *IEEE Transactions on Microwave Theory and Techniques* 40(12): 2424-2432.

[4.10] Wilker C. et al (1991) "5 GHz high-temperature-superconductor resonators with high Q and low power dependence up to 90K". *IEEE Transactions on Microwave Theory and Techniques* 39(9): 1462-1467.

[4.11] Takemoto J.H. et al (1989) "Microstrip ring resonator technique for measuring microwave attenuation in high-T_c superconducting thin films". *IEEE Transactions on Microwave Theory and Techniques* 37(10): 1650-1652.

[4.12] Namordi M.R. et al (1991) "Comparison of high-temperature-superconductor and metal-based resonators". *IEEE Transactions on Microwave Theory and Techniques* 39(9): 1468-1474.

[4.13] Porjesz T. et al (1993) "Magnetic field controlled superconducting microwave microstrip resonators". *Applied Superconductivity* 1(10-12): 1707-1713.

[4.14] Subramanyam G. et al (1993) "TlCaBaCuO high T_c superconducting microstrip ring resonators designed for 12 GHz". *Applied Superconductivity* 1(10-12): 1605-1614.

[4.15] Suzuki K. et al (1993) "High T_c superconductor microwave resonators and filters". *Applied Superconductivity* 1(10-12): 1575-1593.

[4.16] Tellmann N. et al (1994) "High Q $LaAlO_3$ dielectric resonator shielded by YBCO-films" *IEEE Transactions on Applied Superconductivity* 4(3): 143-148.

[4.17] Jenkins A.P. et al (1995) "An HTS microstrip resonator stabilised voltage controlled oscillator". In D. Dew-Hughes (ed.) *Applied Superconductivity 1995 Volume 2*. Bristol: IoP Publishing: 1183-1183.

[4.18] Jenkins A.P. et al (1993) "Microwave characteristics of Tl-Ba-Ca-Cu-O thin film microstrip resonators". In H.C. Freyhardt (ed.) *Applied Superconductivity*

1993 Vol. 2. Oberürsel, Germany: DGM Informationsgesellschaft mbH: 1033-1036.

[4.19] Talisa S.H. et al (1991) "Low- and high-temperature superconducting microwave filters". *IEEE Transactions on Microwave Theory and Techniques* 39(9): 1448-1454.

[4.20] Mei K.K., Liang G. (1991) "Electromagnetics of superconductors". *IEEE Transactions on Microwave Theory and Techniques* 39(9): 1545-1581.

[4.21] Schmidt M.S. et al (1991) "Measured performance at 77K of superconducting microstrip resonators and filters". *IEEE Transactions on Microwave Theory and Techniques* 39(9): 1493-1497.

[4.22] Kang K. et al (1993) "Fabrication and characterization of high-T_c superconducting bandpass filter made on MgO and $LaAlO_3$". *Applied Superconductivity* 1(10-12): 1691-1698.

[4.23] Matthaei G.L., Hey-Shipton G.L. (1993) "Novel staggered resonator array superconducting 2.3 GHz bandpass filter". *IEEE Transactions on Microwave Theory and Techniques* 41(12): 2345-2352.

[4.24] Jenkins A.P. et al (1995) "Microwave surface resistance measurements of air-atomised spray deposited Tl-Ba-Ca-Cu-O thick films". *IEEE Transactions on Applied Superconductivity* 5(2): 1095-1098.

[4.25] Track E.K. et al (1991) "Fabrication and characterization of YBCO microstrip delay lines". *IEEE Transactions on Magnetics* 27(2): 2936-2939.

[4.26] Hofer G.J. et al (1993) "HTS coplanar delay lines". *IEEE Transactions on Applied Superconductivity* 3(1): 2800-2803.

[4.27] Liang G.C. et al (1994) "HTS devices on sapphire". *IEEE Transactions on Microwave Theory and Techniques* 42(1): 34-40.

[4.28] Du Pont Superconductivity (1993) "25 ns low-loss delay line". *Technical Data Sheet*. Delaware, USA: Du Pont Superconductivity.

[4.29] Jenkins A.P. et al (1994) "A novel on board satellite spread spectrum correlator". In *Proceedings of the IEEE Third International Symposium on Spread Spectrum Techniques & Applications Volume 2/2*. Piscataway, NJ: IEEE: 362-366.

[4.30] Dolan G.J. et al (1981) "Superconducting tunnel junctions as mixers at 115 GHz". *IEEE Transactions on Microwave Theory and Techniques* 29(2): 87-91.

[4.31] Konopka J. et al (1990) "Microwave detectors based on granular high-T_c thin films". *IEEE Transactions on Microwave Theory and Techniques* 38(2): 160-165.

[4.32] Jenkins A.P. (1994) *Microwave Applications of High-Temperature Superconductors*. Unpublished D.Phil. thesis, University of Oxford.

[4.33] Ruggiero S.T. et al (1991) "Mixing in TlBaCaCuO superconducting films at 61 GHz". *IEEE Transactions on Magnetics* 27(2): 3070-3072.

[4.34] Hong J.P. et al (1991) Millimeter wave mixing from deliberate grain-boundary weak links in epitaxial $Tl_2CaBa_2Cu_2O_8$ films". *Applied Physics Letters* 59(8): 991-993.

[4.35] Konopka J. et al (1988) "Microwave detection and mixing in Y-Ba-Cu-O thin films at liquid-nitrogen temperatures". *Applied Physics Letters* 53(9): 796-798.

[4.36] Jenkins A.P. et al (1995) "Subharmonically pumped BSCCO microwave mixers operated at Ka band and at 77K". *Superconductor Science and Technology* 8: 613-616.

[4.37] Butler D.P. et al (1993) "Conversion gain and noise of $YBa_2Cu_3O_7$ weak-link mixers". *IEEE Transactions on Applied Superconductivity* 3(1): 2269-2272.

[4.38] Butler D.P. et al (1992) "Conversion loss of a $YBa_2Cu_3O_7$ grain boundary mixer at 20 GHz". *Applied Physics Letters* 61(3): 333-335.

[4.39] Chew W., Fetterman H. (1989) "Printed circuit antennas with integrated FET detectors for millimeter-wave quasi-optics". *IEEE Transactions on Microwave Theory and Techniques* 37(3): 593-597.

[4.40] Ramisch R. et al (1991) "A tapped-delay-line superconductive chirp filter in shielded microstrip". *IEEE Transactions on Microwave Theory and Techniques* 39(9): 1575-1581.

[4.41] Jenkins A.P. et al (1993) "Novel on-board processing architectures for satellite spread spectrum communications". In *Proceedings of the Third IEE European Conference on Satellite Communications*. London: IEE: 280-283.

[4.42] Khanna A.P.S. et al (1991) "A superconducting resonator stabilized low phase noise oscillator". *Microwave Journal* 34(February): 127-130.

[4.43] Gerdemann R. et al (1995) "Asymmetric high temperature superconducting Josephson vortex-flow transistors with high current gain". *Applied Physics Letters* 67(7): 1010-1012.

[4.44] Gross R. et al (1995) "Physics and performance of high temperature superconducting vortex flow transistors". *Applied Superconductivity* 2(7/8): 1-17.

[4.45] Alff L. et al (1994) "Magnetic-field-effect three-terminal device on $YBa_2Cu_3O_{7-\delta}$ grain boundary junctions". *Journal of Applied Physics* 75(3): 1843-1845.

Chapter 5

Devices

Chapters 2 and 3 have already explained how the low R_s of HTS can be measured by different techniques and that low R_s results have been achieved in the course of this research. Although, a review of the R_s measurement techniques was important and the achievement of low R_s results significant, the ultimate aim of this research was to produce microwave devices with performances better than conventional devices. Such improvements also needed to be produced in packages smaller and lighter than would have been possible in a waveguide or coaxial construction. Once produced these devices could also be compared against other HTS devices made around the world and reviewed in chapter 4.

The design philosophy with regard to which devices to fabricate had to take into consideration the quality of films available, the size and material properties (e.g. the dielectric constant) of the substrates used, microwave modelling constraints and device patterning control. In addition, devices that might have use within a satellite or mobile base station were singled out to demonstrate the potential of HTS commercially.

Many of the devices constructed were of the microstrip geometry and this required them to be patterned using photolithographic and wet etch techniques. The control

of this process was critical to the production of reliably performing devices time after time. Therefore, this chapter begins with a section on this topic.

Microstrip resonators had already been fabricated and used for R_s measurement after patterning. These served a dual purpose as they are also devices in their own right with application in local oscillators, for instance. The results from these resonators are reported on in this chapter, but with particular emphasis upon their Q values and the improvement over similar copper devices.

Continuing the theme of resonators, but using a different geometry, results for dielectric resonators are given showing that Q values in excess of 100,000 can be achieved. Such results are only possible with the low R_s of HTS.

Filters are important elements of a satellite or mobile base station and this chapter reviews the results for different types fabricated on various substrates. There is also a comparison with similar copper implementations of these devices showing that good performance and patterning accuracy, obtained by optimization of the patterning process by using accurate masks and gentle etches, can be achieved.

Finally, this chapter puts forward the proposition of integrating an HTS filter and an HTS dielectric resonator together with semiconductor elements in order to produce a very low phase noise oscillator.

5.1 Device Patterning

Device patterning was achieved by use of standard photolithographic techniques and wet etches using acetate and glass masks (the latter provided by the Rutherford-Appleton Laboratories). The processes were optimized initially by A.P. Jenkins and further improved by K.L. Jim (Engineering Science Department, Oxford University). In general the following steps are needed [5.1]:

1. Spin a thin layer of photoresist onto the film (typically 1.0-1.5 μm).
2. Bake for greater than 5 minutes at 80°C.
3. Place mask over film surface and expose to UV light for 15 seconds.
4. Immerse film in developer solution for 1 minute.
5. Rinse in DI water.
6. Immerse film in $FeCl_3$ checking periodically by eye and microscope.
7. Remove photoresist in acetone bath.

This process was improved by K.L. Jim [5.2] firstly, by pre-baking the substrate before stage 1. This step leaves a dry surface to which the photoresist sticks better. Secondly, another baking step is placed between the developing and etching stages. This reduces undercut of lines and sharpens line edge definition. Thirdly, before etching the sample should be immersed in a soap solution (1 ml in 1 l DI water) for 1 minute. This reduces surface tension between the photoresist and the HTS film and allows the etch to produce a cleaner edge. Finally, by changing the etch to a 1 molar citric or adipic solution the etch rate is slowed to minutes rather than seconds. This allows greater control over stage 6.

Initially, masks were produced using a commercial drawing package and then translated into a standard printer format. These were then printed out onto acetate using a high definition plotter with a final resolution of 2400 dpi (approximately 10 μm per dot) at the Oxford University Computing Services. Later, this process was improved by translating the mask required into a different format which could then be sent to the Rutherford-Appleton Laboratories where glass masks with an accuracy of 1 μm could be produced.

5.2 Resonators

Microstrip resonator results have already been summarized in chapter 3 where the results were used to determine the R_s of films after patterning. However, for convenience's sake, Table 5.1 highlights the best results obtained for microstrip resonators. The mask type refers to the type of resonator patterned and the exact description was given in section 3.3.

Sample	Mask Type	f_o (GHz)	P_{in} (dBm)	Q_{sc}	R_s at 10 GHz ±7% (mΩ)
La56	L	2.33, 2.60*	-20, -50*	101, 570*	489, 62.5*
JDMGO16	M	3.68, 3.81*	-50, -50*	625, 233*	39.1, 123*
ABTM24	L	8.00 8.00 8.00	0 -20 -40	222 397 484	61.6 31.8 25.0
ABTM31	L	7.70 7.70 7.70 7.70	0 -20 -40 -60	166 325 461 532	87.6 41.7 27.6 23.1
ABTM33	L	8.39 8.40 8.40	0 -20 -40	215 335 390	60.8 36.9 30.9
ABTM35	L	8.24 8.30 8.30	0 -20 -40	148 244 355	92.6 53.5 34.9
ABTM37	L	8.04 8.04 8.04	0 -20 -40	360 525 544	35.5 22.5 21.5

Table 5.1 Microstrip Resonator Results

Key: * Two results indicate a resonator patterned without coupling gaps and then with gaps.
L Linear Resonator Mask
M Meander Line Resonator Mask

The results show improvement over a similar silver resonator constructed which had a unloaded Q of 300. The results do show significant power dependency and this is associated with the current distribution in a microstrip structure. Fig. 5.1 shows an idealized graph of the current distribution in a microstrip line of width, d.

In a microstrip line the current density is at its highest at the edges. The density here can be as much as two orders of magnitude higher than in the centre [5.3]. Therefore, the quality of the HTS edges can critically determine the performance of a resonator and should more power be inserted into the resonator we may find the current density in the edges exceeding J_c and going normal. This effect will show up

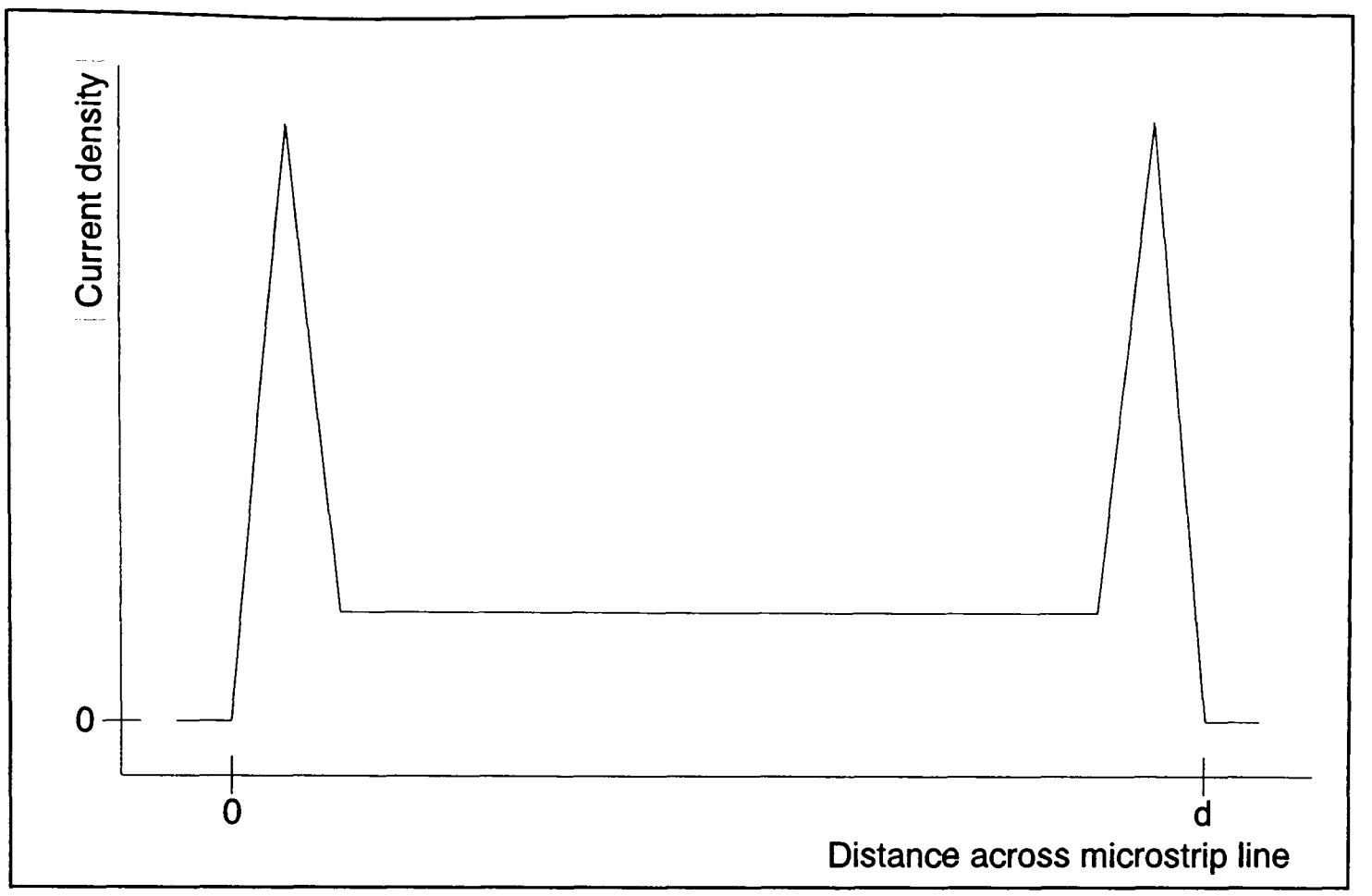

Figure 5.1 Current Distribution across a Microstrip Line

as a degradation in Q as the power is increased.

The resonator results compare poorly with those given in section 4.2. The best result given above is two orders of magnitude lower than the best recorded in the world. Therefore, film quality needs to be improved and further investigations are needed into the effect of etches on patterned films especially around the crucial edge regions. All resonators given above were patterned using the process developed by A.P. Jenkins. Therefore, $FeCl_3$ was used as an etch and this may have been too harsh especially for good quality line edges.

More promising though are the results obtained from the dielectric resonators. Table 5.2 reviews the results giving the puck material and the films used (further details of the latter have been given in chapter 3). The input power in all cases was -10 dBm.

Type	f_o (GHz)	Unloaded Q	T(K)
Sapphire puck (25.4mmØx12mm length), A394 and LaB9	5.58	117,305 121,471*	77
Sapphire puck (4mmØx4mm length), La99 and La100	24.75	90,991	80
$LaAlO_3$ puck (4mmØx1.75mm length), La99 and La100	22.85	47,877	80
$LaAlO_3$ puck (4mmØx3.5mm length), La99 and La100	23.23	53,223	80

Table 5.2 DR Results

Key: Ø=diameter

* Result with 20 dB attenuation.

As can be seen unloaded Qs in excess of 100,000 can be obtained when high quality films are used. As explained in chapter 3 these values could be increased providing very low loss tangent materials are used for pucks. There is less power dependency for a DR than for a microstrip resonator as the circulating currents are distributed over a larger area.

5.3 Filters

5.3.1 13 GHz Filter

The first attempt at an HTS filter was a 13 GHz centre frequency, 4% bandwidth, 4-pole coupled line bandpass filter. Such a filter had already been fabricated by Macdonald et al [5.4] who had produced a filter that very closely matched the specification and they had provided line lengths, widths and spacings for a filter to be produced on 1cm square $LaAlO_3$. Using this design would serve two purposes. Firstly, it would show up any inconsistencies in the patterning process control as the performance of the constructed filter could be compared against a known standard. Secondly, it would help with future microwave modelling on high (greater than 10) dielectric constants. It has been found [5.4, 5.5] that using quasi-static models for device design is only reliable for dielectric constants less than around 10. This is because many modelling packages do not have stored empirical data for components on dielectrics with dielectric constants greater than 10 and so any prediction depends on extrapolating data and this leads to inaccuracies. $LaAlO_3$ has a dielectric constant of 24 and so any improvement to modelling on it using the Department of Engineering Science's quasi-static model would be very useful.

As a first step, the line dimensions of Macdonald et al [5.4] were put into the HP EEsof Touchstone quasi-static CAD package used in the Department of Engineering Science, Oxford University and the dielectric constant varied so that a satisfactory

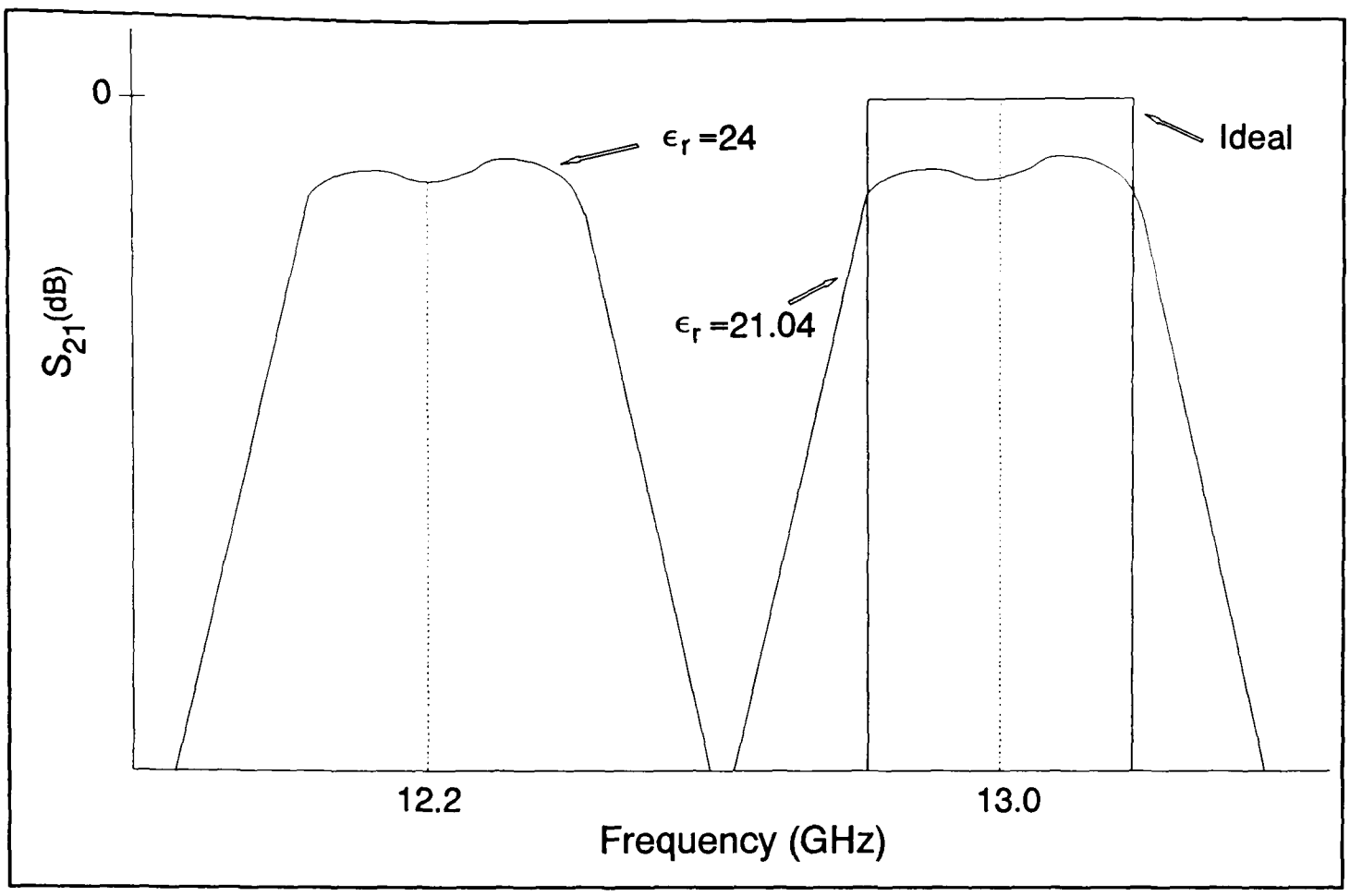

Figure 5.2 Effect of dielectric constant on centre frequency

response was obtained. Fig. 5.2 shows the effect of different dielectric constants. Fig. 5.2 clearly shows that if a dielectric constant of 24 is used the centre frequency of the filter is predicted as being less than 13 GHz. A better value to use, found from varying the dielectric constant in Touchstone, was 21.04 as this lines up well with the ideal filter response. In the future, providing there is continued use of quasi-static analysis, it would perhaps be better to use the latter value to model for $LaAlO_3$. The slight "humpiness" of the two modelled responses is due to inaccuracies in the Touchstone model and shows that changing the dielectric constant is not a complete solution to producing accurate modelling.

Therefore, an alteration to the dielectric constant is only a first step. It, for instance, takes no account of cross-coupling between pairs of coupled lines which can be

significant with very small filters on high dielectric constant substrates. Taking such factors into consideration with the current analysis would be difficult and a full-wave or finite element analysis is recommended as being better [5.4]. The adjustment in dielectric constant may find greater use, though, with the modelling of microstrip resonators where the length of the line is critical in determining the resonant frequency.

Once the analysis had been completed an acetate mask was designed and manufactured and the filter patterned onto a Tl(2212) coated 1cm square $LaAlO_3$ substrate (sample La105) fabricated by S.M. Morley, Materials Department, Oxford University using the process of A.P. Jenkins referred to in section 5.1. This used $FeCl_3$ as the etch. A gold ground plane of 3 μm thickness was sputtered onto the back of the substrate.

Fig. 5.3 shows the filter characteristic at different power levels and 79K. At 0 dB attenuation the input power is -10 dBm. The graphs show that there is little change in the transmission loss (S_{21}) when the attenuation is changed from 20 to 40 dB. The insertion loss at the peak is less than 5 dB. Macdonald et al [5.4] had measured an insertion loss of 2.5 dB and the shape of their response in the passband was flatter than the one shown in Fig. 5.3. The reason for the loss of flatness was patterning errors. Some of the lines used to make this filter were as narrow as 60 μm and using $FeCl_3$ (with an etch time of around 10 seconds) it was difficult to control line widths accurately. In addition, an acetate mask was used with line accuracies of ± 10 μm. An

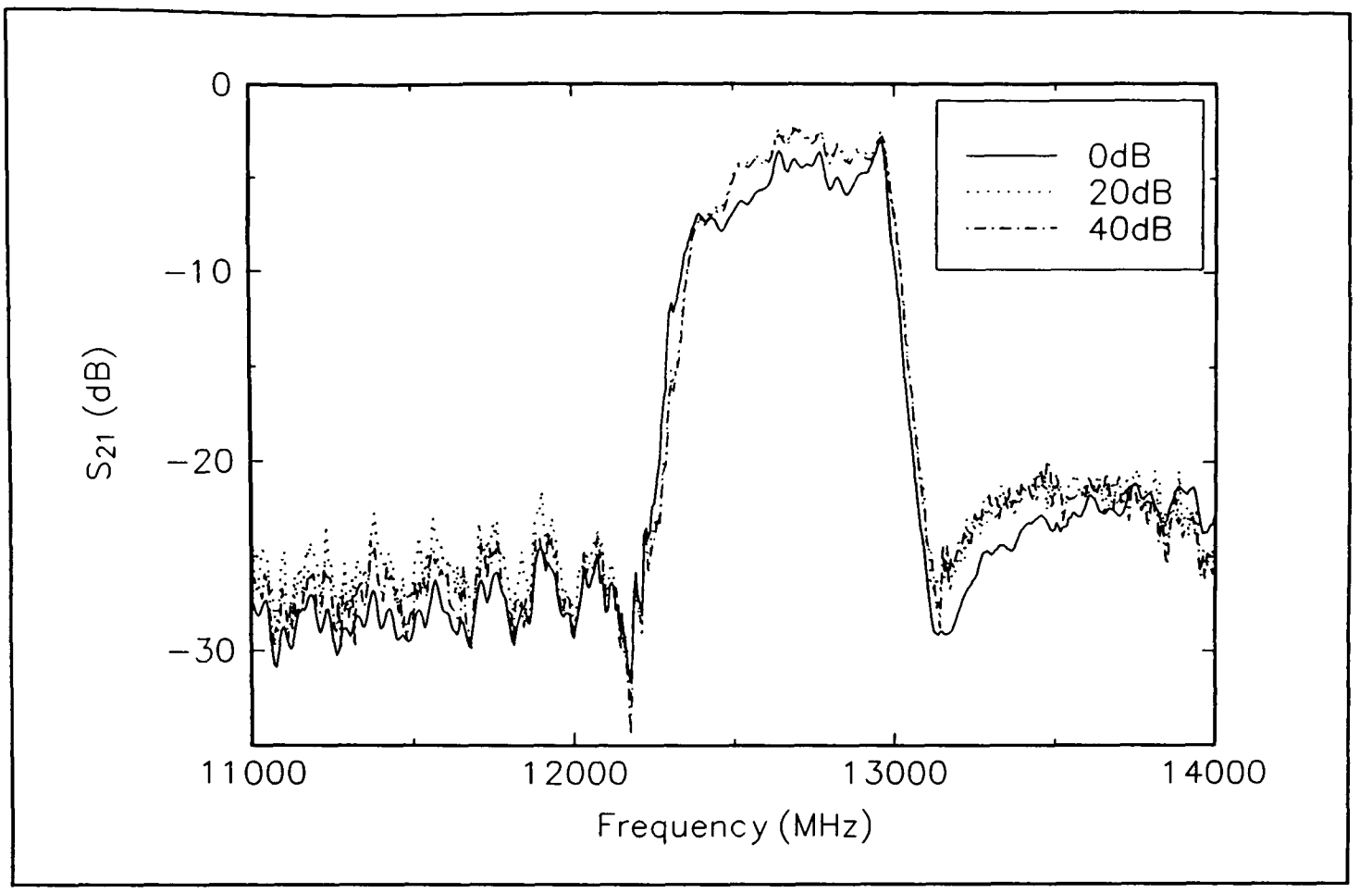

Figure 5.3 Filter response at different power levels

improvement to this could be achieved if citric or adipic acid is used as an etch (as this has an etch time in minutes) [5.2] together with a glass mask with an accuracy of ± 1 μm. This was found to be the case with another filter produced (see section 5.3.3).

The centre frequency of the filter does not match the result of Macdonald et al [5.4] which was 13.0 GHz. Line lengths affect the centre frequency of the filter so it is possible that the use of acetate masks (accuracy ± 10 μm) may have caused this error because the lines were too long so reducing the centre frequency. However, this seems unlikely as the smallest line length was 1.36mm on which ± 10 μm is a very small error. Therefore, the cause of the shift in centre frequency is much more likely to be a difference in the dielectric constant used by Macdonald et al [5.4] and the

one used here. There is some evidence to support this with measured values varying between 23.5-24.5 [5.6]. It would therefore seem that to produce reliable devices on $LaAlO_3$, cost effectively, there needs to be further work done on improving the consistency of the dielectric constant even when the $LaAlO_3$ is sourced from different suppliers.

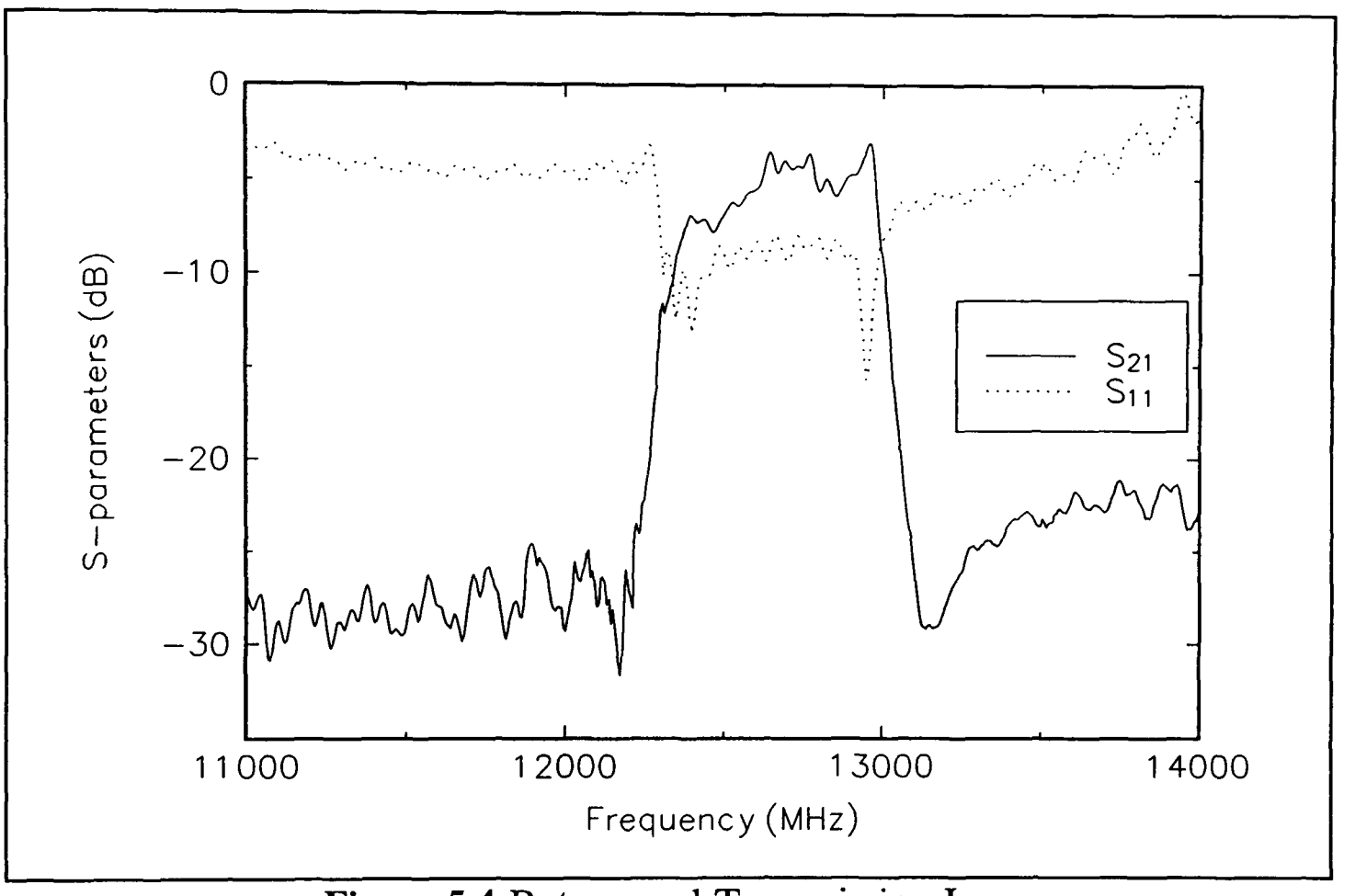

Figure 5.4 Return and Transmission Loss

Fig. 5.4 shows the return loss (S_{11}) and transmission loss (S_{21}) for the filter at 0 dB attenuation and 79K. A return loss below -10 dB was desirable (as this had been achieved by Macdonald et al [5.4]) throughout the passband and this was very nearly achieved.

Fig. 5.5 shows a picture of the actual device.

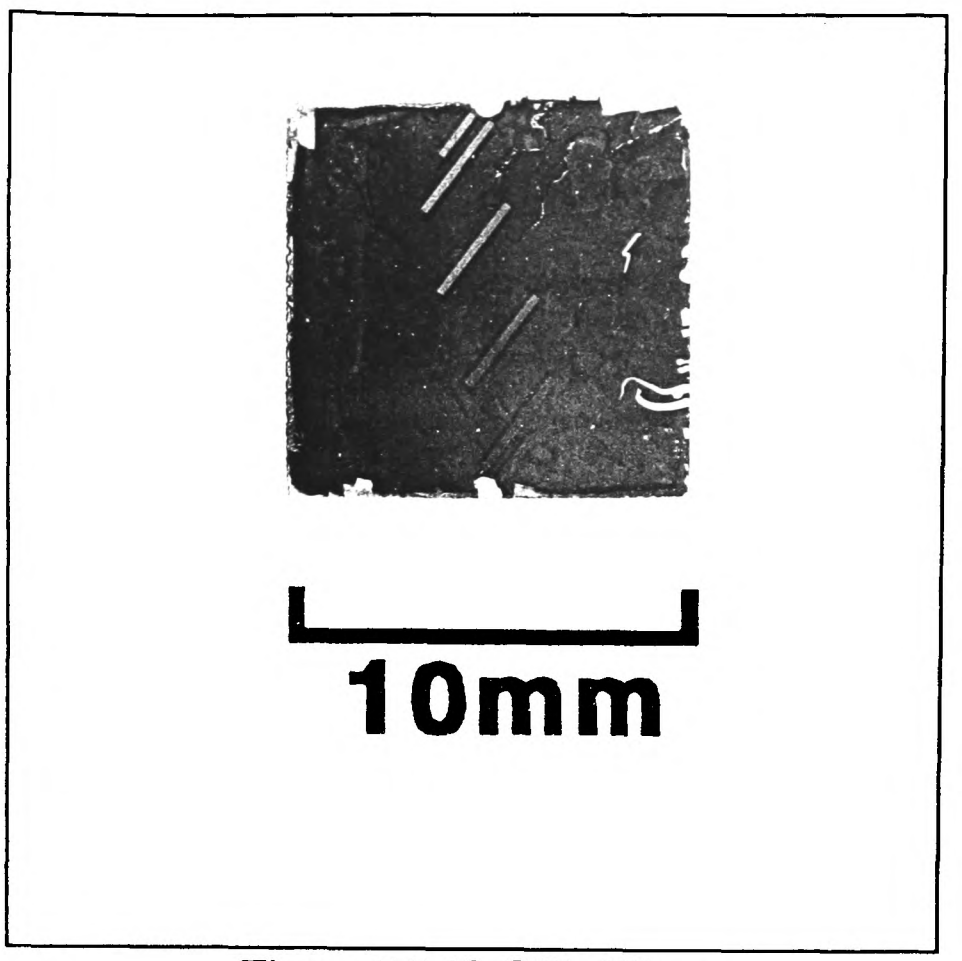

Figure 5.5 13 GHz Filter

5.3.2 Channel Filters

Two HTS channel filters were modelled and constructed. Such filters are useful in satellite transponders [5.7] where several carrier frequencies need to be received. It is important to eliminate as much cross-talk between channels as possible as this destroys the effectiveness of the satellite's operation. Often banks of channel filters are combined together in a demultiplexer for reception of signals and in a multiplexer for transmission of signals. Production of HTS channel filters which could be placed within a single cryocooler would significantly reduce the weight of satellites as filters on light substrates would replace waveguide filters made from solid copper.

The first channel filter was designed for a centre frequency of 10 GHz, 2% bandwidth and to have 4 poles. The second for 10.63 GHz, 2% bandwidth and 4 poles. These two filters were also constructed from copper coated Duroid for comparison purposes. The HTS filters were patterned onto 2cm square MgO substrates (samples MgO112 and MgO113) fabricated by A.P. Bramley, Materials Department, Oxford University. The patterning process used acetate masks and $FeCl_3$ as the etch. Gold ground planes were sputtered onto the substrates' back sides.

Fig 5.6 shows a transmission loss comparison between the 10 GHz HTS on MgO filter and a similar copper on Duroid filter both tested at 79K. The graphs show the HTS filter having a similar performance to the copper filter, but that in the case of

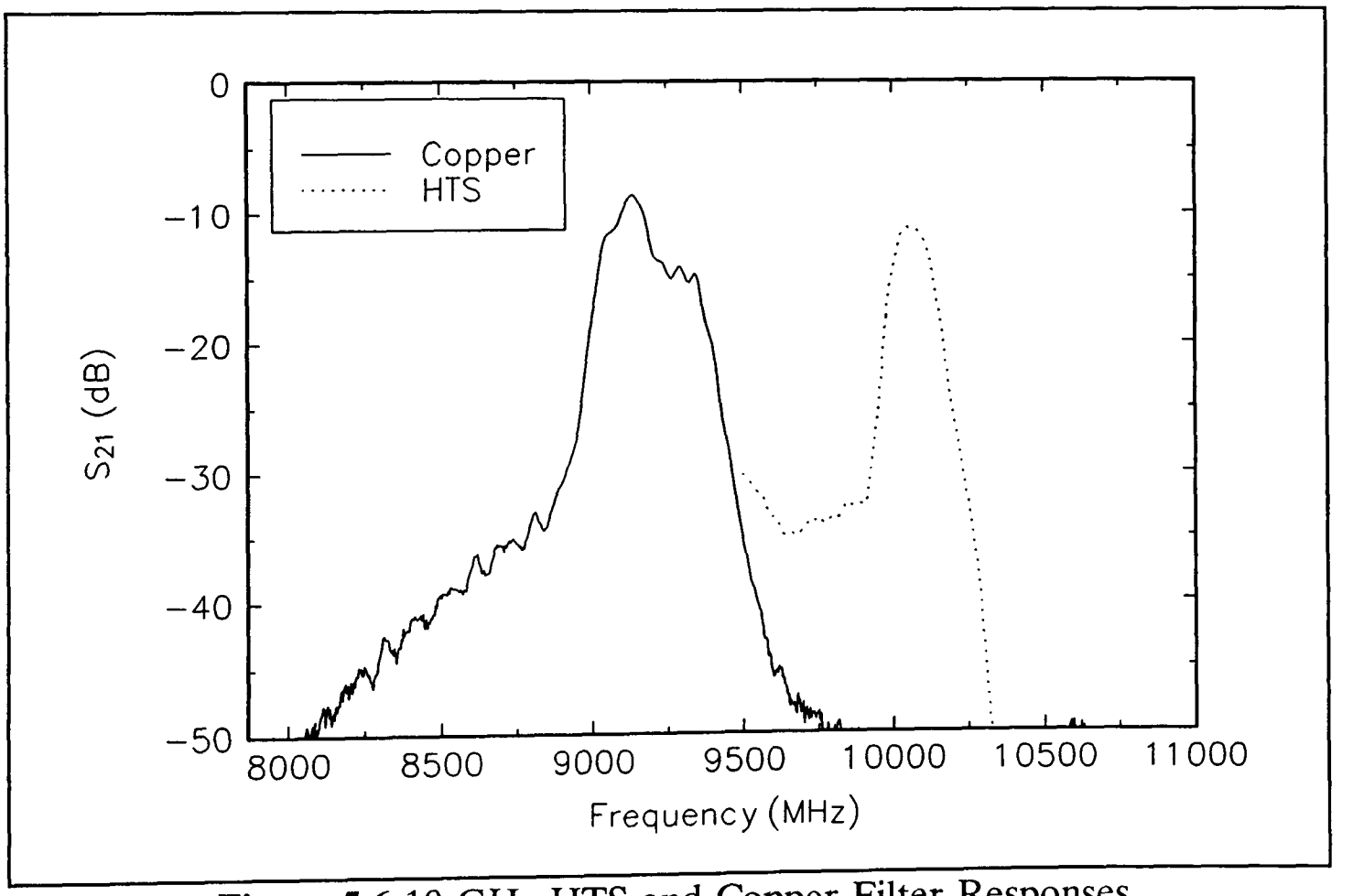

Figure 5.6 10 GHz HTS and Copper Filter Responses

the HTS filter the centre frequency has not shifted considerably from 10 GHz. The

shift in the copper filter is due to the change in the dielectric constant of Duroid due to cooling to 79K. Also noticeable on this graph is the shoulder at the beginning of the HTS bandpass response. This is due to a box mode caused by the metal enclosure of the filter. One possible way to remove this is to decrease the distance between the enclosure's lid and the substrate making the cavity smaller and raising the frequency of any box modes. The measured centre frequency of the HTS filter was 10.06 GHz which is only very slightly in error showing the accuracy that is possible with modelling with dielectric constants less than 10 (MgO has a dielectric constant of 9.8). The slight inaccuracy is likely to be due to small patterning errors. The smallest line width for this HTS filter was 380 μm and so the use of acetate masks and $FeCl_3$ was good enough to produce accurate results unlike the 13 GHz filter reported on in section 5.3.1.

Fig. 5.7 shows a similar comparison for the 10.63 GHz filter. Once again there is comparable performance (and a box mode for the HTS filter response), but the centre frequency of the HTS filter is closer to the intended one than the copper equivalent at 10.67 GHz. This once again shows the accuracy possible with the patterning process providing line widths are in the hundreds of microns (the smallest width here was 480 μm).

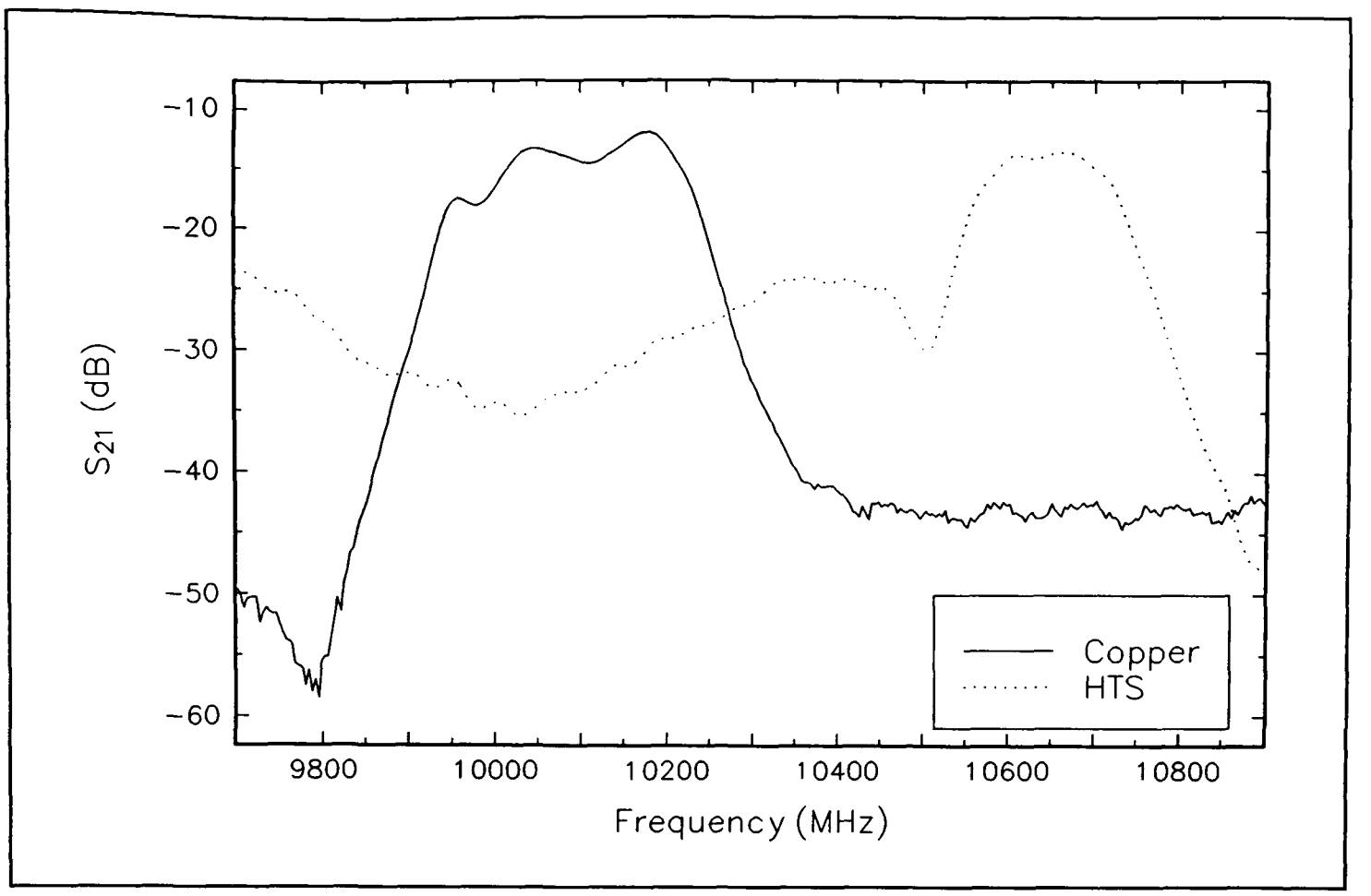

Figure 5.7 10.63 GHz HTS and Copper Filter Responses

5.3.3 Oscillator Filter

An intention of this research was to produce a very low phase noise HTS oscillator (further details are given in section 5.4). One of the building blocks of this oscillator was to be a 5.58 GHz centre frequency, 200 MHz bandwidth, 3-pole bandpass filter to be used in conjunction with the 5.58 GHz DR and a gain element. This filter design was modelled using the HP EEsof Touchstone microwave modelling CAD package and then patterned onto a double sided Tl(2223) on MgO 2cm square sample (sample ABTM83), produced by A.P. Bramley, Materials Department, Oxford University. A glass mask designed in-house, but manufactured by the Rutherford-Appleton Laboratories and a wet etch of adipic acid was used for the patterning (i.e.

the process of K.L. Jim described in section 5.1). A filter with the same intended centre frequency and bandwidth and the same number of poles was made from copper coated Duroid for comparison.

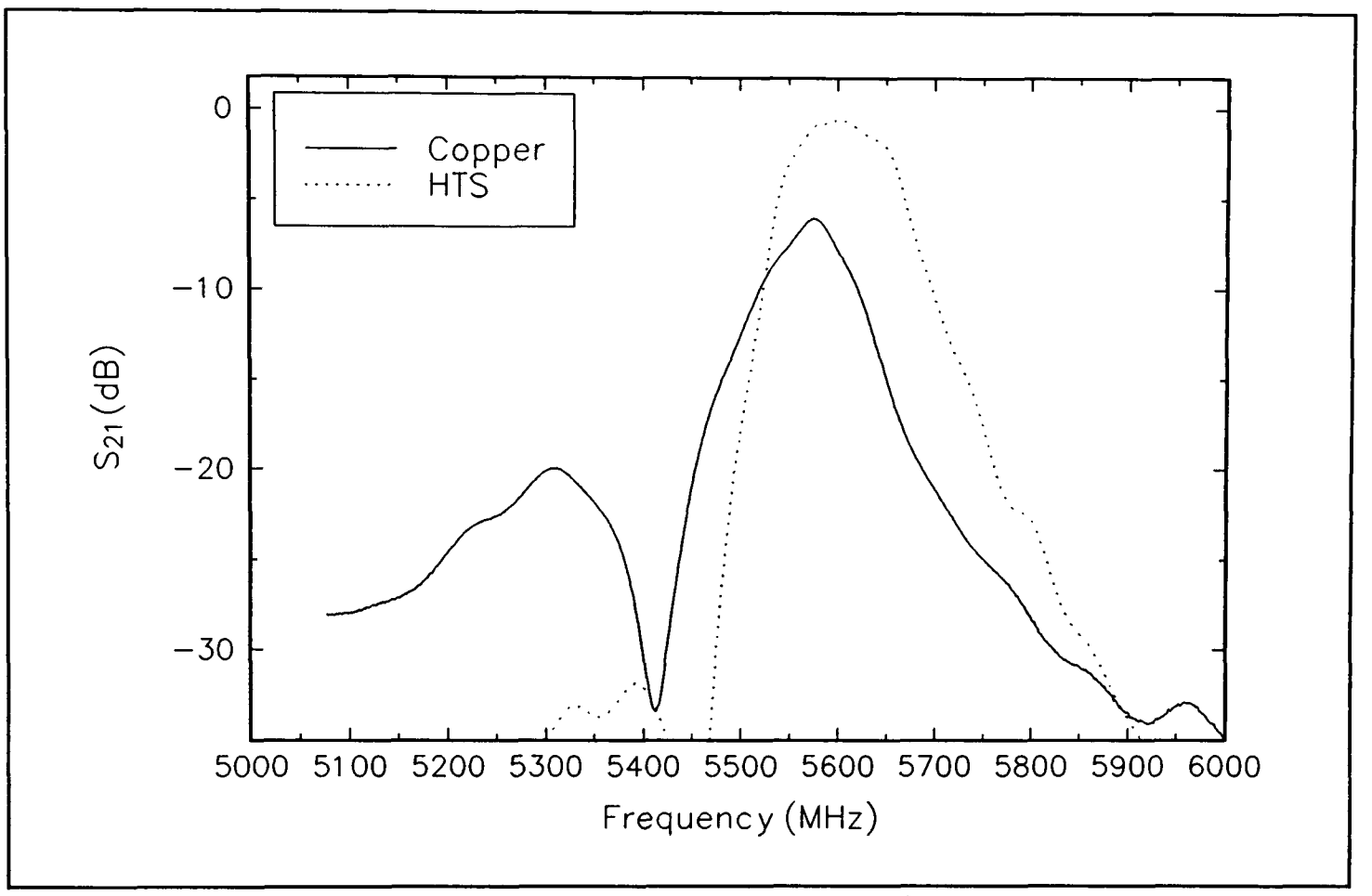

Figure 5.8 5.58 GHz HTS and Copper Filter Responses

Fig 5.8 shows the passband responses of the copper and HTS filters both tested at 79K. The HTS filter has an insertion loss at the peak of the response of only 0.5 dB and this compares favourably with other results reported (see section 4.3) and especially well against the copper filter which has a loss of greater than 5 dB. The HTS filter was cycled four times between room temperature and 79K and showed no degradation in performance. The bandwidth of the passband was narrower than modelled at 118 MHz. However, the shape of the response was less "peaky" than for copper on Duroid. The centre frequency was also found to be only very slightly detuned at 5.60 GHz demonstrating the accuracy of the patterning process.

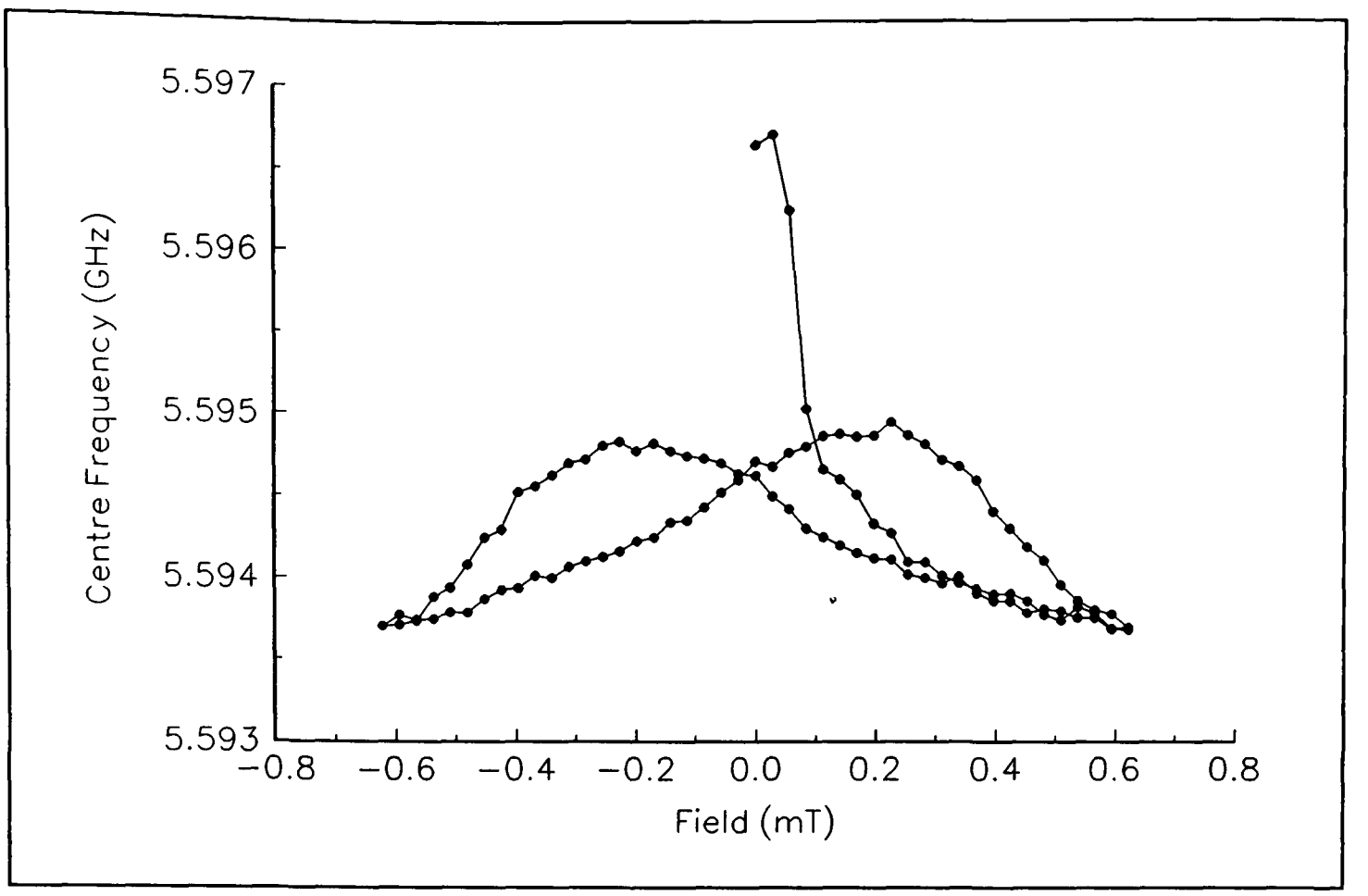

Figure 5.9 Centre Frequency vs Field

As this filter was to be used with the 5.58 GHz DR and gain elements to produce an oscillator it was considered worthwhile to investigate whether it would be possible to adjust the centre frequency (which was slightly detuned at 5.60 GHz) with the application of a magnetic field. It has already been demonstrated that the resonant frequency of a resonator can be changed by the application of a magnetic field perpendicular to the film [5.8]. Helmholtz coils designed and built by A.P. Jenkins, Engineering Science Department, Oxford University were used to provide a controllable dc magnetic field for this experiment. As the field produced by these coils was directly proportional to the voltage applied this raised the possibility of a voltage controlled oscillator if the centre frequency was found to change. Fig. 5.9 shows the effect on centre frequency of applying a magnetic field. The result shows that it was possible to change the centre frequency of the filter by around 1 MHz

depending on the field applied. This is, to best knowledge, the first demonstration of a tunable HTS thin film filter. The curve is hysteretic and this was also found to be the case when the insertion loss was compared against the applied field (Fig. 5.10).

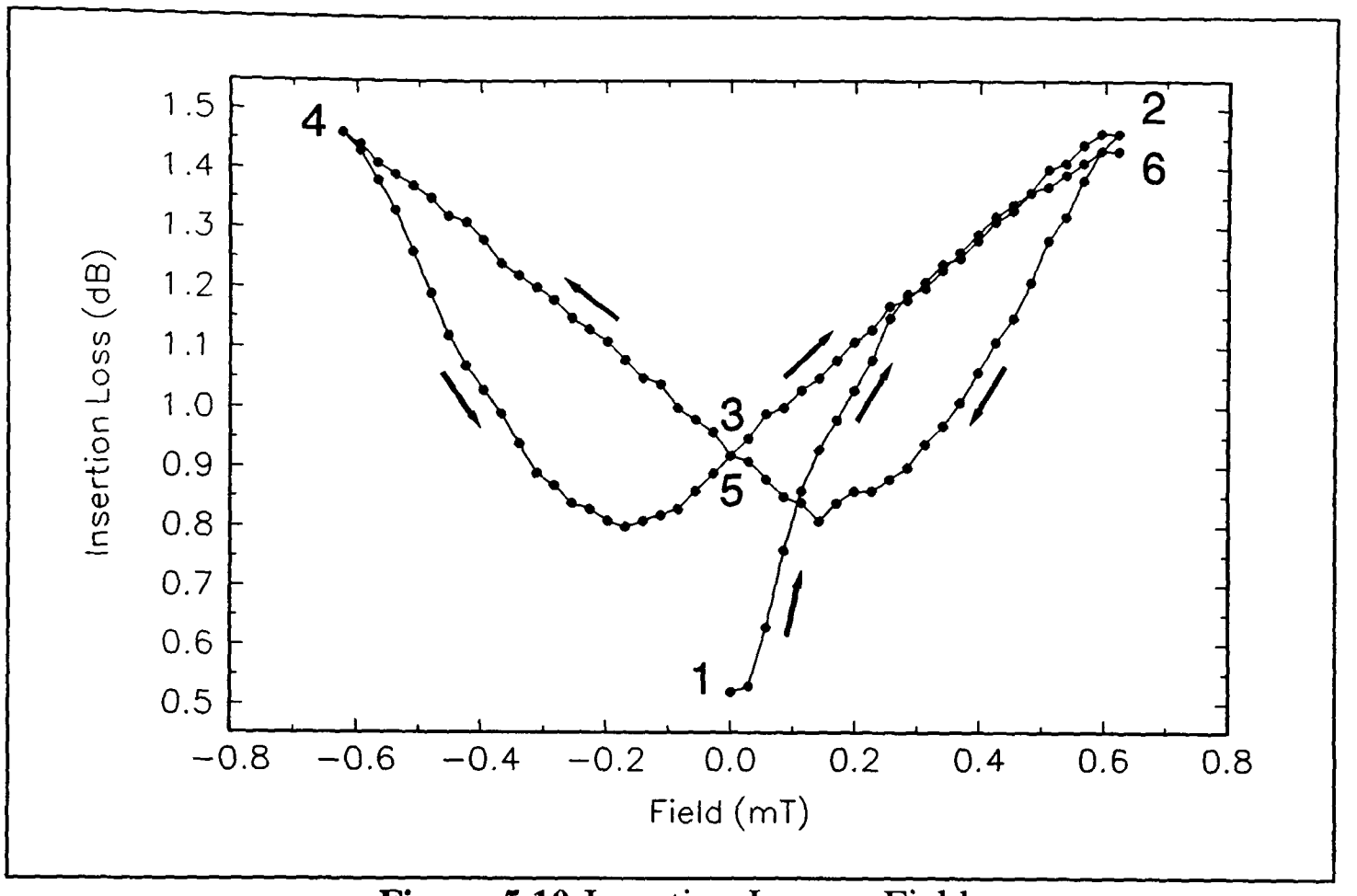

Figure 5.10 Insertion Loss vs Field

Examining this curve we see that on returning to the zero field (point 3) the insertion loss did not return to its former level (point 1). This suggested a trapped field in the HTS. It has been suggested that such behaviour is due to weak link characteristics in the HTS [5.9]. As the field is applied the penetration depth, λ_L, changes which then lowers the conductivity across the weak links. This in turn raises the R_s and so the insertion loss is increased. However, the exact nature of this effect needs further study.

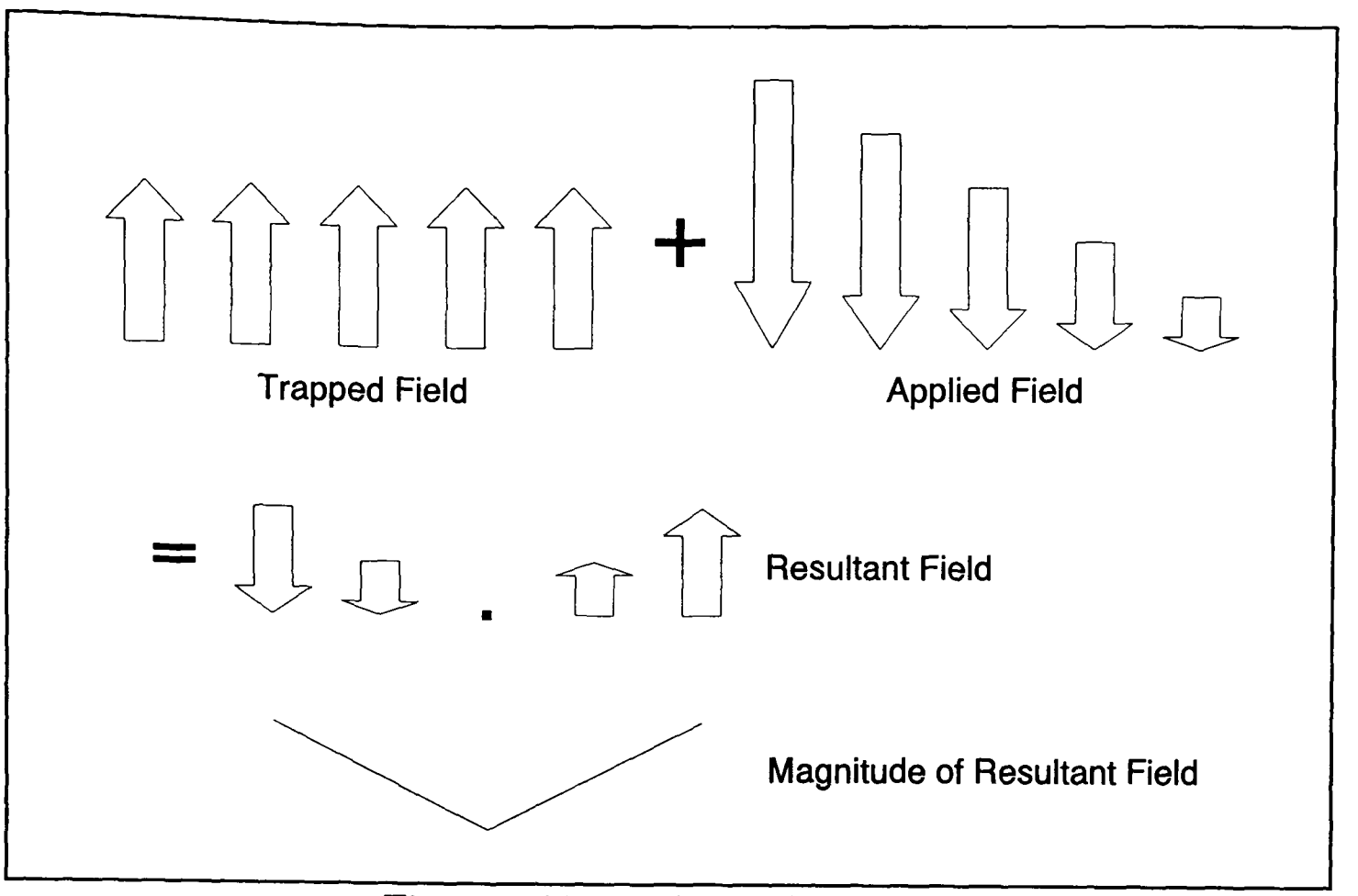

Figure 5.11 Resultant Field Effect

Further examination of the curve shows the possible interaction of the trapped field and the applied field leading to a V-shaped curve around ±0.2 mT. Fig. 5.11 demonstrates a possible explanation. As the applied field was reduced the resultant field also decreased until it just cancelled the trapped field. Beyond this point, the resultant field increased once more. The magnitude of the resultant field was thus V-shaped and the insertion loss followed this.

Fig. 5.12 shows the effect on the bandwidth of the filter. There appeared to be less hysteresis than for the insertion loss, but there was a definite change in bandwidth. However, this change is most likely explained as a secondary effect of the change on the insertion loss as this caused a narrowing of the filter response. The filter was cycled four times between room temperature and 79K and the hysteretic effects

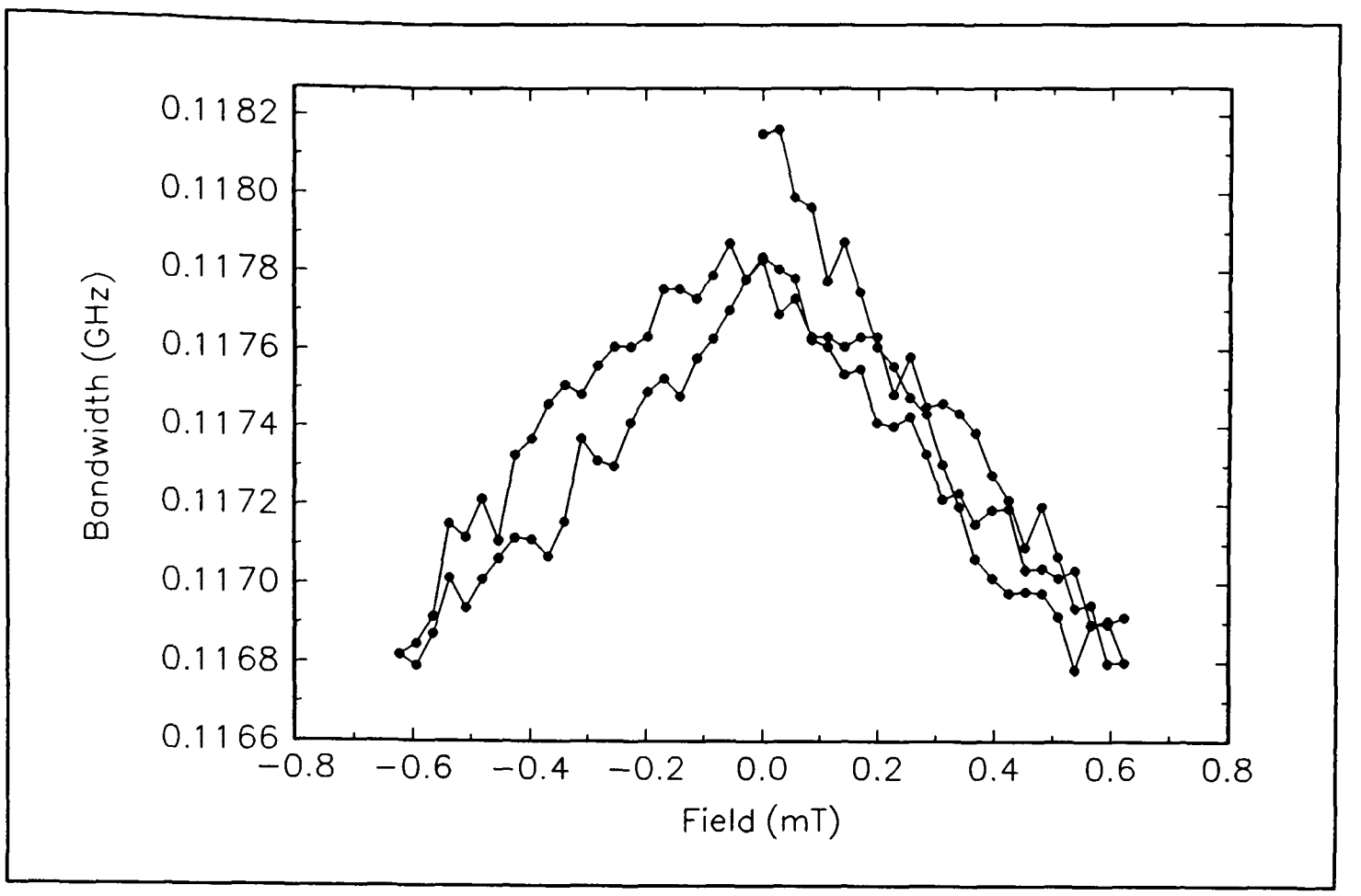

Figure 5.12 Bandwidth vs Field

shown in Figs. 5.9, 5.10 and 5.12 were found to be repeatable.

Fig. 5.13 compares the filter responses at zero field and maximum field (0.62 mT). The change in shape is hardly detectable.

Finally, Fig. 5.14 shows a picture of the actual device.

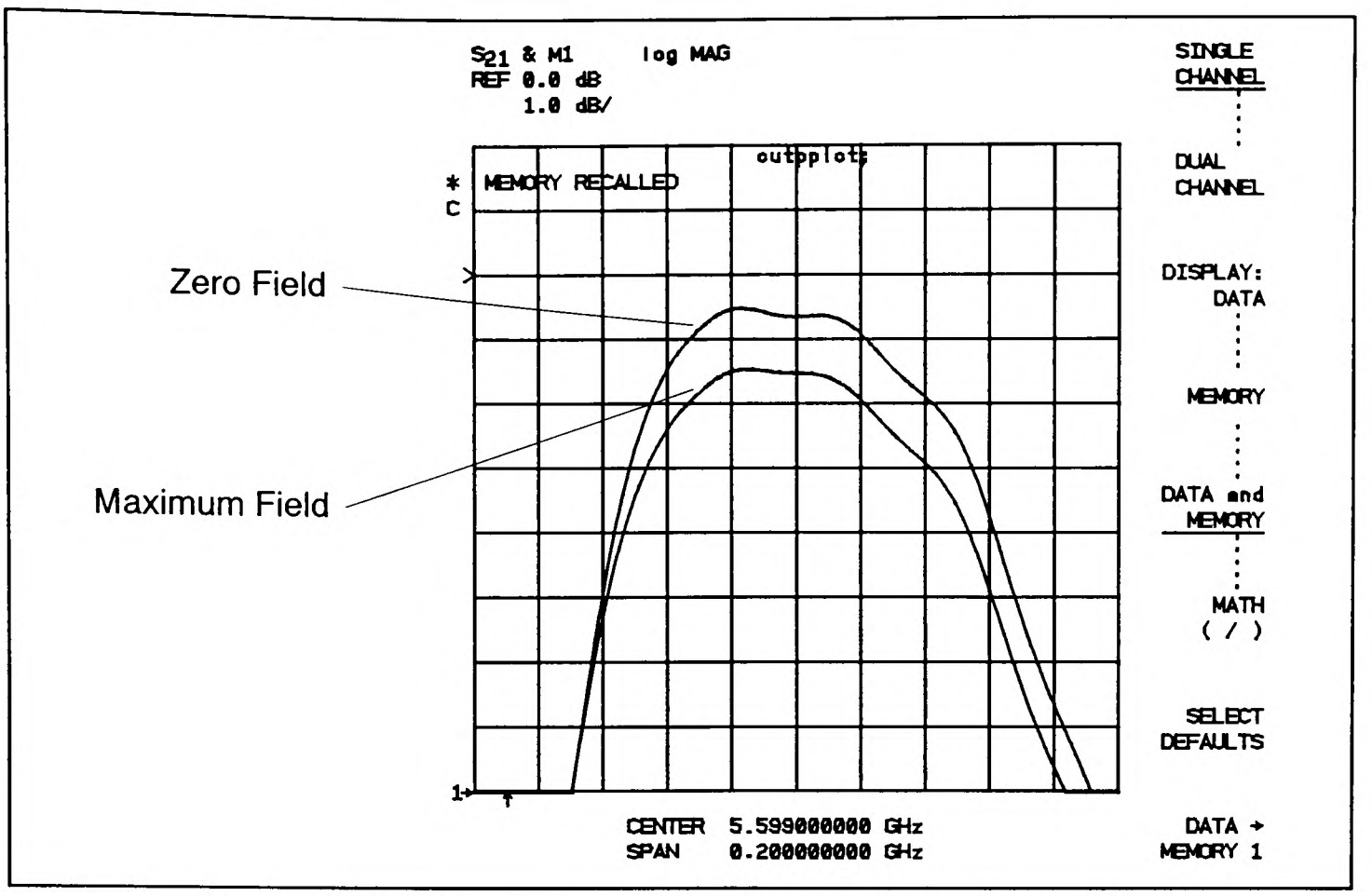

Figure 5.13 Filter Response at Zero and Maximum Field

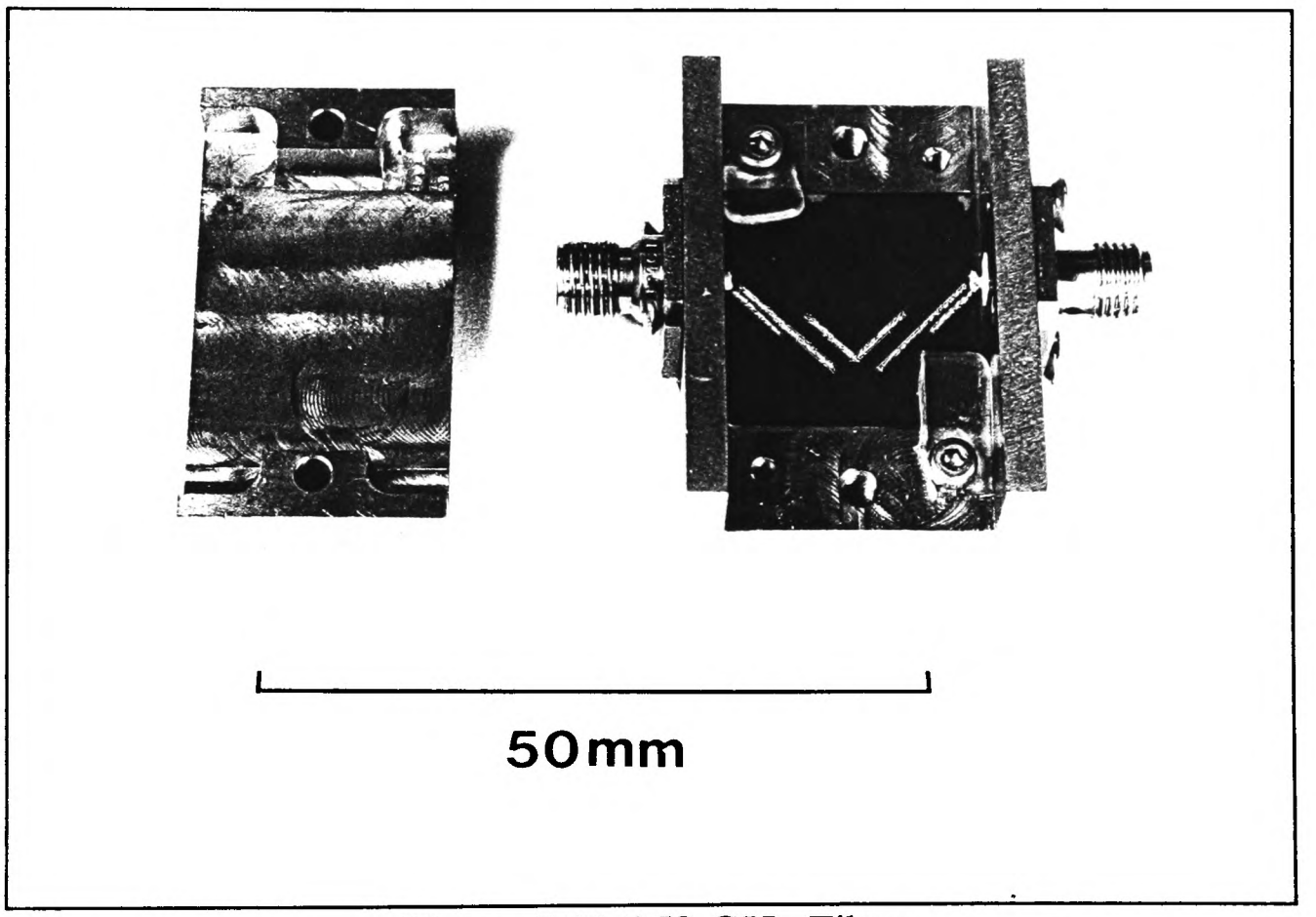

Figure 5.14 5.58 GHz Filter

5.4 Oscillators

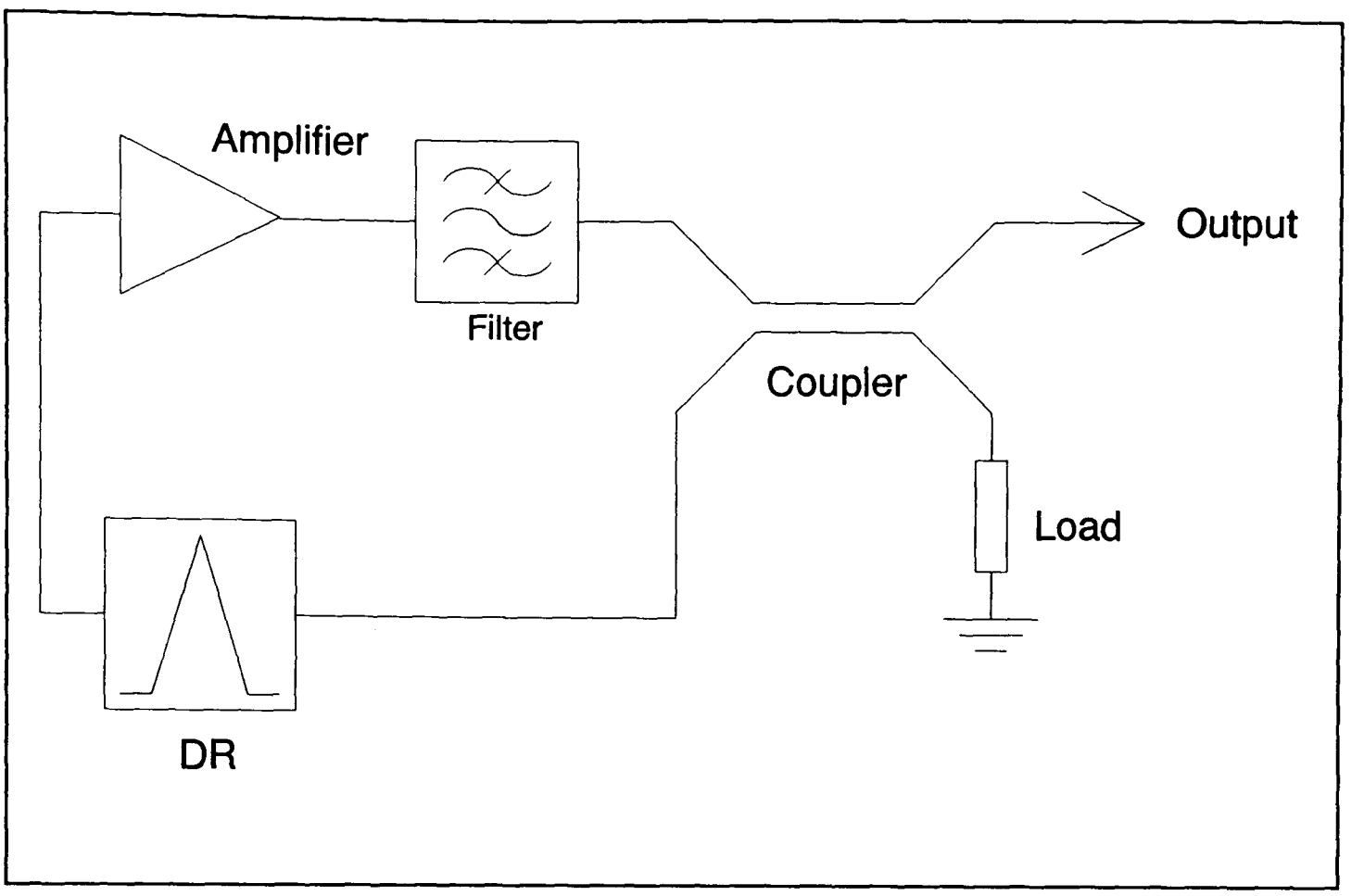

Figure 5.15 5.58 GHz Oscillator Schematic

The Oxford group has already shown considerable success by producing a hybrid HTS/semiconductor 3.1 GHz oscillator with a phase noise of less than -61 dBc/Hz at 10 kHz offset which was an improvement of 29 dBc/Hz over the equivalent copper implementation [5.10]. To follow on from this it was intended to use the 5.58 GHz filter, the 5.58 GHz DR and a gain element to produce a feedback oscillator with very low phase noise. Fig. 5.15 shows the schematic for such a device.

However, within the constraints of this research it has not been possible to construct this oscillator together with a suitable set-up that would be capable of measuring its phase noise. This has been left as further work.

5.5 Conclusions

This chapter has reviewed a number of HTS microwave devices that have been built and tested. The performance of the filters is especially promising and would yield considerable benefits for satellite front ends as high performance can be delivered in a small, light package. A reliable patterning process for these filters and other devices using glass masks and an adipic acid etch has been developed. There has also been a demonstration, for the first time, of an HTS filter whose centre frequency can be tuned with the application of a magnetic field. Other experiments on this filter have shown similar effects on insertion loss and bandwidth. Such tuning has exhibited hysteresis and it has been postulated that this is due, in some part, to the existence of a trapped field in the superconductor. However, further investigation of this is necessary to determine the exact cause of this effect.

In addition, by using a 13 GHz centre frequency filter patterned onto HTS coated $LaAlO_3$ it has been shown that careful consideration needs to be given to modelling devices and the accuracy of microwave CAD packages should not be taken for granted, especially when dielectric constants greater than 10 are used. It has been suggested that for quasi-static analysis on $LaAlO_3$ a dielectric constant of 21.04 is better for modelling, but this is only a first step and takes no consideration of other effects such as cross-coupling between lines.

A schematic for a 5.58 GHz oscillator using an HTS filter and dielectric resonator has been given, but further work is required in order to produce this. Given sufficient time and resources this could be achieved and its phase noise measured.

5.6 References

[5.1] Jenkins A.P. (1994) *Microwave Applications of High Temperature Superconductors*. Unpublished D.Phil. thesis, University of Oxford.

[5.2] Jim K. (1995) *Superconducting Microwave Devices*. Unpublished final year project dissertation, University of Oxford.

[5.3] El-Ghazaly S.M. et al (1992) "Analysis of superconducting microwave structures: application to microstrip lines". *IEEE Transactions on Microwave Theory and Techniques* 40(3): 499-508.

[5.4] Macdonald P. et al (1994) "HTS microstrip matching networks and filters". *IEEE Transactions on Microwave Theory and Techniques* 42(3): 523-525.

[5.5] York R.A., Compton R.C. (1990) "Experimental evaluation of existing CAD models for microstrip dispersion". *IEEE Transactions on Microwave Theory and Techniques* 38(3): 327-328.

[5.6] Hollmann E.K. et al (1994) "Substrates for high-T_c superconductor microwave integrated circuits". *Superconductor Science and Technology* 6(1): 1-13.

[5.7] Edwards D.J. (1995) (Private Communication).

[5.8] Jenkins A.P. et al (1993) "Microwave characteristics of Tl-Ba-Ca-Cu-O thin film microstrip resonators". In H.C. Freyhardt (ed.) *Applied Superconductivity 1993 Volume 2*. Obersürsel, Germany: DGM Informationsgesellschaft mbH: 1033-1036.

[5.9] Wosik J. et al (1992) "Effect of the weak links on the surface resistance of YBCO bulk materials" In *Proceedings of MRS Spring Meeting, Symposium S, USA, May*.

[5.10] Jenkins A.P. et al (1995) "An HTS microstrip resonator stabilised voltage controlled oscillator". In D. Dew-Hughes (ed.) *Applied Superconductivity 1995 Volume 2*. Bristol: IoP Publishing: 1183-1186.

Chapter 6

Conclusions

This chapter will review the achievements of the research which show that HTS films can be characterized for microwave applications and can be used to produce high performing devices. Characterization has been done by different techniques and is a necessary step for deducing the quality of films produced. The devices made demonstrate that HTS can perform better than conventional conductors in the microwave field. This chapter also makes suggestions for future research work.

6.1 Research Summary

The research described in this thesis has concentrated upon the microwave characterization and applications of HTS. It has been shown, in a number of ways, that there is considerable potential for HTS to be exploited to produce higher performance devices in smaller packages leading to significant cost savings.

The following is a review of the research's main achievements.

1. The use of several techniques for the measurement of the R_s of HTS films on different substrates. These have included the parallel plate resonator, complete and partial end wall replacement, the microstrip resonator and different sizes of dielectric resonator. These techniques have been compared and contrasted. Thallium-based thin films with an R_s as low as 54-69 $\mu\Omega$ at 80K and scaled to 10 GHz have been measured on 1 cm square $LaAlO_3$ substrates. Two inch diameter thin films on $LaAlO_3$ have also been tested and the lowest R_s measured on these was 4.37 m$\Omega\pm$14.0% at 77K and scaled to 10 GHz. The lowest R_s measured on a 2 cm square $LaAlO_3$ sample was 0.6 m$\Omega\pm$14.9% at 80K and scaled to 10 GHz. The R_s of double sided MgO 2 cm square samples has also been measured and the lowest result achieved here was 0.6 m$\Omega\pm$16.5% at 80K and scaled to 10 GHz, although the other side of this film had an R_s of 92.9 m$\Omega\pm$1.1% showing that double sided deposition needs very careful control of processing conditions. Of the thick film samples

tested one was found to have one of the lowest R_s values in the world of 2.7 m$\Omega \pm 8.0\%$ at 77K and scaled to 10 GHz.

2. The dielectric resonator as an R_s measurement tool has been examined in great detail. Consideration has been given to losses that are present in the walls of an enclosure that holds a resonator (an area that has been neglected in the past). This has shown that for all the dielectric resonators made and used during this research programme the effect of these walls could be considered as negligible.

3. The dielectric resonator has been used to investigate the loss tangent of dielectric materials, especially sapphire. This has shown that the loss tangent of sapphire is not as low as reported by some researchers and the highest quality sapphire should be used in dielectric resonators if very high Q values are to be achieved.

4. Microstrip resonators with Q values better than the equivalent copper designs have been made and have served the dual purpose of R_s characterization and operating as devices in their own right.

5. A variety of filters with centre frequencies in the range 5.58-13 GHz have been made and tested. Various processing routes have been used for the patterning of these filters. It was found that to control dimensions very

accurately, especially for the most detailed designs, the use of glass masks and adipic acid is recommended. The 13 GHz filter has been used to improve future modelling on high dielectric constants by adjustment of the dielectric constant in the Touchstone CAD package, although this is not a complete solution. Two channel filters have been constructed with centre frequencies of 10 and 10.63 GHz and have shown the possibility of using banks of filters in a small, light package capable of replacing waveguide components. A 5.58 GHz filter constructed has an insertion loss in the passband of 0.5 dB which is significantly better than the equivalent copper model and compares well with other HTS filters made in the world.

6. Magnetic measurements on this filter have shown effects on the centre frequency, insertion loss and bandwidth resulting in hysteretic "butterfly" curves as the field is cycled. It has been postulated that these effects may, in some part, be attributed to a trapped field in the HTS. The influence of the magnetic field on the centre frequency has allowed for the first demonstration of a tunable HTS thin film filter.

6.2 Further Work

There are a number of areas where the research described in this thesis can be extended. Firstly, given the limitations that a dielectric without a very low loss tangent can place upon the performance of a dielectric resonator it would be a good

proposal to obtain sapphire with a loss tangent of less than 10^{-7} at microwave frequencies. This will have two benefits: make the measurement of HTS R_s easier and more accurate and allow a higher Q to be achieved. Such high quality sapphire is available and has been used by Du Pont to produce a dielectric resonator with a unloaded Q value in excess of 10^6 [6.1].

Secondly, the 5.58 GHz dielectric resonator and 5.58 GHz HTS filter could be combined with a gain element to produce a very low phase noise oscillator. This was an original intention of this research but due to resource and time constraints it was not possible to produce this. A schematic was given in the last chapter of how such an oscillator could be manufactured.

The phase noise of the oscillator can be measured in various ways. One method may be to compare the output of the oscillator with a low noise source operating at the same frequency and then mixing the two signals down to baseband. Any phase fluctuation in the oscillator output would result in a voltage fluctuation at the output of the mixer which would indicate the amount of phase noise present [6.2].

However, as the intention is to produce a very low phase noise oscillator and given the high Q values that can be obtained from a dielectric resonator it is possible that the phase noise of the oscillator may be below that of the source. Therefore, Fig. 6.1 shows an alternative that requires the use of only the oscillator as source combined with other discriminator elements.

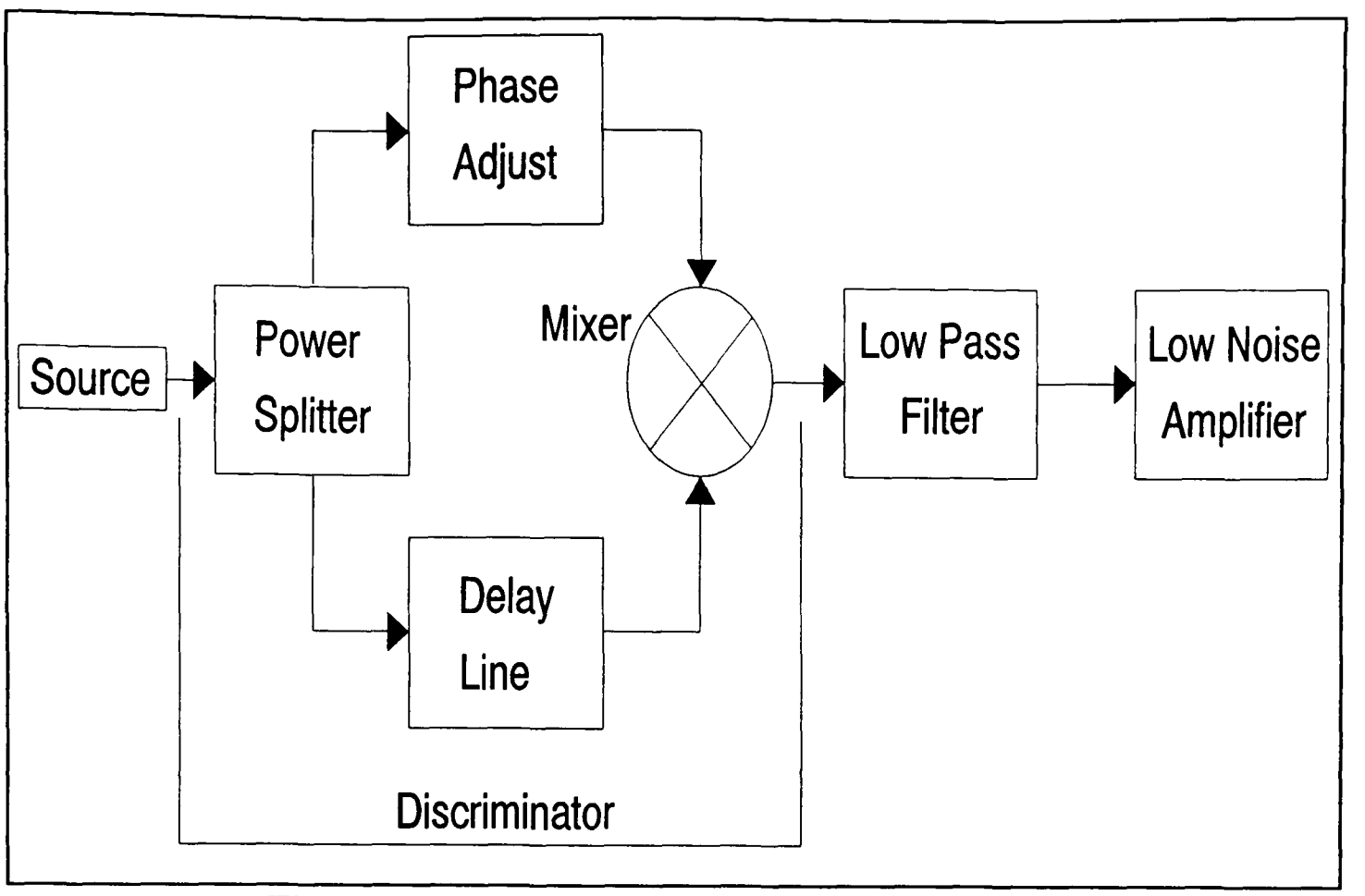

Figure 6.1 Phase Noise Measurement [after 6.2]

The delay line serves to uncorrelate the noise of the source from the upper path after power splitting and converts the frequency fluctuations of the source into phase fluctuations which the mixer then translates into voltage fluctuations which can then be converted into a phase noise figure.

This approach to phase noise measurement not only reduces the hardware required for measurement, but is also useful in cases where there is a high degree of drift in the output of the source which would occur if, for instance, the temperature of the dielectric resonator varied [6.3]. However, the simplicity of the arrangement would be most useful for testing at different temperatures without having to re-set the frequency of another reference source.

Thirdly, the performance of the microstrip resonators needs to be improved. The best unloaded Q value obtained in this research was only 625 which is two orders of magnitude lower than the best obtained in the world using the same geometry. This improvement seems possible given that less harsh etches are now in use and the R_s of films are now low enough. Indeed our group has recently reported on a microstrip resonator with an unloaded Q of 1491 at 77K operating at 3.078 GHz with an input power of -30 dBm [6.4]. Coupled with the reliable patterning process route described in section 5.1 such resonators could produce not only high Q values, but be manufactured to operate at the desired frequency without the need of tuning.

It is also possible to investigate different geometries for resonators that do not place such a heavy burden in terms of high current densities. For instance, disk resonators would lower the current density across the film considerably at the expense of using a larger area of substrate [6.5]. Such resonators would also find application in high power applications of microwave devices, such as high power filters, extending the range of HTS use and driving down costs at a systems level.

To summarize, this research has investigated the characterization of HTS films showing that they can have very low R_s values compared to normal conductors such as copper. The R_s of these films has been measured by a number of techniques. In some cases the same films have been tested using different methods to compare different R_s measurement techniques and to find the dependence of R_s on frequency. Such characterization was performed as a means to an end with the ultimate aim of

producing working HTS devices. Many different types of these have been made and tested. The devices show the potential for the application of HTS components in satellites and mobile base stations.

6.3 References

[6.1] Shen Z. et al (1992) "High T_c superconductor-sapphire microwave resonator with extremely high Q-values up to 90K". *IEEE Transactions on Microwave Theory and Techniques* 40(12): 2424-2432.

[6.2] Decker T., Temple B. (?) "Choosing a phase noise measurement technique: concepts and implementation". *Technical Data Sheet, HP RF & Microwave Measurement Symposium and Exhibition*.

[6.3] Suter W.A. (1995) "Phase noise measurements for under $250". *RF Design* 18(September): 60-69.

[6.4] Jenkins A.P. et al (1995) "An HTS microstrip resonator stabilised voltage controlled oscillator". In D. Dew-Hughes (ed.) *Applied Superconductivity 1995 Volume 2*. Bristol: IoP Publishing: 1183-1186.

[6.5] Jenkins A.P. et al (1996) "Microstrip disk resonators for filters fabricated from TBCCO thin films". Presented at the *Applied Superconductivity Conference 1996*, Pittsburgh, PA, USA, 25-30 August.

Appendix A

Complex Conductivity

The following is a derivation of the complex conductivity for superconductors.

For normal electrons in an electric field:

$$m\frac{dv_N}{dt} + \frac{mv_N}{\tau} = eE$$

where: m=mass of electron

v_N=electron velocity

τ=relaxation time

e=electron charge

E=electric field

let:

$$E = E_o e^{j\omega t} \qquad and \qquad v_N = V_N e^{j\omega t}$$

$$\Rightarrow \quad mj\omega V_N e^{j\omega t} + \frac{m}{\tau} V_N e^{j\omega t} = eE_o e^{j\omega t}$$

$$\Rightarrow \quad V_N = \frac{\left(\frac{e\tau}{m}\right)E_o}{1 + j\omega\tau} \qquad (A.1)$$

For the superconducting electrons starting from the second London equation:

$$\frac{m}{n_S q^2}\frac{dJ_S}{dt} = E \qquad (A.2)$$

where: q=superelectron charge=2e

J_S=superelectron current density

n_S=superelectron number density

And we have:

$$J_S = n_S q v_S \qquad \Rightarrow \qquad \frac{dJ_S}{dt} = n_S q \frac{dv_S}{dt} \tag{A.3}$$

where: v_S=superelectron velocity

Combining (A.2) and (A.3):

$$m\frac{dv_S}{dt} = qE$$

With the sinusoidal variations:

$$E = E_o e^{j\omega t} \qquad and \qquad v_S = V_S e^{j\omega t}$$

$$\Rightarrow \quad V_S = \frac{qE_o}{jm\omega} \tag{A.4}$$

The total current density is given by:

$$J = J_N + J_S$$
$$\therefore \quad J = n_N e V_N + n_S q V_S$$

Substituting (A.1) and (A.4) gives:

$$J = \left[\frac{(n_N e^2\tau/m)}{1 + j\omega\tau}\right]E_o + \frac{n_S q^2 E_o}{jm\omega}$$
$$= \frac{(n_N e^2\tau/m)}{1 + \omega^2\tau^2}E_o(1 - j\omega\tau) - \frac{jn_S q^2}{m\omega}E_o$$
$$= E_o\left(\frac{n_N e^2\tau}{m(1 + \omega^2\tau^2)} - j\left[\frac{n_N e^2\tau^2\omega^2}{m\omega(1 + \omega^2\tau^2)} + \frac{n_S q^2}{m\omega}\right]\right)$$

But since τ is small and $\omega^2\tau^2 << 1$ we have:

$$J = E_o\left(\frac{n_N e^2\tau}{m} - j\left[\frac{n_S q^2}{m\omega}\right]\right)$$

and the complex conductivity is defined as:

$$\sigma_{eff} = \frac{J}{E_o} = \frac{n_N e^2\tau}{m} - j\left[\frac{n_S q^2}{m\omega}\right] \qquad (A.4)$$

and the London penetration depth given by:

$$\lambda_L^2 = \frac{m}{\mu n_S q^2}$$

but q=2e:

$$\Rightarrow \qquad \lambda_L^2 = \frac{m}{4\mu n_S e^2} \quad or \quad e^2 = \frac{m}{4\mu n_S \lambda_L^2} \qquad (A.5)$$

(A.5) in (A.4) gives:

$$\sigma_{eff} = \frac{1}{\omega\mu\lambda_L^2}\left[\frac{\omega\tau}{4}\left(\frac{n_N}{n_S}\right) - j\right] \qquad (A.6)$$

Appendix B

Cavity End-Wall Replacement Theory

Figure B.1 shows a cavity of radius a and length d together with cylindrical co-ordinate axes.

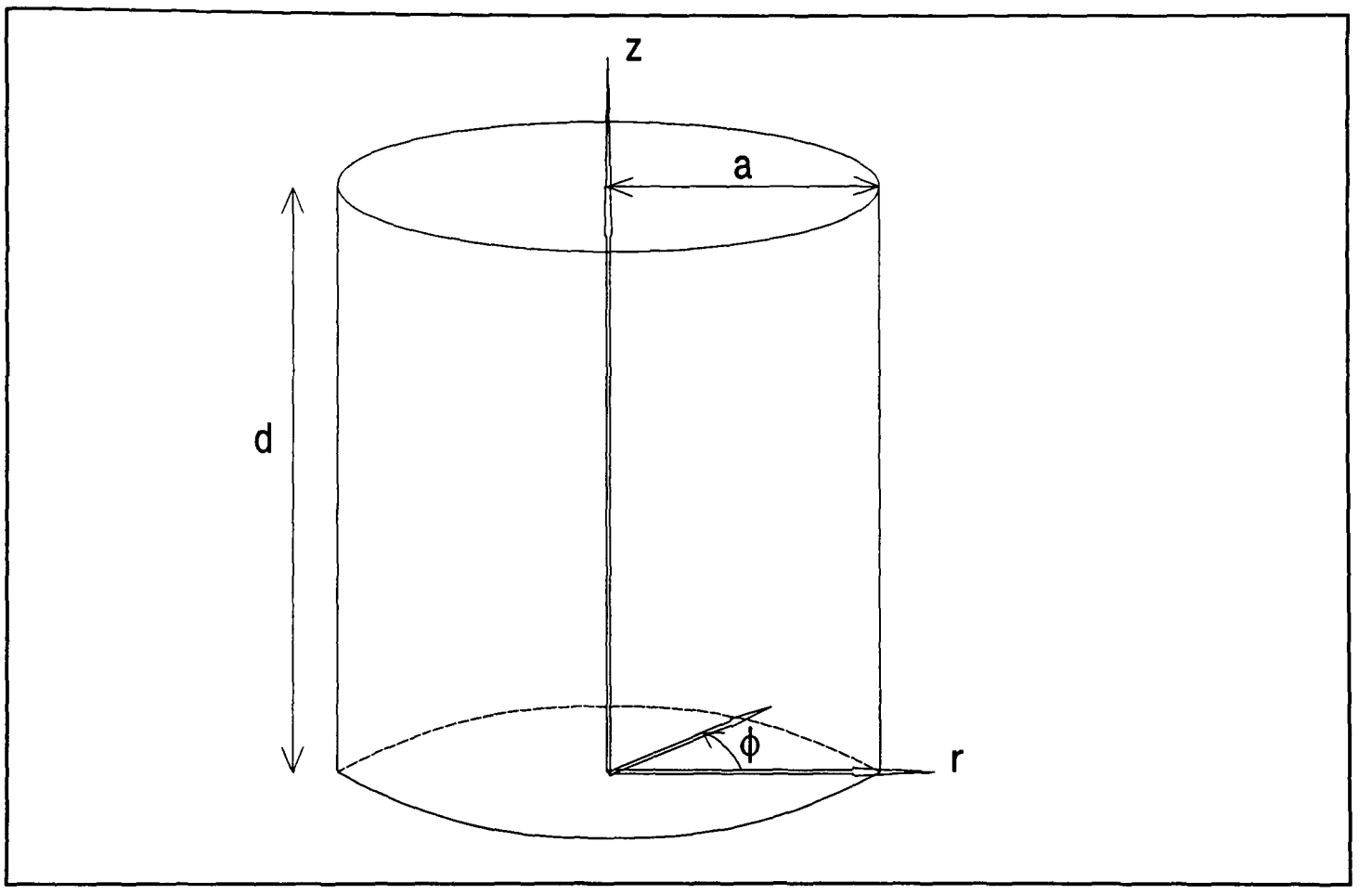

Figure B.1 Cavity

In the cavity we have a propagating wave in the z direction and so the Helmholtz equation is [B.1]:

$$\nabla^2 H_z + k^2 \epsilon_r H_z = 0 \qquad \text{(B.1)}$$

where: $k=\sqrt{(\omega^2 \mu_o \epsilon_o)}$ = propagation constant in free space.

The dielectric constant, ϵ_r, has been included in the equation as sometimes cavities are filled with a dielectric that needs to be considered in the analysis (see Appendix

C). The most common mode used for cavity measurements is the TE_{011} mode as it has a high Q (improving accuracy with better resolution on the measurement), currents do not flow across the junction between the end-plates and the cavity wall and the analysis is simplified because many of the field components become zero. Therefore, the following analysis is for this mode. In cylindrical co-ordinates the TE_{011} mode has no ϕ variations and so the wave equation becomes:

$$\frac{\partial^2 H_z}{\partial r^2} + \frac{1}{r}\frac{\partial H_r}{\partial r} + \frac{\partial^2 H_z}{\partial z^2} + k^2 \epsilon_r H_z = 0 \qquad \text{(B.2)}$$

The forward wave solution is:

$$H_z = AR(r)e^{-\gamma z} \qquad \text{(B.3)}$$

where:

$$\gamma = \alpha + j\beta \qquad \text{(B.4)}$$

The α component represents attenuation per unit length and β the phase shift per unit length. (B.3) in (B.2) gives:

$$\frac{R''}{R} + \frac{R'}{rR} = -\gamma^2 - k^2 \epsilon_r = constant = -\xi_1^{\,2} \qquad \text{(B.5)}$$

where:

$$R' = \frac{dR}{dr} \qquad \text{(B.6a)}$$

$$R'' = \frac{d^2 R}{dr^2} \qquad \text{(B.6b)}$$

and ξ_1 = r direction wave number in the cavity.

If we assume that the only losses in the cavity are due to the walls and end-plates of the cavity then $\alpha=0$ and $\gamma=j\beta$. So (B.5) becomes:

$$\frac{R''}{R} + \frac{R'}{rR} = \beta^2 - k^2\epsilon_r = constant = -\xi_1^2 \qquad \text{(B.7)}$$

The solution to (B.7) is:

$$H_z = A[J_o(\xi_1 r) + jY_o(\xi_1 r)]e^{-j\beta z} \qquad \text{(B.8)}$$

where: J_o and Y_o are zeroth order Bessel's functions of the first and second kind respectively.

However, this is the forward wave solution and we also have a backward wave to consider (as we have a resonant cavity) giving:

$$H_z = [AJ_o(\xi_1 r) + BY_o(\xi_1 r)][e^{-j\beta z} + e^{+j\beta z}] \qquad \text{(B.9)}$$

The first boundary condition is:

$$z = 0,\ H_z = 0 \qquad \text{(B.10)}$$

$$\Rightarrow H_z = AJ_o(\xi_1 r)[e^{-j\beta z} - e^{j\beta z}] \qquad \text{(B.11)}$$

$$H_z = AJ_o(\xi_1 r)\sin(\beta z) \qquad \text{(B.12)}$$

(B.12) is the solution for the magnetic field in the z direction. However, in order to completely solve for the cavity other field components need to be found. For these we use Maxwell's equations in cylindrical co-ordinates:

$$\underline{\nabla}\times\underline{E} = \frac{1}{r}\begin{vmatrix} \hat{\underline{r}} & r\hat{\underline{\phi}} & \hat{\underline{z}} \\ \frac{\partial}{\partial r} & \frac{\partial}{\partial \phi} & \frac{\partial}{\partial z} \\ E_r & rE_\phi & E_z \end{vmatrix} = -j\omega\mu\underline{H} = -\frac{\partial \underline{B}}{\partial t} \tag{B.13}$$

$$\Rightarrow \frac{1}{r}\frac{\partial E_z}{\partial \phi} - \frac{\partial E_\phi}{\partial z} = -j\omega\mu H_r \tag{B.14}$$

$$\frac{\partial E_r}{\partial z} - \frac{\partial E_z}{\partial r} = -j\omega\mu H_\phi \tag{B.15}$$

$$\frac{1}{r}\left(\frac{\partial (rE_\phi)}{\partial r} - \frac{\partial E_r}{\partial \phi}\right) = -j\omega\mu H_z \tag{B.16}$$

Note that $\mu = \mu_o\mu_r$.

Also:

$$\underline{\nabla}\times\underline{H} = \frac{1}{r}\begin{vmatrix} \hat{\underline{r}} & r\hat{\underline{\phi}} & \hat{\underline{z}} \\ \frac{\partial}{\partial r} & \frac{\partial}{\partial \phi} & \frac{\partial}{\partial z} \\ H_r & rH_\phi & H_z \end{vmatrix} = j\omega\epsilon E_r \tag{B.17}$$

$$\Rightarrow \frac{1}{r}\frac{\partial H_z}{\partial \phi} - \frac{\partial H_\phi}{\partial z} = j\omega\epsilon E_r \tag{B.18}$$

$$\frac{\partial H_r}{\partial z} - \frac{\partial H_z}{\partial r} = j\omega\epsilon E_\phi \tag{B.19}$$

$$\frac{1}{r}\left[\frac{\partial (rH_\phi)}{\partial r} - \frac{\partial H_r}{\partial \phi}\right] = j\omega\epsilon E_z \tag{B.20}$$

Note that $\epsilon = \epsilon_o\epsilon_r$

(B.19) in (B.14) gives:

$$\left(\frac{\partial^2}{\partial z^2} + \omega^2\mu\epsilon\right)H_r = j\frac{\omega\epsilon}{r}\frac{\partial E_z}{\partial\phi} + \frac{\partial}{\partial z}\left(\frac{\partial H_z}{\partial r}\right) \tag{B.21}$$

(B.18) in (B.15) gives:

$$\left(\frac{\partial^2}{\partial z^2} + \omega^2\mu\epsilon\right)H_\phi = \frac{1}{r}\frac{\partial}{\partial z}\left(\frac{\partial H_z}{\partial\phi}\right) - j\omega\epsilon\frac{\partial E_z}{\partial r} \tag{B.22}$$

(B.15) in (B.18) gives:

$$\left(\frac{\partial^2}{\partial z^2} + \omega^2\mu\epsilon\right)E_r = -\frac{\partial}{\partial z}\left(\frac{\partial E_r}{\partial r}\right) + j\frac{\omega\mu}{r}\frac{\partial H_z}{\partial\phi} \tag{B.23}$$

(B.14) in (B.19) gives:

$$\left(\frac{\partial^2}{\partial z^2} + \omega^2\mu\epsilon\right)E_\phi = \frac{1}{r}\frac{\partial}{\partial z}\left(\frac{\partial E_z}{\partial\phi}\right) + j\omega\mu\frac{\partial H_z}{\partial r} \tag{B.24}$$

Equations (B.13)-(B.20) can be used, if required, to find all the field components for all modes in the cavity. However, as only the TE_{011} mode is being analyzed here only E_ϕ, H_z and H_r need be considered. In addition, there are no ϕ variations for this mode. (B.21) becomes:

$$\left(\frac{\partial^2}{\partial z^2} + \omega^2\mu\epsilon\right)H_r = \frac{\partial}{\partial z}\left(\frac{\partial H_z}{\partial r}\right) \tag{B.25}$$

(B.22) and (B.23) become 0=0 and (B.24) becomes:

$$\left(\frac{\partial^2}{\partial z^2} + \omega^2\mu\epsilon\right)E_\phi = j\omega\mu\frac{\partial H_z}{\partial r} \tag{B.26}$$

Equation (B.12) showed that:

$$H_z = AJ_o(\xi_1 r)\sin(\beta z) \tag{B.27}$$

(B.27) in (B.25) gives:

$$\left(\frac{\partial^2}{\partial z^2} + \omega^2\mu\epsilon\right)H_r = -\xi_1\beta AJ_1(\xi_1 r)\cos(\beta z) \tag{B.28}$$

The solution to which is:

$$H_r = -A\frac{\beta}{\xi_1}J_1(\xi_1 r)\cos(\beta z) \tag{B.29}$$

(B.27) in (B.26) gives:

$$\left(\frac{\partial^2}{\partial z^2} + \omega^2\mu\epsilon\right)E_\phi = -j\omega\mu\xi_1 AJ_1(\xi_1 r)\sin(\beta z) \tag{B.30}$$

The solution to which is:

$$E_\phi = -jA\frac{\omega\mu}{\xi_1}J_1(\xi_1 r)\sin(\beta z) \tag{B.31}$$

Remembering that $\beta d=\pi$, the non-zero field expressions for the TE_{011} mode in the cavity can be expressed as:

$$H_z = AJ_o(\xi_1 r)\sin\left(\frac{\pi z}{d}\right) \tag{B.32}$$

$$H_r = -A\frac{\beta}{\xi_1}J_1(\xi_1 r)\cos\left(\frac{\pi z}{d}\right) \tag{B.33}$$

$$E_\phi = -jA\frac{\omega\mu}{\xi_1}J_1(\xi_1 r)\sin\left(\frac{\pi z}{d}\right) \tag{B.34}$$

For a cylindrical cavity $E_\phi=0$ at r=a so (B.34) gives $J_1(\xi_1 a)=0$. That is $\xi_1 a = R_{1n}$ where R_{1n} is the nth root of J_1 and n=1, 2,...

For the TE_{011} mode, n=1, and so $R_{11}=3.83=\xi_1 a$ (from tables). Combining this with equation (B.7) gives:

$$-\beta^2 + k^2\epsilon_r = \frac{3.83^2}{a^2} \tag{B.35}$$

Therefore:

$$\beta = \pm\left[k^2\epsilon_r - \left(\frac{3.83}{a}\right)^2\right]^{\frac{1}{2}} \tag{B.36}$$

For the TE_{011} mode $\beta d=\pi$ hence (B.36) becomes:

$$k = \frac{1}{\sqrt{\epsilon_r}}\left[\left(\frac{\pi}{d}\right)^2 + \left(\frac{3.83}{a}\right)^2\right]^{\frac{1}{2}} \tag{B.37}$$

Now $k=(2\pi f_o)/c$ giving the resonant frequency of the cavity as:

$$f_o = \frac{c}{2\pi\sqrt{\epsilon_r}}\left[\left(\frac{\pi}{d}\right)^2 + \left(\frac{3.83}{a}\right)^2\right]^{\frac{1}{2}} \tag{B.38}$$

The quality factor of the cavity is given by:

$$Q = \frac{2\pi f_o W}{P} \tag{B.39}$$

where: W = time average stored energy

P = energy loss per second.

For the cavity the electrical energy equals the magnetic energy:

$$W_e = W_m \tag{B.40}$$

and:

$$W = W_e + W_m \tag{B.41}$$

giving:

$$W = 2W_e \tag{B.42}$$

In cylindrical co-ordinates:

$$W_e = \frac{\epsilon}{4}\int_0^{2\pi}\int_0^a\int_0^d |E_\phi|^2 \, r\,d\phi\,dr\,dz \tag{B.43}$$

Putting (B.34) in (B.43) gives:

$$W_e = \frac{\epsilon A^2}{4}\left(\frac{\omega\mu}{\xi_1}\right)^2 2\pi\int_0^a\int_0^d r\,|J_1(\xi_1 r)|^2 \sin^2\left(\frac{\pi z}{d}\right)\,dr\,dz \tag{B.44}$$

Carrying out the integration wrt z first:

$$W_e = \frac{\epsilon\pi A^2}{2}\left(\frac{\omega\mu}{\xi_1}\right)^2 \frac{d}{2}\int_0^a r|J_1(\xi_1 r)|^2\, dr \tag{B.45}$$

Isolating the integration wrt r we have [B.2]:

$$\int_0^a r|J_1(\xi_1 r)|^2\, dr = \left[\frac{r^2}{2}\left(J_1^2(\xi_1 r) - \frac{2J_o(\xi_1 r)J_1(\xi_1 r)}{\xi_1 r} + J_o^2(\xi_1 r)\right)\right]_0^a \tag{B.46}$$

But $J_1(\xi_1 a)=0$ so this reduces to:

$$\int_0^a r|J_1(\xi_1 r)|^2\, dr = \frac{a^2}{2}J_o^2(\xi_1 a) \tag{B.47}$$

Giving:

$$W_e = \frac{1}{8}A^2\epsilon\pi d a^2\left(\frac{\omega\mu}{\xi_1}\right)^2 J_o^2(\xi_1 a) \tag{B.48}$$

and:

$$W = \frac{1}{4}A^2\epsilon\pi d a^2\left(\frac{\omega\mu}{\xi_1}\right)^2 J_o^2(\xi_1 a) \tag{B.49}$$

The energy dissipated in the cavity by the wall and end-plates is given by the following surface integral:

$$P = \frac{1}{2}\int_s R_s|H|^2\, ds \tag{B.50}$$

The dissipated energy is now broken down into two contributions: one from the end-plates and one from the cavity wall. First, consider the end-plates. Using equation (B.33) we have:

$$P_{12} = \frac{R_1 + R_2}{2}\int_0^a\int_0^{2\pi} |A\frac{\pi}{d\xi_1}J_1(\xi_1 r)|^2 \; r d\phi dr \tag{B.51}$$

where: R_1 and R_2 are the surface resistances of the end-plates.

$$P_{12} = \frac{R_1 + R_2}{2} 2\pi \frac{A^2\pi^2}{d^2\xi_1^2}\int_0^a r|J_1(\xi_1 r)|^2 \; dr \tag{B.52}$$

$$P_{12} = \frac{R_1 + R_2}{2}\frac{A^2\pi^3 a^2}{d^2\xi_1^2}J_o^2(\xi_1 a) \tag{B.53}$$

Now consider the dissipated energy in the cavity wall (using (B.32)):

$$P_3 = \frac{R_3}{2}\int_0^d\int_0^{2\pi} |AJ_o(\xi_1 a)\sin\left(\frac{\pi z}{d}\right)|^2 \; a \, d\phi dz \tag{B.54}$$

where: R_3 = surface resistance of the cavity wall.

$$P_3 = \frac{R_3}{2} 2\pi a A^2 J_o^2(\xi_1 a)\int_0^d \sin^2\left(\frac{\pi z}{d}\right) dz \tag{B.55}$$

$$P_3 = \frac{R_3}{2}\pi a d A^2 J_o^2(\xi_1 a) \tag{B.56}$$

Letting $\overline{R}_1 = R_1/R_3$ and $\overline{R}_2 = R_2/R_3$ we have:

$$P = P_{12} + P_3 = A^2 J_o^2(\xi_1 a)\pi a R_3\left[\frac{d}{2} + \frac{\bar{R}_1 + \bar{R}_2}{2}\frac{\pi^2 a}{d^2\xi_1^2}\right] \tag{B.57}$$

$$P = \frac{A^2 J_o^2(\xi_1 a)\pi a R_3 d}{2(\xi_1 a)^2}\left[(\xi_1 a)^2 + (\bar{R}_1 + \bar{R}_2)\frac{a^3\pi^2}{d^3}\right] \tag{B.58}$$

Substitute equations (B.49) and (B.58) into (B.39):

$$\Rightarrow Q = \frac{\omega^3 a^3 \epsilon \mu^2}{2R_3\left[(\xi_1 a)^2 + (\bar{R}_1 + \bar{R}_2)\frac{a^3\pi^2}{d^3}\right]} \tag{B.59}$$

and remembering $k^2=\omega^2\epsilon_o\mu_o$ gives:

$$Q = \frac{(ka)^3\sqrt{\frac{\mu_o}{\epsilon_o}}}{2R_3\left[(\xi_1 a)^2 + (\bar{R}_1 + \bar{R}_2)\frac{a^3\pi^2}{d^3}\right]} \times \epsilon_r \mu_r^2 \tag{B.60}$$

The first part of this equation is for an air-filled cavity and the $\epsilon_r\mu_r^2$ factor allows for cavities that are dielectrically and ferro-magnetically loaded. Also $(\xi_1 a)^2 = (ka)^2 - (\beta a)^2$ and $\beta = \pi/d$ giving:

$$(ka)^2 = (\xi_1 a)^2 + \left(\frac{\pi a}{d}\right)^2 \tag{B.61}$$

The free space impedance is given by $\eta = \sqrt{(\mu_o/\epsilon_o)}$ giving:

$$Q = \frac{\eta\left[(\xi_1 a)^2 + \left(\frac{\pi a}{d}\right)^2\right]^{\frac{3}{2}}}{2R_3\left[(\xi_1 a)^2 + (\bar{R}_1 + \bar{R}_2)\frac{a^3\pi^2}{d^3}\right]} \times \epsilon_r \mu_r^2 \tag{B.62}$$

Alternatively, since $\xi_1 a = R_{11}$ for the TE_{011} mode we have:

$$Q = \frac{\eta\left[(R_{11})^2 + \left(\frac{\pi a}{d}\right)^2\right]^{\frac{3}{2}}}{2R_3\left[(R_{11})^2 + (\bar{R}_1 + \bar{R}_2)\frac{a^3\pi^2}{d^3}\right]} \times \epsilon_r \mu_r^2 \tag{B.63}$$

If we have a superconducting end-plate in an otherwise copper cavity then $R_3 = R_{cu}$, $\bar{R}_1 = 1$ and $R_2 = R_{sc}$ giving:

$$Q_{sc} = \frac{\eta\left[R_{11}^2 + \left(\frac{\pi a}{d}\right)^2\right]^{\frac{3}{2}}}{2R_{cu}\left[R_{11}^2 + \pi^2\left(\frac{a}{d}\right)^3\right] + 2R_{sc}\pi^2\left(\frac{a}{d}\right)^3} \times \epsilon_r \mu_r^2 \tag{B.64}$$

For a cavity made entirely of the same material (e.g. copper end-plates and a copper wall), $\overline{R}_1 = \overline{R}_2 = 1$ giving:

$$Q_{cu} = \frac{\eta\left[(R_{11})^2 + \left(\frac{\pi a}{d}\right)^2\right]^{\frac{3}{2}}}{2R_{cu}\left[(R_{11})^2 + 2\pi^2\left(\frac{a}{d}\right)^3\right]} \times \epsilon_r \mu_r^2 \tag{B.65}$$

Let the numerator be denoted by:

$$F = \eta\left[(R_{11})^2 + \left(\frac{\pi a}{d}\right)^2\right]^{\frac{3}{2}} \times \epsilon_r \mu_r^2 \tag{B.66}$$

Then inverting equations (B.64) and (B.65) and subtracting we have:

$$\frac{1}{Q_{cu}} - \frac{1}{Q_{sc}} = \frac{2\pi^2\left(\frac{a}{d}\right)^3 (R_{cu} - R_{sc})}{F} \tag{B.67}$$

or:

$$R_{sc} = R_{cu} - \left[\frac{1}{Q_{cu}} - \frac{1}{Q_{sc}}\right] \frac{F}{2\pi^2\left(\frac{a}{d}\right)^3} \tag{B.68}$$

References

[B.1] Collin R.E. (1992) *Foundations for Microwave Engineering*, 2nd ed. Singapore: McGraw Hill.

[B.2] Gray A., Matthews G.B. (1966) *A Treatise on BESSEL FUNCTIONS and Their Application to Physics*, 2nd ed. London: Constable and Company Ltd.

Appendix C

Dielectric Resonator Theory

The following derivation is for a dielectric resonator, inside a cylindrical metallic enclosure, operating in the TE_{011} mode. Figure C.1 shows the resonator with the relevant dimensions and axes.

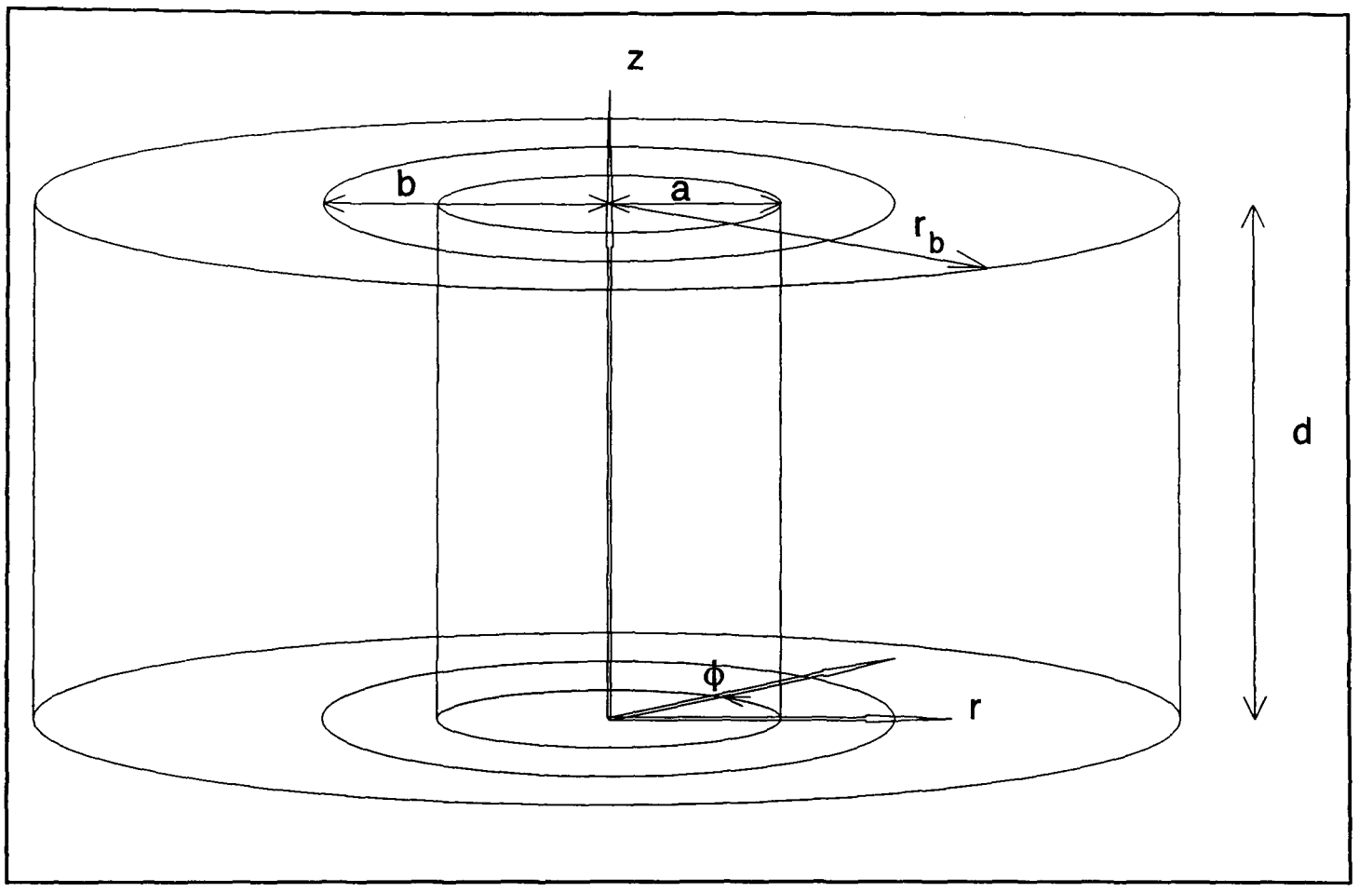

Figure C.1 Dielectric Resonator

Equations (B.32), (B.33) and (B.34) (Appendix B) give the field expressions for this mode inside the dielectric. Outside the dielectric the field expressions are found as follows. Assuming the dielectric is surrounded by air or vacuum then equation (B.7) becomes:

$$\frac{R''}{R} + \frac{R'}{rR} = \beta^2 - k^2 = constant = +\xi_2^2 \qquad (C.1)$$

The solution to (C.1) is:

$$H_z = A[J_o(j\xi_2 r) + jY_o(j\xi_2 r)]e^{-j\beta z} \qquad (C.2)$$

where: J_o and Y_o are zeroth order Bessel's functions of the first and second kind respectively.

But:

$$K_n(\xi_2 r) = \frac{\pi}{2} j^{n+1}[J_n(j\xi_2 r) + jY_n(j\xi_2 r)] \qquad (C.3)$$

where: K_n is the nth order modified Bessel function of the second kind.

So the solution becomes:

$$H_z = BK_o(\xi_2 r)e^{-j\beta z} \qquad (C.4)$$

However, this is the forward wave solution and we also have a backward wave to consider (as we have a resonant cavity) giving:

$$H_z = K_o(\xi_1 r)[Ae^{-j\beta z} + Be^{+j\beta z}] \qquad (C.5)$$

The first boundary condition is:

$$z = 0,\ H_z = 0 \tag{C.6}$$

$$\Rightarrow H_z = BK_o(\xi_1 r)[e^{-j\beta z} - e^{j\beta z}] \tag{C.7}$$

$$H_z = BK_o(\xi_1 r)\sin(\beta z) \tag{C.8}$$

Equations (B.25) and (B.26) (Appendix B) derived from Maxwell's equations still apply. Substituting (C.8) into (B.25) and (B.26) gives:

$$H_r = B\frac{\beta}{\xi_2}K_1(\xi_2 r)\cos(\beta z) \tag{C.9}$$

and:

$$E_\phi = jB\frac{\omega\mu}{\xi_2}K_1(\xi_2 r)\sin(\beta z) \tag{C.10}$$

In summary the non-zero field expressions for a dielectric resonator operating in the TE_{011} mode inside the dielectric (i.e. $r \leq a$) are (equations (B.32), (B.33) and (B.34) (Appendix B) respectively):

$$E_{\phi 1} = -jA\frac{2\pi\mu f}{\xi_1}J_1(\xi_1 r)\sin(\beta z) \tag{C.11}$$

$$H_{r1} = -A\frac{\beta}{\xi_1}J_1(\xi_1 r)\cos(\beta z) \tag{C.12}$$

$$H_{z1} = AJ_0(\xi_1 r)\sin(\beta z) \tag{C.13}$$

Outside the dielectric ($r \geq a$) we have (equations (C.10), (C.9) and (C.8) respectively):

$$E_{\phi 2} = jB\frac{2\pi\mu_o f}{\xi_2}K_1(\xi_2 r)\sin(\beta z) \tag{C.14}$$

$$H_{r2} = B\frac{\beta}{\xi_2}K_1(\xi_2 r)\cos(\beta z) \tag{C.15}$$

$$H_{z2} = BK_0(\xi_2 r)\sin(\beta z) \tag{C.16}$$

where: ξ_2 = r direction wave number outside the dielectric.

and:

$$\beta^2 = k^2\epsilon_r - \xi_1^2 = k^2 + \xi_2^2 \tag{C.17}$$

$$k = \frac{2\pi}{\lambda} = \frac{2\pi f}{c} = 2\pi f\sqrt{\epsilon_o\mu_o} \tag{C.18}$$

At r=a, E_ϕ inside and outside the dielectric are equal and the same applies to H_z giving:

$$\frac{J_1(\xi_1 a)}{\xi_1 a}A + \frac{K_1(\xi_2 a)}{\xi_2 a}B = 0 \tag{C.19}$$

$$J_o(\xi_1 a)A - K_o(\xi_2 a)B = 0 \tag{C.20}$$

The determinant of (C.19) and (C.20) must be zero for non-trivial solutions:

$$\frac{J_1(\xi_1 a)K_o(\xi_2 a)}{\xi_1 a} + \frac{K_1(\xi_2 a)J_o(\xi_1 a)}{\xi_2 a} = 0 \tag{C.21}$$

At z=0 and z=d the electric fields inside and outside the dielectric are zero giving:

$$\beta = \frac{\pi}{d} \tag{C.22}$$

When (C.17), (C.18), (C.21) and (C.22) are solved simultaneously the resonant frequency, $f=f_o$, can be found.

The expressions for Q_c (conductor Q), Q_d (dielectric Q) and Q_r (radiation Q) are found as follows. The free space impedance is given by:

$$\eta = \sqrt{\frac{\mu_o}{\epsilon_o}} = 120\pi = \mu_o \frac{1}{\sqrt{\epsilon_o \mu_o}} = \mu_o c = \mu_o f \lambda \tag{C.23}$$

$$\Rightarrow 2\pi\mu_o f = \frac{240\pi^2}{\lambda} \tag{C.24}$$

Substituting (C.22) and (C.24) in (C.11); (C.22) in (C.12); (C.22) in (C.13); (C.20), (C.22) and (C.24) in (C.14); (C.20) and (C.22) in (C.15); (C.20) and (C.22) in (C.16) gives:

$$E_{\phi 1} = -jA\frac{240\pi^2}{\xi_1 \lambda} J_1(\xi_1 r)\sin\left(\frac{\pi}{d}z\right) \tag{C.25}$$

$$H_{r1} = -A\frac{\pi}{\xi_1 d} J_1(\xi_1 r)\cos\left(\frac{\pi}{d}z\right) \tag{C.26}$$

$$H_{z1} = AJ_o(\xi_1 r)\sin\left(\frac{\pi}{d}z\right) \tag{C.27}$$

$$E_{\phi 2} = jA\frac{240\pi^2}{\xi_2 \lambda}\frac{J_o(\xi_1 a)}{K_o(\xi_2 a)} K_1(\xi_2 r)\sin\left(\frac{\pi}{d}z\right) \tag{C.28}$$

$$H_{r2} = A\frac{\pi}{\xi_2 d}\frac{J_o(\xi_1 a)}{K_o(\xi_2 a)}K_1(\xi_2 r)\cos\left(\frac{\pi}{d}z\right) \tag{C.29}$$

$$H_{z2} = A\frac{J_o(\xi_1 a)}{K_o(\xi_2 a)}K_o(\xi_2 r)\sin\left(\frac{\pi}{d}z\right) \tag{C.30}$$

The conductor Q is defined as:

$$Q_c = \frac{2\pi f_o W_o}{P_c} \tag{C.31}$$

The dielectric Q is defined as:

$$Q_d = \frac{2\pi f_o W_o}{P_d} \tag{C.32}$$

The radiation Q is defined as:

$$Q_r = \frac{2\pi f_o W_o}{P_r} \tag{C.33}$$

The unloaded Q, Q_o of the dielectric resonator is defined as:

$$\frac{1}{Q_o} = \frac{1}{Q_c} + \frac{1}{Q_d} + \frac{1}{Q_r} \tag{C.34}$$

where: P_c, P_d and P_r are the dissipated power in the conductor, dielectric and the cylindrical box enclosure respectively.

The total stored energy in the resonator is given by:

$$W_o = W_{e1} + W_{e2} \tag{C.35}$$

where: W_{e1} and W_{e2} are the peak electrical energies inside and outside the dielectric respectively.

Using equations (C.25) and (C.28) we have:

$$W_{e1} = \frac{\epsilon_o \epsilon_r}{2} \int_{V_1} E_{\phi 1}^* E_{\phi 1} \, dv$$
$$= \frac{\epsilon_o \epsilon_r}{2} \left(\frac{240\pi^2 A}{\xi_1 \lambda} \right)^2 \int_0^{2\pi} d\phi \int_0^d \sin^2\left(\frac{\pi}{d} z \right) dz \int_0^a J_1^2(\xi_1 r) \, r dr$$
$$= \frac{\epsilon_o \epsilon_r \pi d}{2} \left(\frac{240\pi^2 A}{\xi_1 \lambda} \right)^2 \int_0^a J_1^2(\xi_1 r) \, r dr \qquad \text{(C.36)}$$

$$W_{e2} = \frac{\epsilon_o}{2} \int_{V_2} E_{\phi 2}^* E_{\phi 2} \, dv$$
$$= \frac{\epsilon_o}{2} \left(\frac{240\pi^2 A}{\xi_1 \lambda} \right)^2 \left[\frac{\xi_1 J_o(\xi_1 a)}{\xi_2 K_o(\xi_2 a)} \right]^2 \int_0^{2\pi} d\phi \int_0^d \sin^2\left(\frac{\pi}{d} z \right) dz \int_a^\infty K_1^2(\xi_2 r) \, r dr$$
$$= \frac{\epsilon_o \pi d}{2} \left(\frac{240\pi^2 A}{\xi_1 \lambda} \right)^2 \left[\frac{\xi_1 J_o(\xi_1 a)}{\xi_2 K_o(\xi_2 a)} \right]^2 \int_a^\infty K_1^2(\xi_2 r) \, r dr \qquad \text{(C.37)}$$

where: V_1 and V_2 are the volumes inside and outside the dielectric respectively.

Substituting (C.36) and (C.37) into (C.35):

$$W_o = \frac{\epsilon_o \epsilon_r \pi d}{2} \left(\frac{240\pi^2 A}{\xi_1 \lambda} \right)^2 [1 + R] \int_0^a J_1^2(\xi_1 r) \, r dr \qquad \text{(C.38)}$$

where:

$$R = \frac{W_{e2}}{W_{e1}} = \frac{1}{\epsilon_r} \left[\frac{\xi_1 J_o(\xi_1 a)}{\xi_2 K_o(\xi_2 a)} \right]^2 \frac{\int_a^\infty K_1^2(\xi_2 r) \, r dr}{\int_0^a J_1^2(\xi_1 r) \, r dr} \qquad \text{(C.39)}$$

The power dissipated in the conductor is given by:

$$P_c = 2\times\frac{R_s}{2}\left[\int_{S_1} H_{r1}^{*}H_{r1}\ ds + \int_{S_2} H_{r2}^{*}H_{r2}\ ds\right] \tag{C.40}$$

The 2 factor arises because there are two films and S_1 and S_2 are the film surfaces for r<a and r>a respectively. Substituting (C.26) and (C.29) into (C.40):

$$\begin{aligned} P_c &= R_s\left(\frac{\pi A}{\xi_1 d}\right)^2\left\{\int_0^{2\pi} d\phi\int_0^{a} J_1^2(\xi_1 r)\ r dr + \left[\frac{\xi_1 J_o(\xi_1 a)}{\xi_2 K_o(\xi_2 a)}\right]^2\int_0^{2\pi} d\phi\int_a^{\infty} K_1^2(\xi_2 r)\ r dr\right\} \\ &= 2\pi R_s\left(\frac{\pi A}{\xi_1 d}\right)^2 [1 + \epsilon_r R]\int_0^{a} J_1^2(\xi_1 r)\ r dr \end{aligned} \tag{C.41}$$

Substituting (C.38) and (C.41) into (C.31) gives:

$$Q_c = \frac{240\pi^2\epsilon_r}{R_s}\left(\frac{d}{\lambda}\right)^3\frac{1 + R}{1 + \epsilon_r R} \tag{C.42}$$

Using the definition for the dielectric loss tangent:

$$\tan\ \delta = \frac{P_d}{2\pi f_o W_{e1}} \tag{C.43}$$

P_d can be found:

$$P_d = 2\pi f_0 \tan\ \delta W_{e1} = 2\pi f_o \tan\delta\ \frac{W_o}{1 + R} \tag{C.44}$$

Substituting (C.44) into (C.32) we obtain:

$$Q_d = \frac{1 + R}{\tan\ \delta} \tag{C.45}$$

The power dissipated in the box walls is given by:

$$P_r = \frac{R_{sw}}{2}\int_{S_3} H_{z2}^{*} H_{z2}\, ds \tag{C.46}$$

where: S_3 is the surface of the box and R_{sw} is the box wall surface resistance.

Substituting (C.30) into (C.46) gives:

$$\begin{aligned} P_r &= \frac{R_{sw}A^2}{2}\left[\frac{J_o(\xi_1 a)}{K_o(\xi_2 a)}\right]^2 \int_0^{2\pi} d\phi \int_0^{d} K_o^2(\xi_2 r_b)\sin^2\left(\frac{\pi}{d}z\right) r_b\, dz \\ &= \frac{\pi d R_{sw}A^2 r_b}{2}\left[\frac{J_o(\xi_1 a)}{K_o(\xi_2 a)}\right]^2 K_o^2(\xi_2 r_b) \end{aligned} \tag{C.47}$$

where: r_b=radius of box wall.

Substituting (C.38) and (C.47) into (C.33) gives:

$$Q_r = \frac{960\pi^4 \epsilon_r [1 + R]\int_0^{a} J_1^2(\xi_1 r) r\, dr}{\xi_1^2 \lambda^3 R_{sw} r_b \left[\frac{J_o(\xi_1 a)}{K_o(\xi_2 a)}\right]^2 K_o^2(\xi_2 r_b)} \tag{C.48}$$

Appendix D

Matlab Programs

The following pages give listings of programs written in Matlab that were used to calculate the resonant frequency, ratio of energy stored outside the dielectric to that stored in it and the radiation Q for different dielectric resonators.

```
% program to predict resonant frequency of TE011 mode in dielectric
% resonator.

l = 1.75e-3;          % length of puck
epr = 24;             % dielectric constant
c = 3e8;              % speed of light
a = 2e-3;             % radius of puck
f1 = 23.12e9;         % start frequency
f2 = 23.13e9;         % stop frequency
fs = (f2-f1)/100;     % frequency increment
f = f1:fs:f2;         % range of frequencies

xi1 = pi*(sqrt((((2*f/c).^2)*epr) - ((1/l)^2)));  % radial wave number in puck
xi2 = pi*(sqrt(((1/l)^2) - ((2*f/c).^2)));        % radial wave number outside puck

% split up equation
p1 = (bessel(1,xi1.*a).*besselk(0,xi2.*a))./(xi1.*a);
p2 = (besselk(1,xi2.*a).*bessel(0,xi1.*a))./(xi2.*a);
y = p1 + p2;

plot (f, y)
grid on
title ('Prediction of TE 011 resonant frequency with box wall ignored')
```

```
xlabel ('f (Hz)')

ylabel ('y=function(f)')
```

```
% program to calculate ratio of energy outside to inside the puck

function y=R(x)

a = 2e-3;          % radius of puck
l = 1.75e-3;       % length of puck
epr = 24;          % dielectric constant
f = 23.129e9;      % frequency of oscillation
lam = 3e8/f;       % wavelength

xi1 = pi*(sqrt((((2/lam)^2)*epr) - ((1/l)^2)));        % radial wave number in puck
xi2 = pi*(sqrt(((1/l)^2) - ((2/lam)^2)));              % radial wave number outside puck

% expressions for diff's of k1(xi2*a) and j1(xi1*a)
k1d = ((-1/(xi2*a))*besselk(1,xi2*a)) - (besselk(0,xi2*a));
j1d = ((-1/(xi1*a))*bessel(1,xi1*a)) + (bessel(0,xi1*a));

% split up equation into handy segments
t1 = xi1*bessel(0,xi1*a);
b1 = xi2*besselk(0,xi2*a);
t2 = ((a^2)/2)*((k1d^2) - ((1 + (1/((xi2*a)^2)))*((besselk(1,xi2*a))^2)));
b2 = ((a^2)/2)*((j1d^2) + ((1 - (1/((xi1*a)^2)))*((bessel(1,xi1*a))^2)));
```

```
% the final expression

y=(1/epr)*((t1/b1)^2)*(t2/b2);
```

```
% program to calculate box wall losses quality factor (radiation Q)

function y=Q(x)

a = 2e-3;          % radius of puck
l = 1.75e-3;       % length of puck
epr = 24;          % dielectric constant
f = 23.129e9;      % frequency of oscillation
lam = 3e8/f;       % wavelength

xi1 = pi*(sqrt((((2/lam)^2)*epr) - ((1/l)^2)));        % radial wave number in puck
xi2 = pi*(sqrt(((1/l)^2) - ((2/lam)^2)));              % radial wave number outside puck

R = 0.0046;        % ratio of energy outside/inside the puck
rb = 4.5e-3;       % radius of box wall
rs = 38.8e-3;      % the rs of the box wall

% split up equation into handy segments
t1 = 960*(pi^4)*epr*(1+R);
t2 = ((a^2)/2)*((bessel(0,xi1*a))^2) - ((2*bessel(1,xi1*a)*bessel(0,xi1*a))/(xi1*a))
+ ((bessel(1,xi1*a))^2);
b1 = (xi1^2)*(lam^3)*rs*rb*((besselk(0,xi2*rb))^2);
b2 = ((bessel(0,xi1*a))/(besselk(0,xi2*a)))^2;
```

```
y = (t1*t2)/(b1*b2);
```

Appendix E

Papers

The research carried out and described in this thesis has led to the following publications and presentations.

[1] Jenkins A.P., Su L.Y., Kale K.S., Goringe M.J., Burgoyne J.W., Dew-Hughes D., Grovenor C.R.M. (1995) "Microwave surface resistance of air-atomised spray deposited Tl-Ba-Ca-Cu-O thick films". *IEEE Transactions on Applied Superconductivity* 5(2): 1095-1098.

[2] Jenkins A.P., Kale K.S., Dew-Hughes D., Bramley A.P., Grovenor C.R.M. (1996) "TBCCO thin film microwave devices". In *Superconducting Microwave Circuits Colloquium Digest*. London: IEE: 3/1-3/5.

[3] Jenkins A.P., Kale K.S., Dew-Hughes D. (1996) "Surface Resistance Measurement Techniques". In A.V. Narlikar (ed.) *Studies in High Temperature Superconductors* Vol. 17 (Part I). New York, NY: Nova Science Publishers: 179-219.

[4] Kale K.S., Jenkins A.P., Jim K.L., O'Connor J.D., Dew-Hughes D., Edwards D.J., Bramley A.P., Glassey B.J., Grovenor C.R.M., Goringe M.J., Pecz B. (1996) "TBCCO thin films and passive microwave devices". In U. Balachandran (ed.) *Proceedings of the TMS Annual Meeting, Anaheim, CA, USA, February*. Warrendale, PA: TMS, in press.

[5] Bramley A.P., Glassey B.J., Grovenor C.R.M., Goringe M.J., O'Connor J.D., Dew-Hughes D., Jenkins A.P., Kale K.S., Jim K.L., Edwards D.J., Pecz B. (1996) "Tl-based thin films for electronic applications". In C. Schneider (ed.) *Proceedings of the HTS-Workshop on Digital Applications, Josephson Junctions and 3-Terminal Devices, Enschede, Netherlands, 21-24 April.* Netherlands: University of Twente, in press.

[6] Bramley A.P., Glassey B.J., Grovenor C.R.M., Goringe M.J., O'Connor J.D., Jenkins A.P., Kale K.S., Jim K.L., Dew-Hughes D., Edwards D.J. (1996) "Tl-Ba-Ca-Cu-O thin films on buffered substrates for microwave device applications". Presented at the *Applied Superconductivity Conference 1996*, Pittsburgh, PA, USA, 25-30 August.

[7] Jenkins A.P., Kale K.S., Edwards D.J., Dew-Hughes D., Bramley A.P., Grovenor C.R.M., Kale S.V. (1996) "Microstrip disk resonators for filters fabricated from TBCCO thin films". Presented at the *Applied Superconductivity Conference 1996*, Pittsburgh, PA, USA, 25-30 August.

[8] Kale K.S., Jenkins A.P., Edwards D.J., Dew-Hughes D., Bramley A.P., Grovenor C.R.M., Morley S.M., Kale S.V. (1996) "HTS-sapphire-HTS dielectric resonators for surface resistance measurements and for low phase noise oscillators". Presented at the *Applied Superconductivity Conference 1996*, Pittsburgh, PA, USA, 25-30 August.

[9] Jenkins A.P., Kale K.S., Bramley A.P. (1996) "TBCCO disk resonators and filters". Presented at the *Fourth Symposium on High-Temperature Superconductors in High-Frequency Fields*, 29 September-20 October, Pacific

Grove, CA, USA.